THESIS

UTILIZING REMOTE SENSING DATA TO ESTIMATE SOIL SALINITY IN IRRIGATED AGRICULTURAL AREAS OF COLORADO'S SOUTH PLATTE RIVER BASIN

Submitted by

Kieri M. Karpa

Department of Civil and Environmental Engineering

In partial fulfillment of the requirements

For the Degree of Master of Science

Colorado State University

Fort Collins, Colorado

Fall 2025

Master's Committee:

Advisor: José L. Chávez
Co-Advisor: Timothy K. Gates

Jessica O'Connell

ABSTRACT

UTILIZING REMOTE SENSING DATA TO ESTIMATE SOIL SALINITY IN IRRIGATED AGRICULTURAL AREAS OF COLORADO'S SOUTH PLATTE RIVER BASIN

With the global population projected to reach 10 billion by 2050, agricultural output will need to increase by about 50%. This increase must occur with little to no expansion of farmable land, as climate change is expected to reduce the amount of land available for agriculture. Additionally, there is limited availability of water resources to aid in the increasing output, as irrigated agriculture already accounts for 72% of freshwater withdrawals worldwide – 40% of which is unsustainable. Farmers are being asked to produce more with fewer resources, while challenges like soil salinization complicate the process.

In the South Platte River Basin (SPRB) of Colorado, farmers are facing increasing soil and water salinity, which leads to a decrease in crop yields. Remote sensing data provide potential for the development of low-cost methods for monitoring changes and effects of salinity. One such method uses satellite remote sensing data to estimate the soil saturation extract electrical conductivity (EC_e, dS/m). Current models for predicting EC_e using remote sensing data utilize vegetation indexes to relate crop health to soil health.

In this study, two previous methods of estimating salinity were tested and revised to calibrate an equation for the estimation of soil salinity in the SPRB. These EC_e modeling methods focused on the application of three different vegetation indexes [i.e., the Normalized Difference Vegetation

Index (NDVI), the Canopy Response to Salinity Index (CRSI), and the Crop Water Stress Index (CWSI)], plus weather data from agricultural weather stations.

When these existing EC_e mapping methods failed to produce accurate EC_e results in the SPRB, multiple regression analyses were run using remote sensing data, and new explanatory variables, to calibrate a local model. Both single year and multiyear data EC_e models were created utilizing three datasets: one dataset included all fields surveyed, one included only the corn fields surveyed, and one included only the non-corn fields surveyed.

Using the highest coefficient of determination (R^2) statistic, 20 models from each dataset (60 models total) were selected for further testing. The Corrected Akaike Information Criterion (AICc) was calculated for each of these models to identify the best model for each dataset. When the selected models were tested against data collected during surveys, they showed very small biases (Mean Bias Error less than +/- 0.16 dS/m, Normalized Mean Bias Error less than 6%). For the dataset that included all fields surveyed and the dataset that included only the non-corn fields surveyed, even the most promising models (R^2 between 0.63 and 0.7) had poor accuracy with a Normalized Root Mean Square Error (NRMSE) of greater than 30% (33.34-40.83%).

The dataset with all surveyed fields was calibrated with observed EC_e data that ranged from 0.00-13.33 dS/m with an average of 2.78 dS/m, and the most promising model calibrated on this data predicted EC_e values between 0.75-4.43 dS/m with an average of 2.67 dS/m. The dataset which included only the non-corn fields was calibrated with observed EC_e data that ranged from 0-13.33 dS/m with an average of 2.91 dS/m, and the most promising model calibrated on this data predicted EC_e values between 0.76-5.15 dS/m, with an average of 2.78 dS/m.

The modeling results from corn field dataset were generally better at estimating soil salinity with R^2 values around 0.84 and NRMSEs of around 20%. The corn field data set was calibrated with observed EC_e data that ranged from 0.43-6.86 dS/m with an average of 2.40 dS/m, and the most promising model calibrated on this data predicted EC_e values between 1.23-4.81 dS/m with an average of 2.40 dS/m.

All tested models from all datasets were accurate to around +/- 1 dS/m (Root Mean Square Error) indicating these models may be useful for field-level management decisions. The number of independent explanatory variables included in the 60 best-performing equations ranged from 2 to 8, with 5-variable models being the most common. Every equation incorporated at least one weather-related variable (precipitation or temperature). Although NDVI was not used as a sole predictor, it was included in nearly all of the top equations (58 out of 60), underscoring its importance in estimating soil salinity. CRSI and CWSI were also prevalent, appearing in approximately two-thirds of the best equations (41 and 42 out of 60, respectively). Additionally, 47 of the 60 equations incorporated the crop growth development-phase data for either vegetation indexes or weather variables, suggesting that the crop development stage is an influential factor in salinity prediction models.

ACKNOWLEDGEMENTS

I would like to thank the Colorado Water Center at Colorado State University, the Colorado Agricultural Experiment Station at Colorado State University, and the Colorado Department of Natural Resources – Colorado Water Conservation Board, who all contributed funding to the research projects supporting this thesis.

I would also like to thank my advisors, Dr. José L. Chávez and Dr. Timothy K. Gates, who brought me onto the projects and provided guidance and assistance through every setback.

This research would not have been possible without the entire student research team, including Gracie Gooch, Muhammad Fawad, and especially Lucas Lenoch and Mike Ryan, who were instrumental in conducting soil surveys, teaching me how to use equipment, writing field-work guides, drilling wells, and sending out soil samples.

A big thanks goes to Dr. Allan Andales for allowing us to borrow his truck for fieldwork and letting us overrun his lab with drying soil samples throughout this project.

I also want to thank my professors for everything their classes have taught me. A special thanks goes to Dr. Jessica O'Connell for agreeing to be on my thesis committee.

I am also so grateful for my community and friends who became more like family throughout my time in Colorado and who cared about me even when I was stressed and difficult to be around.

Finally, as I finish my educational journey at CSU and look forward to what comes next, I want to thank my parents and brother for always supporting me, not just through this program but throughout my entire life. I would not have become the person I am today without them.

TABLE OF CONTENTS

LIST OF FIGURES

LIST OF TABLES

CHAPTER 1:BACKGROUND, LITERATURE REVIEW, AND STUDY OBJECTIVES

1.1 Global Agricultural Water Use

Agriculture is one of the most important industries in the world. Not only is agriculture crucial for providing food for earth's growing population, but it has also been widely utilized to raise income for those in extreme poverty and stimulate economic growth (World Bank Group, 2024). With the population of earth expected to reach 10 billion by 2050, it is necessary to increase agricultural output by an estimated 50% (Michel, 2023; Ranganathan et al., 2018; Heggie, 2019; Giordano et al., 2019). Currently, about 50% of vegetated land is used for agriculture (Ranganathan et al., 2018). Expansion of cropped land is a potential option for increasing agricultural production, but the land available is often less than ideal (Heggie, 2019; Giordano et al., 2019), and it is limited by soil degradation, pollution, and climate (Heggie, 2019). Climate is a major concern for agriculture as the world is estimated to lose half its' farmable land due to climate change (Heggie, 2019). While there are methods for bringing infertile lands into production, agricultural expansion carries major consequences including the destruction of natural habitats and ecosystems both of which cause biodiversity loss (Hanson et al., 2022). Since expanding agricultural land is likely not a sustainable option, other methods of increasing agricultural production need to be considered.

One common method for increasing agricultural output is the use of irrigation (United States Department of Agriculture, 2025). Currently, 72% of freshwater withdrawals around the world are used for agriculture (Michel, 2023; Food and Agriculture Organization of the United Nations, 2022). However, to meet global demand for agriculture, it is estimated that water withdrawals will need to be increased by 30% (Michel, 2023). Currently, groundwater withdraws for irrigated agriculture are increasing at about 2.2% each year (Food and Agriculture Organization of the

United Nations, 2022). This level of pumping is widely regarded as unsustainable as even today 40% of global agricultural relies on unsustainable groundwater extraction (Ingrao et al., 2023). The Food and Agriculture Organization of the United Nations predicts that by 2025 two thirds of the world will be facing water stress and 1.8 billion people will be living in areas with “absolute” water scarcity (Food and Agriculture Organization of the United Nations, 2017).

Water scarcity occurs when demand for water exceeds the available water supply or when water quality prevents water use (United Nations, 2025). “Absolute” scarcity is defined when a region has a volume of water less than 500 m^3/year per capita while “water stress” is defined as having between 500 m^3 – 1000 m^3/year per capita (Food and Agriculture Organization of the United Nations, 2025). If water were only used for domestic uses (toilet, shower, drinking, etc.), this amount would not cause a problem as the average person in a developed nation like the United States uses 138 m^3 of water per year (100 gallons/day) (Philadelphia Water Department, 2024). However, in the United States alone, over 830 m^3/year per capita (600 gallons/day per person) are being used for agriculture (United States Bureau of Reclamation, 2020). Of the areas already facing water scarcity, 60% of croplands are facing a decrease in water availability and 80% of crop lands will face an intensification of water scarcity (Liu et al., 2022). These predictions are based on climate change projections alone and do not consider further pressure from population increase or urban expansion which will continue to limit water resources. Aqueduct 4.0, a model of water stress developed by the Water Resources Institute, shows in their model of 2019 (baseline model) that many areas of the world are facing medium to high water stress (Kuzma et al., 2023). Most of the western United States, Mexico, India, the Middle East and parts of Europe and China face extreme water stress with withdraws accounting for more than 40% of total available water (Figure 1.1).

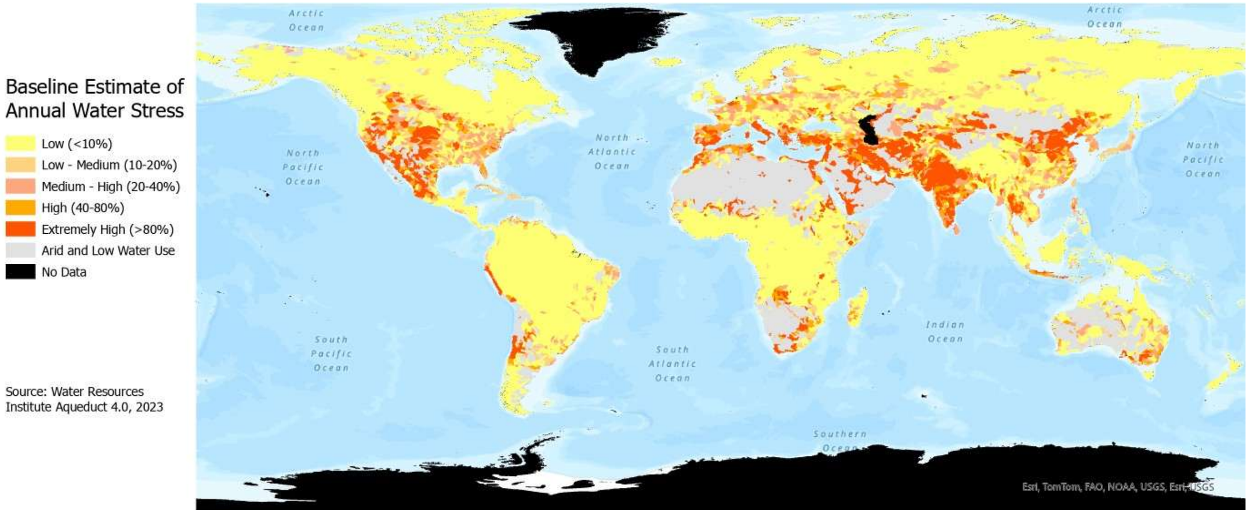

Figure 1.1 Sustainable Development Goal Indicator 6.4.2 "Level of water stress: freshwater withdrawal as a proportion of available freshwater resources" estimates for 2019 indicate the western United States faces high to extremely high levels of water stress. Map created in ArcGIS Pro using data from Aqueduct 4.0 (Kuzma et al., 2023).

1.2 Colorado Agricultural Water Use

In the United States, irrigated agriculture accounts for less than 20% of crop land but crops produced on that land account for nearly 54% of crop sales as of 2017 (United States Department of Agriculture, 2025). More than 143 million ha (58 million acres) of US cropland is irrigated with the majority being in the west (United States Department of Agriculture, 2025). Colorado is ranked 6th in the United States for most irrigated agricultural land containing 4.8% of the United States' total irrigated agricultural land (United States Department of Agriculture, 2025). Colorado agriculture is spread out across 74 million ha (30 million acres) containing about 36,000 farms, directly employs 195,000 people, and generates 47 billion dollars per year (Kelly, 2024). While agriculture is disbursed across the state, the most highly productive areas of Colorado are concentrated in the eastern plains (Kelly, 2024), but this area in particular is facing extreme water scarcity (Figure 1.2) (Kuzma et al., 2023).

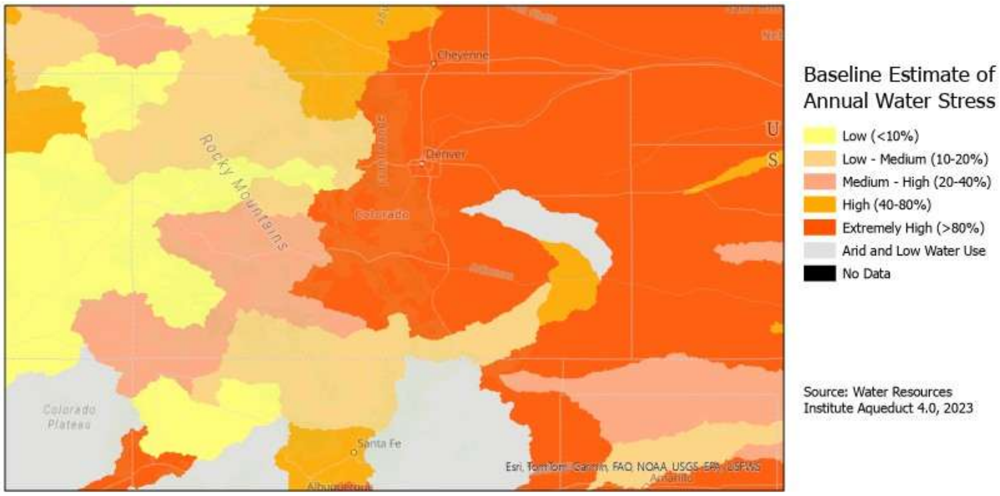

Figure 1.2 Water Stress Map of Colorado indicates extreme water stress in much of eastern Colorado which continues into neighboring states. Map created in ArcGIS Pro using data from Aqueduct 4.0 (Kuzma et al., 2023).

Water scarcity can be either physical or economic. Physical water scarcity is when there is physically not enough water in an area to meet demand whereas economic water scarcity is when there could be enough water to meet demand if there was money for infrastructure to deliver the water from rivers, reservoirs, or aquifers to the areas where it is needed (Giordano et al., 2019). The water stress faced in the United States is usually from physical water scarcity.

In Colorado, 16.8 billion m^3 (13.7 million acre-feet) of precipitation is received annually, but due to interstate agreements only 6.5 billion m^3 (5.3 million acre-feet) are allowed to be consumed within Colorado's borders for agricultural, municipal, and industrial uses each year (Colorado Water Center, 2020). Of the 6.5 billion m^3 (5.3 million acre-feet) consumed, 87% is supplied by surface water while 17% is supplied by groundwater (Colorado Water Center, 2020). The majority of water consumed, 5.8 billion m^3 (4.7 million acre-feet), is used for agriculture (Colorado Water Center, 2020). An additional challenge is presented with the continental divide as 80% of water falls and flows west while the majority of irrigated agricultural lands are on the eastern side of the divide (Colorado Water Center, 2020).

One method of increasing water supply in water limited areas such as the eastern side of Colorado is through the use of return flows. Not all water used is consumed on the first use, much of it becomes return flows which allows water to be used multiple times before leaving Colorado (Colorado Water Center, 2020), however, this can negatively affect water quality. Even with the reuse of water, it is estimated that for the crops grown in Colorado to be fully irrigated, 2.5 billion m^3 (2 million acre-feet) more water would be necessary (Colorado Water Center, 2020). This gap between supply and demand for water is likely to increase in the coming years causing irrigated agriculture in the state to decrease by 15-20% by 2050 (Colorado Water Center, 2020).

Colorado farmers also face pressure due to Colorado's prior appropriation method for determining water rights (Colorado Water Center, 2019). As municipalities expand, they often need more water for their growing population and buy farmland for its water rights or buy water rights directly from the agricultural producers who have legacy water rights (Conran, 2013). Once water rights have been sold, it is often the case that agriculture stops on the land (Conran, 2013). Growing populations put pressure on agricultural producers to sell their land, along with the water rights, which reduces agricultural output (Conran, 2013). To conserve more water for the growing population, many farmers are encouraged to switch from flood irrigation to more efficient sprinkler or drip irrigation systems (Water Education Colorado, 2023a). While these irrigation methods can reduce evaporation, they also reduce deep percolation (Water Education Colorado, 2023a) which can pose its' own challenges such as the intensification of salinity as salts are no longer leached out of the plant root zone.

1.3 South Platte River Basin (SPRB)

The South Platte River Basin (SPRB) includes most of northeastern Colorado and parts of Wyoming and Nebraska (Figure 1.3) (United States Geological Survey, 2000). This area is home to 80% of Colorado's population and includes metropolitan areas like Denver and Fort Collins in addition to agricultural areas (South Platte River Basin Stakeholders Group, 2025). The population of this region is expected to increase to more than 8 million people by 2050, increasing the municipal and industrial water needs (Svaldi, 2017). Besides urban areas, within this basin exist approximately 336,000 ha (831,000 acres) of irrigated agricultural land which provides about 72% of Colorado's agricultural output (South Platte River Basin Stakeholders Group, 2025).

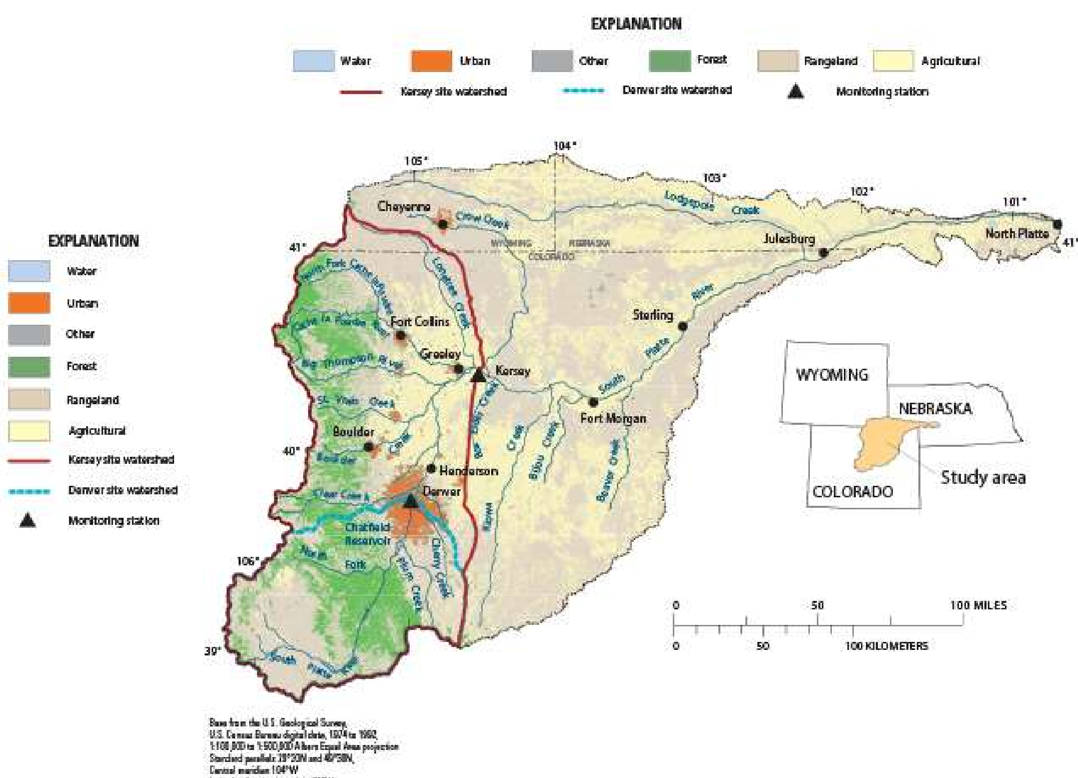

Figure 1.3 The South Platte River Basin covers most of northeastern Colorado as well as parts of Wyoming and Nebraska. Map retrieved from United States Geological Survey (2000).

Both surface water and groundwater are used to meet water needs. Throughout the basin, there are more than 18,600 water diversion points for surface water (Waskom, 2013). The surface water of the South Platte River is connected to an alluvial aquifer which provides water for most of Colorado's front range and agricultural communities (Colorado Water Science Center, 2012). There are over 8,200 high-capacity wells which pump water out of the underground aquifer (Waskom, 2013). Due to declining water levels, strict limits have been imposed on pumping and efforts are being made to recharge the aquifer (Waskom, 2013).

Water in the South Platte is often a result of snow melt from precipitation in the mountains of northern Colorado as well as transbasin diversions from the Colorado river, and the Arkansas, North Platte, and Laramie river basins (Water Education Colorado, 2023b). Low annual precipitation and high evaporative losses already put the majority of Colorado in a water deficit and climate change is predicted to further limit water supply as temperatures are predicted to increase between 2.5°C and 5°C without an expected increase in precipitation (Colorado Water Conservation Board, 2022).

In addition to water quantity, water quality is a major concern. While surface and groundwater quality in forested and mountain regions are generally good and indicate little human influence, water quality in the agricultural areas indicate high levels of nitrate and salinity (Dennehy et al., 1998). NEIRBO Hydrogeology (2020) found increasing salinity in the surface water of the South Platte moving downstream with concentrations of total dissolved solids (TDS, mg/L) increasing from 569 mg/L TDS in Denver to 700 mg/L TDS in Kersey and 1,165 mg/L TDS in Julesburg near the Colorado-Nebraska border. The increasing concentration of contaminants has been linked to large water withdraws for agricultural and urban uses reducing the dilution of contaminants in the South Platte River (Dennehy et al., 1998) and irrigation return flows which largely contribute to stable river flow but often contain nitrates, dissolved solids, and pesticides affecting the downstream water quality (Dennehy et al., 1998; Waskom, 2013). Return flows also indicate that surface and ground water are reused multiple times before the water in the basin leaves Colorado (Dennehy et al., 1998).

Regardless of the exact cause, the increase of TDS in the downstream reaches of the SPRB is of concern to both water quality and agricultural productivity. The concentration of TDS within the SPRB exceeds the United States Environmental Protection Agency's (2015a) secondary drinking water standard of 500 mg/L TDS, which is also the threshold where salt-sensitive crops—such as beans, carrots, and onions, all of which are grown in the SPRB—begin to show yield reductions (Colorado Water Center, 2025). Even more resilient crops like corn and alfalfa, which are among Colorado's most commonly grown crops, begin to experience yield losses when salinity reaches 1,000–2,000 mg/L TDS (Colorado Water Center, 2025). Because TDS levels in downstream areas are approaching or exceeding these thresholds, these regions warrant close monitoring to ensure water quality does not impair agricultural viability—even for salt-tolerant crops.

When used for irrigation, the increasingly contaminated water may leave behind salts in the soil profile. The adoption of more efficient irrigation systems, like sprinklers, while beneficial for water conservation, can exacerbate soil salinity problems as less excess water is available to flush salts beyond the root zone. Without proper irrigation water management, this buildup poses a long-term risk to soil health and agricultural productivity.

1.4 Irrigation Water Management and Soil Salinity

Irrigation has been used throughout history to safeguard food supplies against droughts (Hoffman and Evan, 2007). Today, irrigation is necessary for production in 20% of the world's

cultivated lands producing about 40% of the global food supply (Hoffman and Evan, 2007).
Good irrigation water management practices means applying the right amount of water at the right time to fulfill plant needs without wasting water, soil and plant nutrients, or degrading the soil quality (United States Natural Resources Conservation Service, 1997). While the idea behind irrigation water management is to create a sustainable agricultural system, irrigation can exacerbate some issues like soil salinization (Hoffman and Evan, 2007; Stavi et al., 2021).

Soil salinity is simply the presence of salts in soil (Singh, 2021). This presence can be measured in many ways, but the concentration of TDS (mg/L) and electrical conductivity (EC, dS/m) are two of the most common methods for measuring soil salinity. All surface and ground water contain some amount of dissolved salts, so the presence of some salts in soil is expected and natural (Hoffman and Evan, 2007). A high concentration of salts, however, is a threat to crop production (Hoffman and Evan, 2007; Singh, 2021). High levels of soil salinity can decrease crop yields (Figure 1.4) and can make soils unusable for agriculture which is the likely cause of civilization collapse for Mesopotamia and the Viru Valley of Peru (Shahid et al., 2018).

With the rise in sea level caused by climate change, soil salinization has been intensively studied in coastal areas where saltwater intrusion and capillary rise play large roles in soil salinization, but there is a lack of research conducted in inland areas where lack of precipitation and poor irrigation management are thought to be the primary causes of soil salinization (Eswar et al., 2021). In inland areas, soil salinization occurs when precipitation and irrigation are not able to both meet crop water requirements – the amount of water a plant requires for evapotranspiration (ET) to prevent water stress – and leach salts out of the root-zone (Shahid et al., 2018). When irrigation is used efficiently to meet the crop water requirement, the naturally present salts in the water are left behind in the root zone when the soil water is removed through the ET process

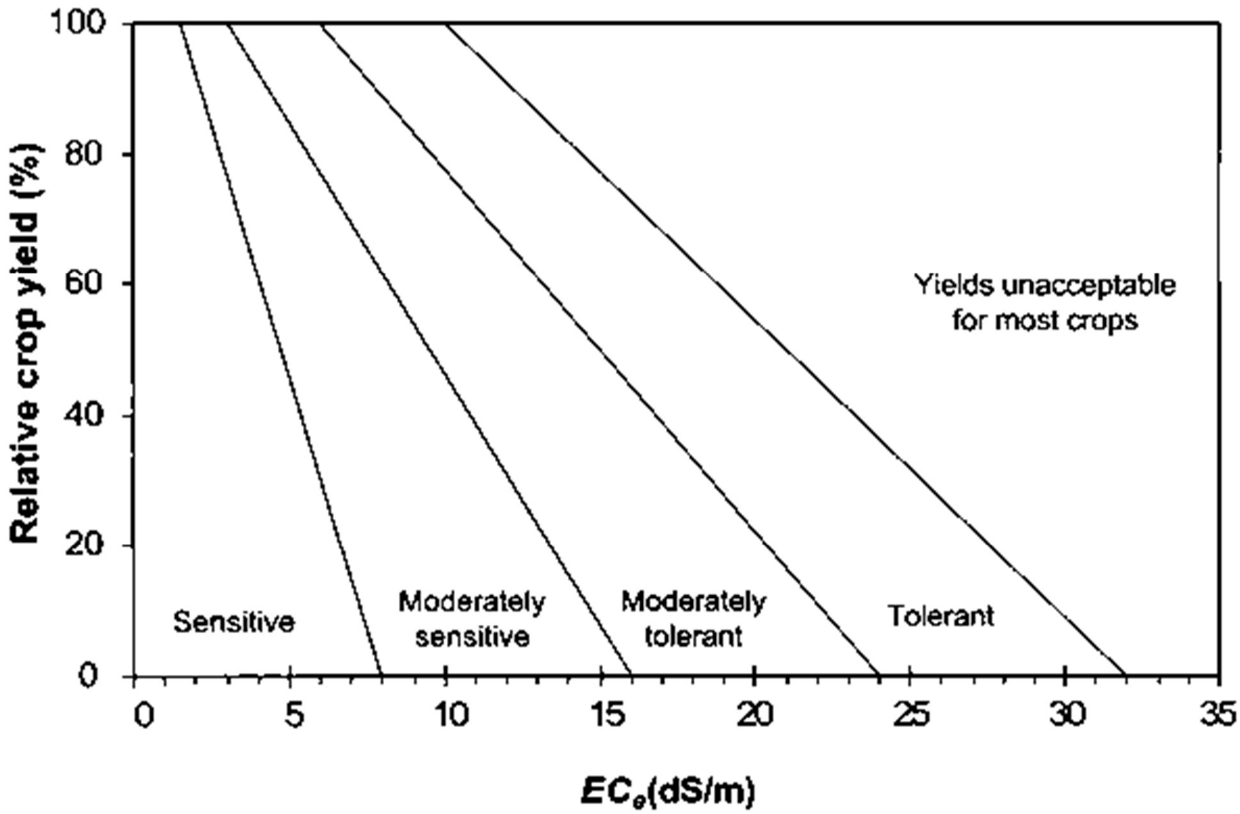

Figure 1.4 Crops exhibit reduced yields as soil salinity increases. Salinity is measured as soil extract electrical conductivity (EC_e, dS/m). Sensitive crops, like beans, carrots, and onions, begin to lose yield at very low salinity levels, around 2 dS/m. Moderately sensitive crops, like corn, alfalfa, and potatoes can tolerate a bit more salinity—up to around 4 dS/m—before yield drops significantly. Moderately tolerant and tolerant crops, like sugar beets, barley, and wheat, maintain yield under higher salinity conditions, but even they begin to show decline after 6-10 dS/m (Food and Agriculture Organization of the United Nations, 2025).

(Hoffman and Evan, 2007). hile this issue is present in most irrigated areas, exceptions include areas where natural rainfall and good soil drainage allow salts to be leached out of the crop root profile and into downstream streams and the groundwater system (Hoffman and Evan, 2007). When irrigation is used in areas without adequate natural rainfall or good soil drainage, extra irrigation water can be used to leach salts out of the soil profile (Hoffman and Evan, 2007). This can pose additional issues, however, as it often increases the salinity of downstream streams and groundwater (Hoffman and Evan, 2007). Since many areas use pumped groundwater for irrigation, the increase in salinity in the groundwater contributes to the soil salinization cycle as it is reapplied to fields leaving behind the salts that were leached into it.

1.5 Electrical Conductivity (EC) as a Proxy for Salinity

Globally, it is estimated that over 1000 Mha are affected by salinity, that is soil having a soil extract electrical conductivity (EC_e, dS/m) equal to or greater than 4 dS/m (Figure 1.5) (Food and Agriculture Organization of the United Nations, 2015; Eswar et al., 2021; Nachtergaele et al., 2009). Electrical conductivity (EC) is a common measure of salinity and describes how well soil water can carry electrical currents (United States Natural Resources Conservation Service,

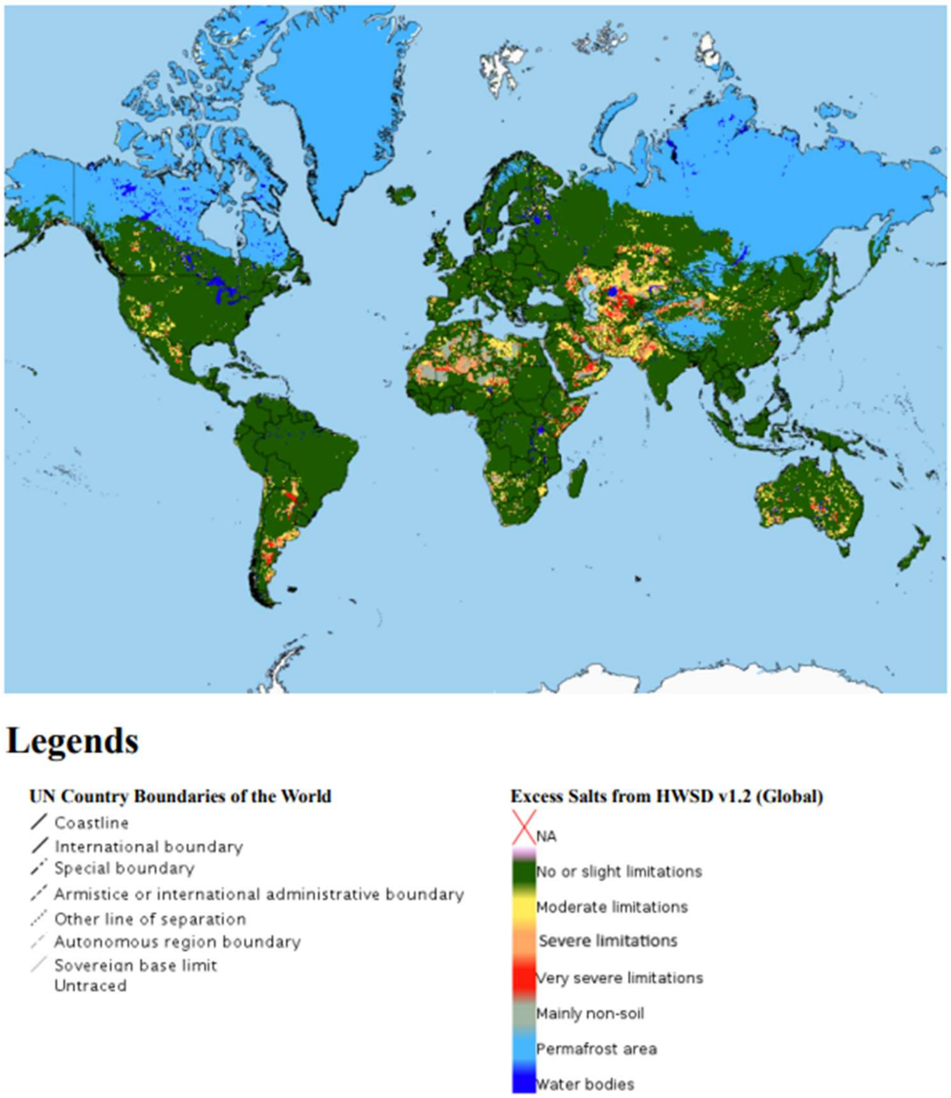

Figure 1.5 A global map of salt-affected soils shows moderate to severely affected soils in parts of the Western United States, Northern Africa, Central and South Asia, and South America. Map retrieved from the Food and Agriculture Organization of the United Nation's Global Soil Information System, Harmonized World Soils Database V1.2, Excess Salts (Food and Agriculture Organization of the United Nations, 2020).

2011; Corwin and Yemoto, 2017). It can be used as a proxy for salinity as the cations and anions which carry the current come from dissolved salts (United States Natural Resources Conservation Service, 2011). Although the exact relationship between salt content and EC varies based on the type of ions present, a strong positive correlation between total soluble salt concentration and soil EC has been demonstrated, with EC increasing as salt content increases (Ismayilov et al., 2021).

Different classifications of EC are measured in different ways. The two classifications used in this study are soil saturation extract EC (EC_e) and apparent or bulk EC (EC_a). EC_e is a standardized method of estimating soil salinity. Measurements of EC_e are made in a laboratory by mixing an air-dried soil sample with distilled water until it reaches saturation (Romić et al., 2021). After saturation is reached, the mixture will be left alone for 24 hours before water is extracted from the mixture (Romić et al., 2021). The EC of the water is measured at a given temperature then adjusted to what would be an equivalent value at 25°C (Corwin and Lesch, 2005). While EC_e is a standardized measurement of EC, it is far more time intensive than most methods used to measure EC_a.

EC_a is a measure of EC in bulk soil, meaning the value is measured leaving the soil structure intact with pores. This value is useful across a homogenous area for comparisons of relative salinity but is not standardized and can be influenced by factors other than salinity alone such as soil structure, soil texture, water content, and temperature (Corwin and Lesch, 2005). Because of this, when EC_a data are collected, usually soil information or soil samples are also collected to calibrate the EC_a data to EC_e.

Transforming EC_a to EC_e requires the use of a calibration equation. Each device used for the estimation of EC_a uses a method of calibration which may change based on soil factors which affect the readings (Bennett et al., 1995). Most devices will provide basic calibration equations which can be used when exact values are not needed. If exact values are desired, to ensure accuracy of the calibration, samples will need to be taken (Bennett et al., 1995). The basic calibration process involves using a device to survey the bulk EC of a field. After a survey is complete, a representative set of soil samples are collected at different locations which represent the variety of the area in terms of salinity, soil type, soil texture, and soil water content. The EC_e estimated for each of the samples can be used in a regression analysis to calibrate the rest of the EC_a values to EC_e.

1.6 Benefits of Mapping Electrical Conductivity (EC) Over Large Areas

Soil salinity is a dynamic soil property affected by pedogenic, edaphic, meteorological, biological, and anthropogenic factors (Corwin and Scudiero, 2019; Craig, 2023) making spatial variation a major concern. Previous studies found coefficients of variation for salinity across study areas near 80% (Peng et al., 2019). Changes in soil management will also affect salinity – specifically, changes in the type, frequency, and amount of irrigation as well as the source of irrigation water can affect the ability of salts to be leached from the surface into groundwater. Since many factors affecting soil salinity (i.e., land use, climate, irrigation management) change not only with location but also with time, monitoring salinity changes is difficult without temporal data (Metternicht and Zinck, 2003; Corwin and Scudiero, 2019; Peng et al., 2019; Craig, 2023). Unfortunately, often data from a single point in time, such as that collected by a soil survey, are all that is available, since surveys are not usually conducted at regular intervals. Monitoring salinity not only on a large temporal scale but also on a large spatial scale allows for changes in soil salinity to be observed relative to potential contributing factors. Meteorological factors (i.e. rainfall and temperature) and anthropogenic factors (i.e. farming practices) are thought to be major contributing factors for the variability of salinity in agricultural areas. Scudiero et al. (2015) utilized weather data along with a vegetation index to find a relatively accurate equation to estimate soil salinity which also accounted for farming practices by differentiating between cropped and fallow land. Craig (2023) suggests that changes in irrigation – specifically moving from flood irrigation to sprinkler or drip irrigation which are less water intensive – may contribute to an increase in salinity as salts cannot be adequately leached from the soil. This can be exacerbated when the irrigation water used is low-quality containing high salt concentrations (Singh, 2021). It is possible to track these – weather data, irrigation type, and water quality – and other potential contributing factors across large areas with historical data and combine them with salinity maps to evaluate their impact on soil salinity.

Large scale mapping of soil salinity through soil surveys has never been completed on a regional or country scale. Some government entities do provide large scale soil mapping. For example, the United States Department of Agriculture's Natural Resources Conservation Service provides information including soil type and surface salt concentrations from the United States soil survey for free through the Soil Survey Geographic Database (SSURGO). However, the data provided by SSURGO is based on the soil type alone and does not account for salinity variations caused by location, land use, or natural processes making SSURGO salinity data unusable for field level salinity management decisions and likely inaccurate for tracking regional salinity patterns (Natural Resources Conservation Service, 2019).

1.7 Methods of Estimating Electrical Conductivity (EC)

Five historically utilized methods for estimating soil EC include visual observations, laboratory analysis of soil samples, in situ measurement of electrical resistivity, in situ electrical conductance measured with time domain reflectometry, and in situ electrical conductance measured by electromagnetic induction (Corwin, 2003; Corwin and Scudiero, 2019). Although quick and relatively cheap, visual observations are the least standardized of all EC detection methods because they rely on expert observation of plant and soil health and lack quantitative analysis (Corwin, 2003; Corwin and Scudiero, 2019). Because opinion can change from expert to expert and conditions change markedly from location to location within a given field, it is unreliable to use visual observations as a method for determining salinity at a field level much less interpolating across multiple fields or regions. Laboratory analysis of soil samples is a standard method of EC estimation which is used for determining EC_e values. While a few different laboratory methods exist for estimating soil EC_e, they all require soil samples, the collection of which tends to be time and labor intensive (Corwin, 2003; Corwin and Scudiero, 2019). Additionally, laboratory analysis of soil samples merely provides point data which cannot be accurately extrapolated over a field if the variability of the field has not already been established (Corwin, 2003).

With difficulty in obtaining EC_e from laboratory data and the unreliability of visual observations, in situ measurements of EC_a are more commonly utilized. One such method of measuring EC_a involves measuring electrical resistivity by placing electrodes in the soil and applying an electrical current between the electrodes (Corwin, 2003; Corwin and Scudiero, 2019). The potential is measured across the electrodes to estimate EC_a (Corwin, 2003; Corwin and Scudiero, 2019). While this technique can be used on a field scale, it has major limitations. Because this method measures EC_a over a large volume of soil at once, it tends to reflect the average EC_a value and mask variations of EC_a within a field (Corwin, 2003; Corwin and Scudiero, 2019). Additionally, the requirement of good contact between the soil and the electrodes can lead to unreliable estimates when used in dry, frozen, or stoney soils (Corwin, 2003; Corwin and Scudiero, 2019).

Although originally intended for measuring soil water content, time domain reflectometry has been adopted for use in measuring EC_a (Corwin, 2003; Corwin and Scudiero, 2019). This method involves measuring the time a voltage pulse takes to move down a probe and return (Corwin, 2003; Corwin and Scudiero, 2019). The EC_a can be determined by measuring the reduction of the voltage signal as it travels through the soil (Corwin, 2003; Corwin and Scudiero, 2019). The procedure for time domain reflectometry is relatively noninvasive (Corwin, 2003; Corwin and Scudiero, 2019). After installation, the probes can take automatic measurements, detect small changes in EC_a when representative soil conditions are present, and typically do not require calibration (Corwin, 2003; Corwin and Scudiero, 2019). However, it is unrealistic for use over areas larger than a single field as the device is stationary and has very coarse resolution (Corwin, 2003; Corwin and Scudiero, 2019).

Electromagnetic induction is well suited for field scale measurements because it can be used efficiently over a large area (Corwin, 2003; Corwin and Scudiero, 2019); however, unlike other field scale devices, electromagnetic induction methods do not require the instrument to be in direct contact with the soil. Electromagnetic induction is done using a transmitter coil to induce eddy-current loops in the soil near the instrument (Corwin, 2003; Corwin and Scudiero, 2019). The eddy-current creates a secondary electromagnetic field which is proportional to the current flowing within that loop (Corwin, 2003; Corwin and Scudiero, 2019). A receiver coil on the opposite end of the instrument intercepts part of the induced electromagnetic field and sums the signals to produce an output voltage related to the soil EC_a (Corwin, 2003; Corwin and Scudiero, 2019). Soil properties will affect the amplitude and phase of the secondary field, so these factors are still relevant in the calibration of EC_a to EC_e (Corwin, 2003; Corwin and Scudiero, 2019). Common devices used for electromagnetic induction can take readings over the top 1.5 m of the soil profile which is beneficial in agricultural settings as it corresponds to the root zone of many plants (Corwin, 2003; Corwin and Scudiero, 2019). Because it is a noninvasive method of determining EC_a, it can be used in dry, frozen, or stoney soil where other methods like electrical resistivity would be inaccurate (Corwin, 2003). However, electromagnetic induction instruments are often expensive ($5,000-$10,000) and renting a device costs around $95 per day which may make monitoring salinity with these devices impractical for large fields or regional scale mapping (Environmental Equipment and Supply, 2025). An additional challenge of electromagnetic induction equipment is the labor required. Commonly, the device is walked or pulled in transects through a field to measure EC_a. Also, soil samples must be gathered and analyzed for calibration of the device's EC_a readings to EC_e. This often requires a full day of work to collect data for just part of a field. This method does, however, establish field level variability which can be used in conjunction with emerging remote sensing methods to calibrate an EC_e map over large areas.

1.8 Remote Sensing

While the historical methods of monitoring EC have been used for at least the last 20 years, one method of EC estimation that is relatively new is remote sensing. Remote sensing is the collection of data from the electromagnetic spectrum and includes data collected from eyesight, photography, airplanes, satellites, and other instruments (Khorram et al., 2016); however, generally the term is used to refer to geospatial data collected using ground-level, airborne, or satellite-based sensors. The electromagnetic spectrum describes the energy produced by vibration of charged particles as they move through space (National Aeronautics and Space Administration, 2021a). These particles move in waves with shorter wavelengths indicating higher energy in the particle (National Aeronautics and Space Administration, 2021a). Remote sensing instruments are a way to gather information not only about the particles themselves but also from other objects based on how these particles and the objects interact.

Two types of remote sensing instruments exist, active and passive (Figure 1.6). Active instruments provide a source of energy which can be collected and analyzed when it rebounds off objects of interest (National Aeronautics and Space Administration, 2021a). Most active instruments operate in the longer, lower energy parts of the electromagnetic spectrum like radiowaves or microwaves and have been used to detect things like forest structure, precipitation, and topography (National Aeronautics and Space Administration, 2021a). Passive remote sensing

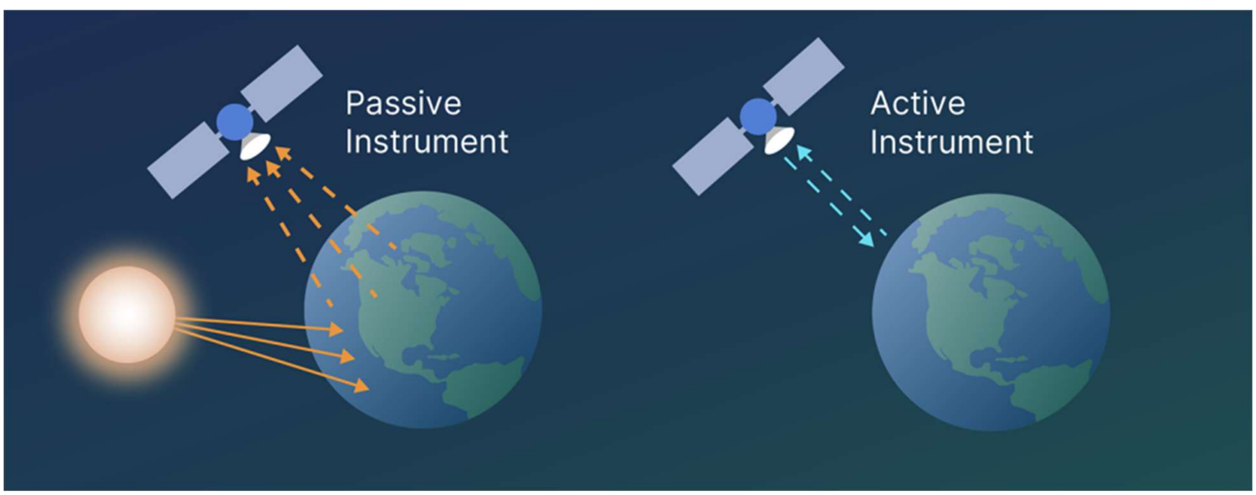

Figure 1.6 Passive and active remote sensing can be used to collect information about objects on earth (National Aeronautics and Space Administration, 2021a). Passive instruments use the sun as an energy source and detect reflected energy while active instruments send out energy and measure the reflected energy. This study uses data collected through passive instruments.

instruments, like those utilized in this study, use the sun as an energy source and detect reflected electromagnetic radiation, most commonly in the visible, near-infrared (NIR), and shortwave infrared portions of the spectrum (National Aeronautics and Space Administration, 2021a). Features of an object can be identified based on the parts of the electromagnetic spectrum they absorb and reflect. For example, visible light is a part of the electromagnetic spectrum and the part of the visible spectrum that an object reflects is the color we see. Reflectance profiles, or reflectance curves, are created to show the areas of the electromagnetic spectrum that an object reflects (Kumar, 2013). These profiles can be used to identify land covers and monitor health in plants (Figure 1.7). Healthy vegetation strongly absorbs red light (around 0.65 μm) for photosynthesis and reflects a lot of near-infrared light (around 0.8–1.3 μm). Soil shows a more gradual increase in reflectance with wavelength and does not exhibit that same red-NIR contrast that can be seen in healthy vegetation. Water generally absorbs all parts of the electromagnetic spectrum.

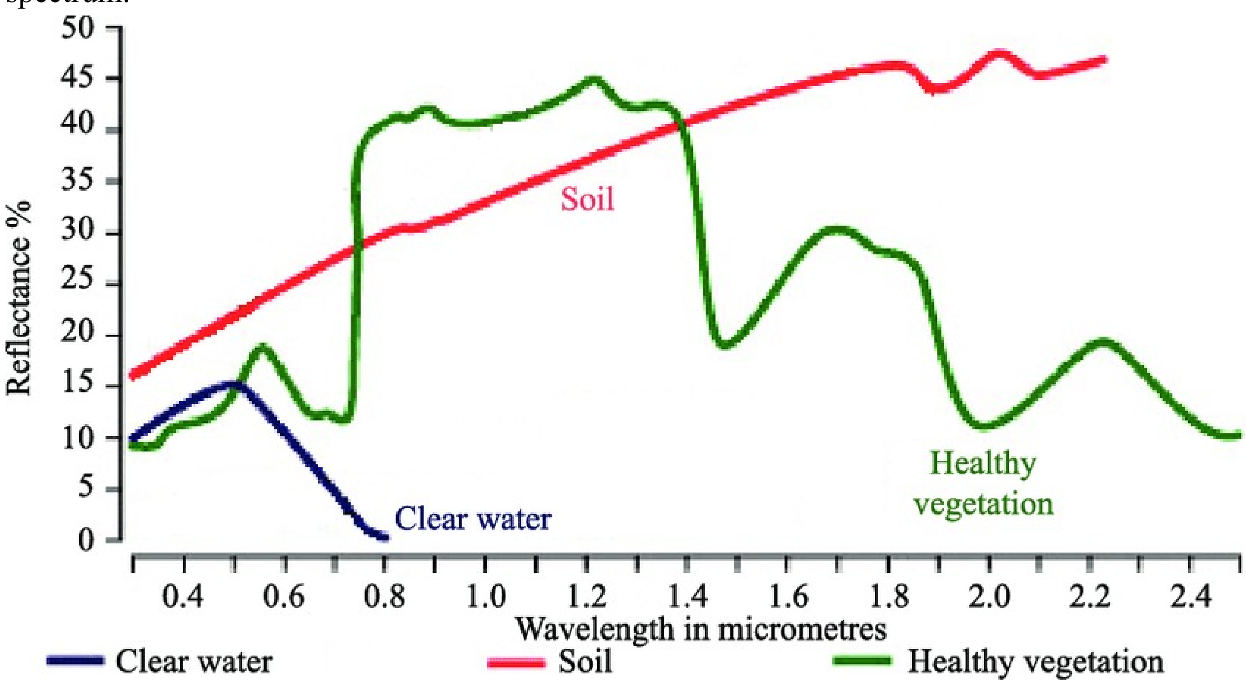

Figure 1.7 The electromagnetic energy reflected from different types of land covers can be used for idetification and monitoring of land cover (Kumar, 2013). Vegetation health in particular can be monitored based on the vegetation's reflectance profile.

1.9 Remote Sensing Approaches to Monitoring Soil Salinity

Surface reflectance profiles provide a basis for reflectance indexes which can be used to monitor changes in land cover – specifically with regards to vegetation. Reflectance indexes can be used to monitor vegetation health, and vegetation health typically declines with increasing soil salinity. For that reason, multiple studies have used vegetation indexes to predict soil salinity levels (Shrestha, 2006; Douaoui et al., 2006; Bouaziz et al., 2011; Scudiero et al., 2014; Scudiero et al., 2015; Scudiero et al., 2016; Peng et al., 2019; Ramos et al., 2020; Craig, 2023; Sehbenu et al., 2023; Cui et al., 2023; Bandak et al., 2024; Wang et al., 2024). This approach is especially useful since salinity usually cannot be identified by visual inspection of an image alone due to vegetation cover (Metternicht and Zinck, 2003). Even when bare soil is present, salinity can appear in multiple different forms from white crusts to black deposits or it can be mixed in with the soil and invisible to the naked eye (Shrestha, 2006). As a result, most salinity studies utilize reflectance driven vegetation indexes to serve as proxies for underlying soil conditions.

Early studies demonstrated that spectral indexes can provide meaningful estimates of soil salinity. Douaoui et al. (2006) used multispectral data from the SPOT2 satellite in the Lower Chéliff Plain in Algeria. The study correlated many spectral indexes and vegetation indexes [normalized differential vegetation index (NDVI), difference vegetation index (DVI), weighted difference vegetation index (WDVI), perpendicular vegetation index (PVI), and transformed soil-adapted vegetation index (TSAVI)] to measured soil EC_e and found that within the context of their study area, vegetation indexes were poor predictors for soil salinity for most of the area likely due to sparse vegetation (Douaoui et al., 2006). Another early study (Shrestha, 2006) used multiple linear regression to link vegetation indexes [NDVI and normalized differential salinity index (NDSI)] calculated from LandSat imagery to measured soil EC_e in northeast Thailand and showed similar results to Douaoui et al. (2006). When utilized in densely vegetated areas like crop lands, vegetation indexes were effective in detecting soil salinity, but their effectiveness declined in sparsely vegetated areas (Shrestha, 2006). Bouaziz et al. (2011) extended this work to northeast Brazil using MODIS imagery to compare spectral indexes and vegetation indexes [soil adjusted vegetation index (SAVI), enhanced vegetation index (EVI), and NDVI] to soil EC_e. The study found that combining vegetation indexes like NDVI with salinity specific indexes like soil index 1 (SI1) could improve the detection of soil EC_e, demonstrating vegetation indexes alone are often not enough to reliably estimate soil EC_e.

Scudiero et al. (2014, 2015, 2016) further developed remote sensing methods to monitor soil EC_e by using LandSat data to estimate soil EC_e in the San Joaquin Valley in California. In their 2014 study, Scudiero et al. use vegetation indexes [NDVI, EVI, green atmospherically resistant vegetation index (GARI), and canopy response to salinity index (CRSI)] along with weather data to estimate soil EC_e and found multiyear reflectance indexes, when combined with weather data, were able to produce promising equations for measuring soil EC_e, further emphasizing that spectral indexes alone likely cannot produce reliable EC_e models. Their 2015 and 2016 papers focus on CRSI models for estimating soil EC_e as they were the most promising of the tested vegetation indexes. In Scudiero et al. (2015), a strong correlation between the multiyear maximum CRSI value and root zone salinity is demonstrated, especially when remote sensing data are combined with weather data. Their 2016 paper compared the maps produced by remote sensing data to those produced by near-ground EC_e measurements and found that especially at low salinity levels remote sensing models have lower accuracy and emphasized that remote sensing methods are good for classifying broad categories of salinity but should not be used for site specific crop management. These studies present the possibility of developing a highly accurate model for estimating soil EC_e but also find that current model accuracy is insufficient for agricultural management decisions, highlighting both the potential and limitations of reflectance-based EC_e estimation. Their work also demonstrates again that spectral indexes alone do not provide sufficient data for estimating EC_e and other factors like weather data must be considered.

More recent studies have increasingly utilized multisource datasets, advanced sensors, and machine learning techniques. Peng et al. (2019) used LandSat imagery to calculate spectral indexes [NDVI, EVI, generalized difference vegetation index (GDVI), non-linear vegetation index (NLI), GARI, CRSI, and SAVI] and correlate those indexes along with terrain variables to measured soil EC_e in the Xinjiang Province of China using a machine learning algorithm. The results showed that vegetation indexes like NDVI and SAVI could produce accurate models when combined with elevation and topographic information, once again demonstrating that vegetation indexes can be used for soil EC_e models but that other information like elevation and topography can improve model accuracy (Peng et al., 2019). The work of Ramos et al. (2020) closely resembles Scudiero et al. (2014) as their study used Sentinel-2 multispectral data in Portugal to test the correlation between vegetation indexes [CRSI, EVI, GARI, GDVI, NDSI, NDVI, NDI, and three-band index (TBI)] and soil EC_e. Like Scudiero et al. (2014, 2015), Ramos et al. (2020) used multiyear maximum index values. In addition to vegetation indexes, Ramos et al. (2020) used other explanatory variables like vegetation cover and soil type. They discovered that the most accurate equations utilized CRSI or GARI in addition to the other independent variables; however, regional-scale implementation of the models was not satisfactory. This suggests that vegetation index-based EC_e models may be able to capture some salinity patterns well, but models may not be transferable over larger areas and local calibration is essential.

Craig (2023) utilized vegetation indexes [NDVI and CRSI] from LandSat multispectral imagery in combination with crop water stress index (CWSI) to predict soil EC_e in the Arkansas River Basin of south-eastern Colorado. Using a multiple linear regression approach, Craig (2023) employed vegetation indexes as well as crop growth phases in the models. He found that vegetation indexes alone could not produce a reliable equation and that incorporating water stress information helped reduce over estimation errors, further emphasizing that vegetation indexes while useful indicators of plant health are insufficient for estimating soil EC_e alone. Stress related metrics like CWSI can provide a more nuanced equation that improves model accuracy.

Bandak et al. (2024) used LandSat and Sentinel 2 imagery for vegetation indexes [NDSI, vegetation soil salinity index (VSSI), SAVI, NDVI, EVI, GDVI, normalized difference water index (NDWI), modified normal difference water index (MNDWI), extended NDVI, extended EVI, CRSI, two-band EVI, and normalized difference infrared index (NDII)] as well as weather and elevation data to find a model for soil EC_e in northern Iran using machine learning. Similar to Peng et al. (2019) and Craig (2023), this study found that vegetation indexes when combined with water stress metrics and elevation information can produce accurate soil EC_e models, underscoring the need for other independent variables to be used with vegetation indexes as opposed to using vegetation indexes alone. Wang et al. (2024) built on the body of research using remote sensing data to estimate soil salinity on a local or regional scale by attempting to estimate soil salinity on a global scale. Using Sentinel 1 and 2 imagery for spectral indexes and vegetation indexes [ratio vegetation index (RVI), enhanced NDVI (ENDVI), infrared percentage vegetation index (IPVI), GDVI, NLI, GARI, NDVI, DVI, EVI, SAVI, optimized SAVI (OSAVI), and global vegetation moisture index (GVMI)] as well as other independent variables like climate/weather data, soil material, groundwater table, and topographic information, machine learning was used to create soil EC_e models based on geographic region. The study identified vegetation health indicators, like NDVI, as significant predictors for soil EC_e and found that, when used in combination with localized data like climate and terrain, relatively accurate salinity models could be created spanning large areas. While regional scale variability could be estimated from these models, it is not nuanced enough for field level management decisions.

Overall, vegetation indexes can contribute to meaningful soil EC_e estimation models but are unable to produce accurate models when used as the sole type of explanatory variables. EC_e estimation models are often non-transferable, and thus local calibration is usually needed. Additionally, models are often not scalable, when calibrated on a small scale of a few fields, regional results suffer. Similarly, when calibrated on a large regional scale, local field-level results suffer.

1.10 Remote Sensing Based Vegetation Indexes

Vegetation indexes previously utilized to estimate salinity include the NDVI (Douaoui et al., 2006; Shrestha, 2006; Bouaziz et al., 2011; Scudiero et al., 2014; Peng et al., 2019; Ramos et al., 2020; Craig, 2023; Bandak et al., 2024; Wang et al., 2024), CRSI (Scudiero et al., 2015; Scudiero et al., 2016; Peng et al., 2019; Ramos et al., 2020; Craig, 2023; Bandak et al., 2024), and CWSI (Craig, 2023).

The estimation of NDVI is as follows:

$$NDVI = \frac{NIR - R}{NIR + R} \tag{1}$$

Using NDVI, healthy vegetation is easily identifiable since the NIR value should be much higher than the R value resulting in an NDVI value near 0.9. This is because healthy vegetation has an abundance of chlorophyll which absorbs red wavelengths while NIR wavelengths which are not used in photosynthesis are reflected (Campbell and Wynne, 2011). Because salinity is detrimental to plant health, NDVI negatively correlates with salinity levels. However, the usefulness of NDVI for estimating soil salinity is debated as some studies found NDVI showed weak or no correlation with EC_e (Shrestha, 2006; Douaoui et al., 2006) while others found it useful for estimating EC_e only in areas with moderate to dense vegetation cover (Scudiero et al., 2014; Peng et al., 2019; Craig, 2023).

CRSI was created to monitor the effects of salts on plant health, and utilizes the visible bands (R, G, and B) as well as the NIR (Scudiero et al., 2014). Like NDVI, CRSI is larger when plants are healthier with high NIR:

$$CRSI = \sqrt{\frac{(NIR \times R) - (G \times B)}{(NIR \times R) + (G \times B)}} \quad (2)$$

Based on work completed by Scudiero et al. (2014, 2015, 2016) in the San Joaquin Valley, CRSI is a promising index for estimating soil salinity, with a value of 1 indicating healthy vegetation and 0 indicating stressed vegetation. While the NIR and green bands are reflected by healthy plants, the reflectance of NIR is much higher than that of the green band (Campbell and Wynne, 2011). Red and blue bands both tend to be absorbed by chlorophyll in healthy plants (Campbell and Wynne, 2011). Generally, as a plant faces more stress, its' reflectance in the red and blue bands increases (Campbell and Wynne, 2011). The product of the NIR and red bands is usually moderate regardless of plant health while the product of the green and blue bands is heavily affected by plant health. When a plant is more stressed, blue light is reflected more while the green band reflectance usually does not substantially change, resulting in a higher product which causes a decrease in CRSI. Using CRSI alongside weather data resulted in equations predicting EC_e with a coefficient of determination (R^2) of approximately 0.7 across both cropped and fallow fields, with ground-truth EC_e values ranging from 0 to 35.2 dS/m, demonstrating strong correlation between this index and EC_e for a large range of soil salinity values (Scudiero et al., 2015). Craig (2023) also demonstrated the value of CRSI in a nonlinear method for estimating EC_e, resulting in a root mean square error (RMSE) of only 0.84 dS/m for corn fields with an observed EC_e ranging from 0 to 14 dS/m.

CWSI relates the actual ET (ET_a) rate of a plant to the expected crop ET (ET_c) rate under non-stress conditions. This is the only index which is not always calculated using reflectance values. Lower values of CWSI, close to 0, indicate ET is occurring at its maximum possible (expected) rate and that the plant has enough water in the soil, while higher values, closer to 1, indicate there is no ET occurring, meaning the plant does not have sufficient water. It is estimated as:

$$CWSI = 1 - \frac{ET_a}{ET_c} \tag{3}$$

ET_c values (mm/d) are generally found using nearby agricultural weather station data where ET_c is calculated using values from a reference ET (alfalfa or clipped grass) multiplied by a crop coefficient K_c, while ET_a (mm/d) is calculated using a water balance or it is found through remote sensing estimates (Gowda et al., 2008). Trout and DeJonge (2018) presented a method for estimating ET_a from remotely sensed data by estimating the crop coefficient K_c based on surface reflectance. Since ET_a is estimated as:

$$ET_a = K_c \times ET_O \tag{4}$$

CWSI can also be estimated as:

$$CWSI = 1 - \frac{K_{c,calc}}{K_c} \tag{5}$$

Where $K_{c,\ calc}$ is the crop coefficient based on surface reflectance data acquired by remote sensing platforms, and K_c is the tabulated crop coefficient from the literature or reported by a local agricultural weather station network.

To get $K_{c,\ calc}$, Trout and Johnson (2007) and Trout (2008) use the fraction of canopy coverage (or fractional vegetation index) estimated as a function of NDVI (Equation 6):

$$f_c = 1.22 \times NDVI - 0.21 \tag{6}$$

Then, in Trout and DeJonge (2018), the fractional coverage is related to the crop coefficient by:

$$K_{c,calc} = 1.10 \times f_c + 0.17 \tag{7}$$

This method estimated crop coefficients using grass-reference ET (ET_o) and was developed for use on corn fields, which limits its' effectiveness across large heterogeneous areas like the SPRB. Trout and Johnson (2007) and Trout and DeJonge (2018) focus primarily on demonstrating that f_c and K_c can be estimated from remote sensing data and provide limited statistical analysis of the equations. From figures in Trout and Johnson (2007), the correlation between NDVI and f_c is highly linear with a R^2 of 0.95. Similarly, the correlation between the calculated K_c and f_c is linear with a R^2 of 0.99 across three different crops. Trout and DeJong (2018) applied the same method for estimating f_c from NDVI and presented a comparison of the calculated K_c from the Trout and Johnson (2007) method with K_c calculated from a water balance which is a widely accepted method. Based on the comparison, it appears K_c calculated from the reflectance index largely agrees with K_c calculated using a water balance method, supporting the validity of a remote sensing-based K_c.

Other studies from around the world have used similar methodologies to estimate f_c and K_c from NDVI with high levels of accuracy (e.g., Barker et al., 2018; Idrisa et al., 2022). However, these studies typically use localized coefficients which differ from the coefficients estimated by Trout and Johnson (2008) and used in Trout and DeJonge (2018). The equation developed in Trout and Johnson (2008) was calibrated with data from the San Joaquin Valley in California and later successfully applied to data from the Great Plains in Trout and Dejong (2018) with high levels of accuracy, indicating the model may be broadly transferable across regions and crops.

This work highlights the principle that vegetation indexes can serve as proxies for crop conditions.

CRSI and NDVI are similar in calculation and range from 0 to 1 with 1 indicating a healthy plant and 0 indicating stress, so it would be expected to see a positive correlation between these indexes. CWSI, on the other hand, is partially calculated based on NDVI and ranges from 0 to 1 with 0 indicating healthy plants and 1 indicating stress, so a negative correlation between CWSI and the other two indexes would be expected.

1.11 Benefits of Remotely Sensed Data

Remotely sensed data offers the opportunity for monitoring soil properties at more frequent intervals than traditional methods. The Natural Resources Conservation Service (2022) recommends agricultural soil testing (quantifying soil pH and health information – including salinity and nutrient levels) every 3 to 5 years as changes in soil health are often slow. Developing a remote sensing-based equation which produces yearly or more frequent estimates for soil EC_e would significantly improve monitoring capabilities compared to soil testing every 3-5 years, allowing for early detection of salinity trends, more responsive management decisions, and better long-term soil health outcomes across agricultural landscapes. Not only can current satellite constellations be used to map near-real time data, but older data can provide important historical information.

1.12 Study Objectives and Hypothesis

Stakeholders in Colorado's SPRB want to understand and address agricultural and environmental concerns relating to salinity in the basin, especially in the downstream regions where salinity in the soil and water have been found at levels that both reduce crop yields and limit the types of crops which can be grown (NEIRBO Hydrogeology, 2020). Soil salinity mapping using remote sensing data provides a method to address these concerns by identifying priority areas for improved land and water management practices to mitigate salt build up in the soil profile.

Soil salinity mapping models using remote sensing data exist for many regions including the San Joaquin Valley (Scudiero et al. 2014, 2015, 2016), the Arkansas River Basin (Craig, 2023), Southern Xinjiang Province in China (Peng, et al., 2019), Portugal (Ramos et al., 2020), Northern Iran (Bandak et al., 2024), Northeast Brazil (Bouaziz et al., 2011), the Lower Chéliff Plain in Algeria (Douaoui et al., 2006), and Northeast Thailand (Shrestha, 2005). There have also been global-scale mapping attempts (Wang et al., 2024). Many of these models have never been tested outside of their area of study and/or the climate they were developed in; hence it is unknown if these models are transferable to other regions and climates. Identifying transferable models allows for EC_e to be mapped in areas with remote sensing data but with little to no ground-truth data which allows farmers, water managers, and researchers in those areas to focus their attention and make better decisions about salinity management and mitigation.

Specific objectives for this study include:

1) evaluating the accuracy of selected remote sensing-based EC_e models relative to ground truth data when used to predict EC_e in Colorado's SPRB; and
2) calibrating selected EC_e models and/or developing new EC_e models for use in the SPRB.

It is hypothesized that established remote sensing-based soil salinity models can be successfully transferred to other regions such as the SPRB when the models are used with local data, and that transferability will require minimal adjustments, such as coefficient recalibration or aligning variables with the local growing season.

CHAPTER 2: METHODS

2.1 Methodology Overview

This study utilized field surveys, groundwater monitoring, remote sensing, and weather data to evaluate soil salinity across the SPRB. Twelve fields across 3 of the 7 regions in the SPRB were used for electromagnetic induction surveys with an EM-38-MK2 system (Geonics Limited, Mississauga, Ontario, Canada). At these fields, soil samples were taken for calibration of each survey and monitoring wells were installed or adopted to collect groundwater quality samples and for continuous measurement of water table level and EC with HOBO sensors (HOBO U24-001 Conductivity Logger and either HOBO U20L-01 or HOBO U20L-04 Water Level Logger, ONSET, Bourne, MA, United States). Multi-year LandSat imagery (2000-2023) and high resolution PlanetScope imagery (2020-2024) were processed to obtain vegetation indexes (NDVI, CRSI, and CWSI) which were used for tracking crop response to salinity. Weather data from 33 agricultural weather stations were incorporated to represent local climate variability. These datasets were integrated into established soil salinity estimation models (Scudiero et al., 2015; Craig, 2023) to produce maps of soil salinity. This methodology was designed to evaluate the transferability of existing remote sensing-based EC_e models from the San Joaquin River Basin (Scudiero et al., 2015) and the Arkansas River Basin (Craig, 2023) to the South Platte River Basin with minimal local calibration, as hypothesized. To clarify the structure of this study, the major methodological steps are summarized in Figure 2.1.

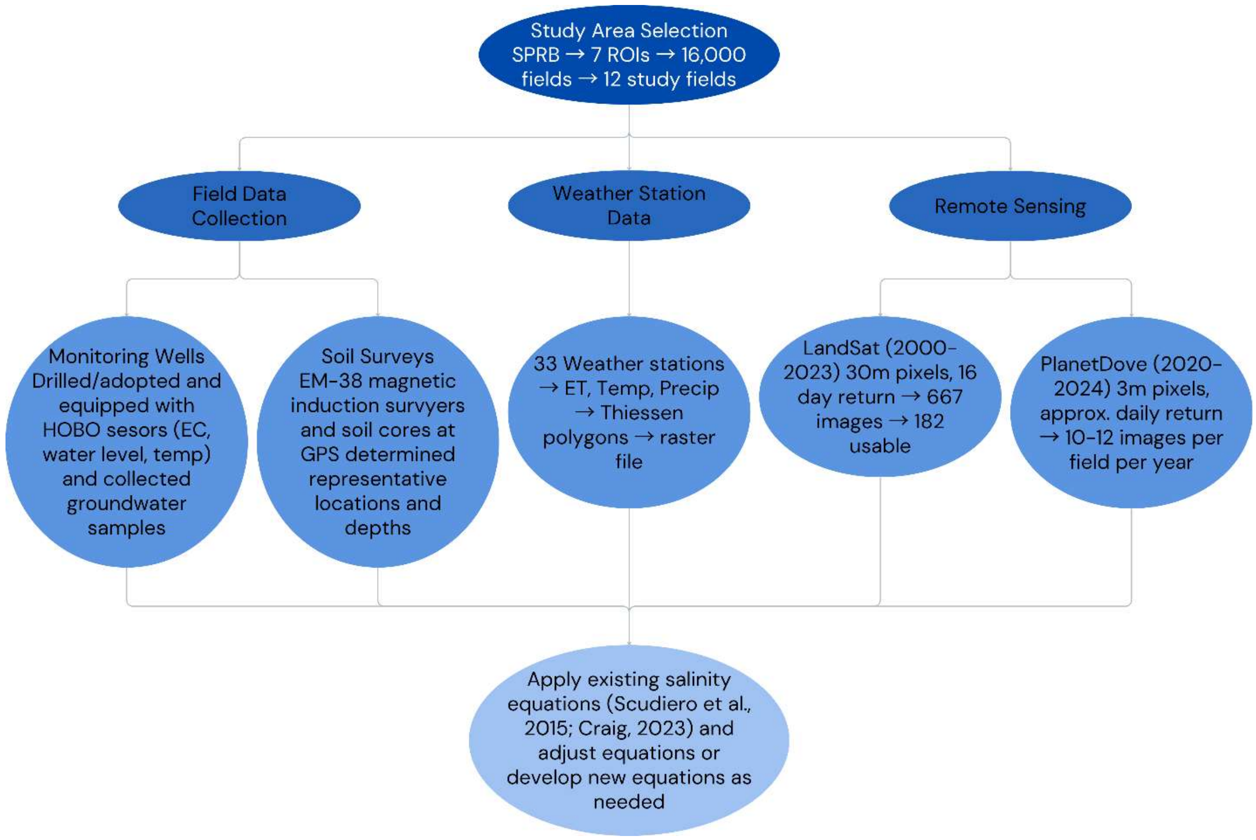

Figure 2.1 Flow chart representation of methodology showing what data was collected and how it was used. Graphic created in Canva.

2.2 Location of Study

Within the SPRB, 7 regions of interest were identified covering most of the irrigated agricultural areas in northeastern Colorado. The regions were identified based on their relationship to the South Platte River (tributary to the South Platte River or following along the South Platte River) and general soil or bedrock type (Figure 2.2) (Colorado Water Center, 2025). Within the overall study area there are approximately 16,000 irrigated fields.

Fields within each region were randomly selected for surveys of soil EC_a. A list of potentially interested farmers of these randomly selected fields or nearby fields was obtained from the Natural Resources Conservation Service and farmers were contacted. If permission was granted

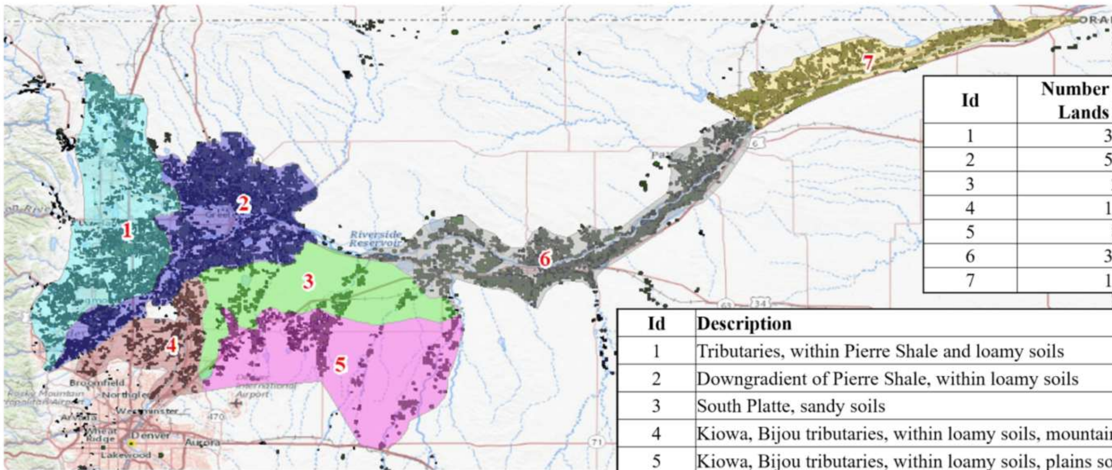

Id	Number of Irrigated Lands in Region
1	3,736
2	5,355
3	252
4	1,003
5	853
6	3,048
7	1,583

Id	Description
1	Tributaries, within Pierre Shale and loamy soils
2	Downgradient of Pierre Shale, within loamy soils
3	South Platte, sandy soils
4	Kiowa, Bijou tributaries, within loamy soils, mountain source
5	Kiowa, Bijou tributaries, within loamy soils, plains source
6	South Platte, bedrock source is Cretaceous (marine)
7	South Platte, bedrock source is Tertiary (terrestrial)

Figure 2.2 The study area of the South Platte River Basin was divided into 7 regions based on geographical location and soil type. Map retrieved from Colorado Water Center (2025).

for the use of their field in this study, a monitoring well was drilled or, when possible, adopted from the nearest Colorado Department of Water Resources' groundwater quality monitoring wells. From this process, 12 fields were identified in 2024. At each field, EC_a soil surveys were conducted along with soil sampling for EC_a-to-EC_e calibration, continuous sensor reading of water table depth and EC_e in the wells, and low flow water sampling from the wells. The fields, located in regions 2, 6, and 7, were planted with different crops including onions, alfalfa, cabbage, corn, soybeans, grass, and hay, and utilized drip, sprinkler, and flood irrigation methods (Table 2.1/Figure 2.3).

Table 2.1 Summary of field names, crop types, and irrigation methods for fields used in this study.

Field Identifier	Crop	Irrigation Method
R2-1	Onion	Drip
R2-2	Alfalfa	Sprinkler
R2-3	Cabbage	Drip
R6-2	Corn	Sprinkler
R6-3	Corn	Sprinkler
R6-4	Alfalfa	Sprinkler
R6-5B	Corn	Flood

R7-1	Soybean	Sprinkler
R7-2	Grass	Flood
R7-4	Hay	Flood
R7-5	Alfalfa	Sprinkler
R7-6	Alfalfa	Sprinkler

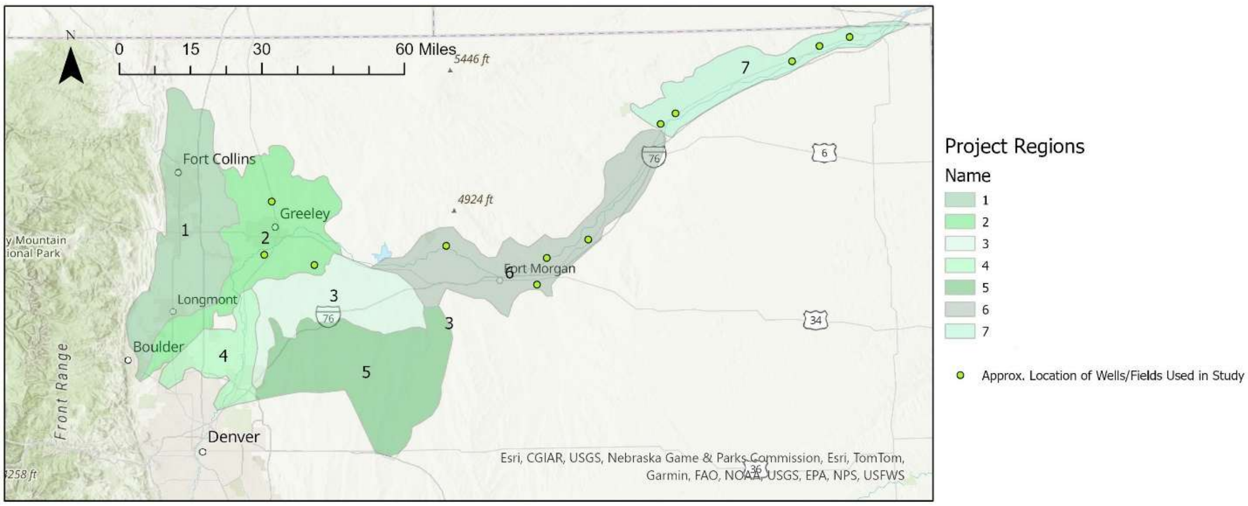

Figure 2.3. Study area regions with approximate locations for the monitoring wells and surveyed fields used in this study. Map created in ArcGIS Pro.

2.3 Data Collection

2.3.1 Soil Salinity Survey

Soil salinity surveys were conducted on each of the 12 fields using an electromagnetic induction instrument: the EM-38-MK2 system (Geonics Limited, Mississauga, Ontario, Canada). Surveys were conducted between June 2024-September 2024, covering at least 23 ha (57 acres) with the average survey area being 57 ha (140 acres). Corwin and Scudiero (2020) outline procedures for conducting soil salinity surveys which were followed for each field. Key points of the initiation of the survey procedure included the recording of date and time of the survey, notation of vegetation grown in the field, and estimation of water content prior to the survey by digging a small hole and checking soil water status by hand (feel and touch method). Often surveys were conducted a few days after irrigation to ensure soil water content was near field capacity but not saturated. Flags were used to mark transects which were walked with the EM-

38-MK2 to collect EC_a data. Since the survey was conducted on foot, metal was not worn by surveyors to avoid error (Geonics Limited, 2016).

For the first field surveys, the initial sampling rate on the EM-38-MK2 was set at 5 hz – 5 samples per second, but this was deemed too high once data were processed, thus the sample rate was lowered to 1 hz – roughly 1 sample per second for the remaining surveys. A Dell rugged tablet field computer with an integrated global positioning system (GPS) was used to collect location (coordinate) information for each point of data collected during the survey. According to its' technical specifications, this system is accurate to a 2-meter radius or about 15 ft (Latitude 7230 Rugged Extreme Tablet, Dell US, Round Rock, TX, United States).

On the same day as the survey, the EC_a data collected was input into the Electromagnetic Sampling and Prediction (ESAP V. 2.35) software which selected 6-12 locations for soil samples to be collected for laboratory analysis. Using this software, sampling locations are strategically selected to characterize the variation in the field based on statistical analysis of the field variability (Brown, 2023). The location for soil samples were then located using the marked transects and GPS data.

Samples taken from the ESAP determined locations were used for calibration of the measured EC_a to EC_e. At each sampling location, soil samples were taken using an auger at a minimum of 5 depths: 0 (just below ground surface), 30, 60, 90, and 120 cm. After the completion of three surveys, samples at a depth of 150 cm and temperature readings for each depth were added to the process to ensure accurate calibration of the EM-38-MK2 based EC_a data. Two soil samples were taken at each depth at each location specified by ESAP – one sample for lab analysis of soil salt contents and the second sample for determination of soil water content. Errors may be present in the surveys due to changing field surveyors as well as the accuracy of the GPS devices used during the survey to identify locations for sample collection.

2.3.2 Water Sampling and Monitoring Wells

Groundwater monitoring wells were also utilized to provide information on the quality of groundwater near the fields surveyed. Unless there was an existing well from Colorado's Department of Water Resources, all monitoring wells for the fields surveyed were drilled using a Giddings rig with a screw-type auger bit. Wells were drilled until groundwater was reached or as deep as possible with depths ranging from 12 ft to 38 ft – some wells never hit water. Once drilled, a 5.08 cm (2 inch) PVC pipe was used as casing with a screen at the bottom to allow water flow. Field procedures for drilling monitoring wells can be found in Appendix A.

Each well was equipped with two HOBO sensors: a HOBO U24-001 Conductivity Logger for recording actual conductivity (µS/cm), temperature (°C), and calculated specific conductance at 25 °C (µS/cm) (HOBO U24-001, ONSET, Bourne, MA, United States) and either a HOBO U20L-01 or a HOBO U20L-04 Water Level Logger for recording water pressure (kPa) and temperature (°C) (HOBO U20L-01, ONSET, Bourne, MA, United States; HOBO U20L-04, ONSET, Bourne, MA, United States). Loggers were set to record one datapoint every hour. Data were downloaded from the loggers every 2-3 months. Water depth and specific conductance data were graphed as time series to identify groundwater trends.

In addition to collecting the data from the HOBO sensors, at the time of soil surveys water samples were taken from the well for laboratory analysis and for verification and calibration of the data acquired with the HOBO sensors. The water sampling from the monitoring wells followed the Environmental Protection Agency's standard procedure for collecting groundwater for site characterization (United States Environmental Protection Agency, 2015). A concise summary of field procedures for collecting groundwater samples can be found in Appendix A. Prior to ground water sampling, 3-6 well volumes were purged, and the water from the well was allowed to stabilize. An Aqua TROLL 500 Multiparameter Sonde (In-Situ, Fort Collins, CO, United States) was used for identifying when the quality of the pumped water stabilized based on three parameters: pH remains at +/- 0.1, temperature remains at +/- 0.5°C, and specific conductance remains at +/- 3% µS/cm. These conditions had to be met for 3 consecutive cycles of 3 minutes before the water sample was taken. Once it was determined that the well had stabilized, the water was discharged into a bottle for laboratory analysis.

Bottles were filled slowly to minimize aeration and put on ice after collection to avoid changes in composition. Samples were shipped to WARD Labs as soon as possible after collection for analysis. The standard water analysis was completed on samples and included pH, sodium adsorption ratio, adjusted sodium adsorption ratio, EC, major cation and anion concentration (sodium, potassium, calcium, magnesium, nitrate, sulfate, chloride, bicarbonate, carbonate, boron), hardness as calcium carbonate, and alkalinity as calcium carbonate.

2.3.3 Remote Sensing

Because no remotely-sensed data are complete and there are tradeoffs with each level of remote sensing, both the United States Geological Survey's LandSat Constellation and Planet Labs' PlanetDove Constellation were used in this study. The differences between these two constellations come in terms of temporal, spectral, and spatial resolution.

Temporal resolution is how often an image of the same location on the earth surface is taken (National Aeronautics and Space Administration, 2021a; O'Connell, 2024). The more often data are collected over an area, the more likely it is that at least some of the data will be usable. Since data usually cannot be collected when it is cloudy, a higher satellite return frequency provides more possibly usable images of the area of study (National Aeronautics and Space Administration, 2021a; O'Connell, 2024). The LandSat Constellation has a return frequency of 16 days which means each point on earth is photographed every 16 days (United States Geological Survey, 2025) while the PlanetDove constellation has a return frequency of 30.3 hours which means every point on earth is being photographed on a near daily basis (Roy et al., 2021). Additionally, the length of operation of the sensor describes the temporal coverage of the system. The original LandSat satellite was launched in 1972 with additional and/or updated satellites being launched every few years since (National Aeronautics and Space Administration, 2021b). The LandSat constellation has effectively been collecting data for about 50 years which can be used in research today. In contrast, the Planet Labs' PlanetDove Constellation has not existed for as long as the LandSat Constellation only achieving the near daily return frequency with their satellite constellation in 2017 (Planet Team, 2025b). Together, the two constellations provide historical and near real time data which can be used to track historical and near real time changes in soil salinity. The differences in temporal resolution and coverage make the LandSat Constellation more beneficial for long term studies while the PlanetDove Constellation provides appropriate data for short term studies and near real-time studies.

Spectral resolution describes what reflected or emitted data from a given surface (the target) are collected over the electromagnetic spectrum (the bandwidths). The electromagnetic spectrum describes wavelengths of energy such as ultraviolet, visible light, infrared, and radio (National Aeronautics and Space Administration, 2021a; O'Connell, 2024). Bands – areas along the electromagnetic spectrum where data are collected – have a range of wavelengths that the sensor detects and computes the average value which is then assigned to the pixel (National Aeronautics and Space Administration, 2021a; O'Connell, 2024). While narrow bands allow for the detection of specific phenomena, broader bands are usually cheaper and more readily available (Campbell and Wynne, 2011; O'Connell, 2024). The blue (B), green (G), red (R), and near infrared (NIR) bands – the bands of the electromagnetic spectrum utilized in this study – detected by these satellites are similar, but not identical. The LandSat 5, 8 and 9 bandwidths are 450-510 nm for B, 530-590 nm for G, 640-670 nm for R, and 850-880 nm for NIR (United States Geological Survey, 2024) while the PlanetDove bandwidths are 464-517 nm for B, 547-585 nm for G, 650-682 nm for R, and 846-888 nm for NIR (Planet Team, 2025b). Because of the differences in wavelengths, the images produced from different satellite constellations will be somewhat different even for data collected on the same day and location.

While the bands differ slightly between the LandSat and PlanetDove constellations, the main difference between these systems is the spatial resolution of the data they provide. Spatial resolution refers to how fine or coarse the pixel size of the image is. A satellite pixel is the smallest picture element in an image that represents a specific ground area and stores the reflectance value measured from that area; with finer spatial resolution, each pixel covers less ground area, so more pixels are needed to represent the same scene (Campbell and Wynne, 2011; National Aeronautics and Space Administration, 2021a; O'Connell, 2024). While finer pixels are advantageous for identifying specific objects, it is usually more expensive to collect data at a finer resolution (Campbell and Wynne, 2011; O'Connell, 2024). The LandSat constellation produces images with 30-meter pixels while PlanetScope images (from Planet Dove mini-satellites) produces images with 3-meter pixels (Figure 2.4). At a field level, the difference in resolution is noticeable as the LandSat image appears pixelated and grainy while the PlanetScope image is smoother.

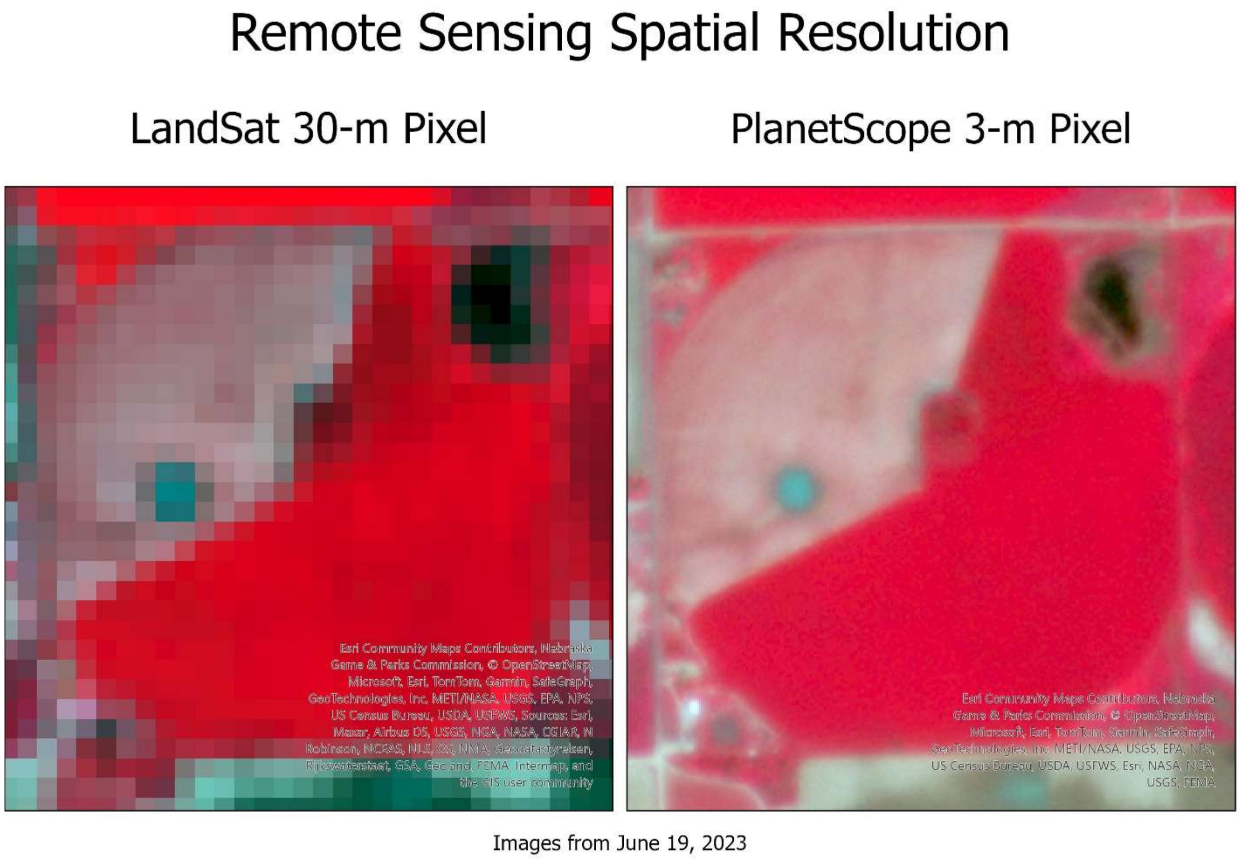

Figure 2.4. The spatial resolution of LandSat's 30-meter pixels is grainy when compared to PlanetScope's 3-meter pixels. Image created in ArcGIS Pro using satellite images retrieved from Metric-EEFlux (Allen et al., 2015) and Planet Team (2025a) for June 19, 2023. The field shown is R6-2 in this study located near Brush, CO.

The remote sensing data, collected from the LandSat satellite network, include images from LandSat satellites 5, 8, and 9 which were active for at least part of the study duration collecting data every 16 days at a 30-meter pixel resolution. The Landsat satellites gather information for B, G, R, NIR, shortwave infrared 1, thermal, and shortwave infrared 2 bands (United States Geological Survey, 2024). Images collected include true color (B, G, R), false color (NIR, R, G), NDVI, and ET_a which were retrieved from EEFlux (Allen et al., 2015).

Satellite acquired multispectral images were collected for all available dates in the March-October time frame for the years 2000-2023. The satellite image data collection period was chosen based on the typical crop growing season in the region. Two Landsat scenes or images (Path 032, Row 032 and Path 033, Row 032) were needed to cover the entire study area resulting in a total of 667 satellite images collected – 325 images covering the east side of the basin and 342 images covering the west side of the basin. The two images used to cover the entire basin were usually taken about a day apart since. For most of the data collection period, multiple satellites were functioning, resulting in a shorter return period. However, there was a section of overlap between images covering the east and west sides of the basin. Since the overlapping areas of the east and west basin images should be virtually identical since the images were taken one day apart, the overlap was removed from one of the images. Overlapping data were removed from the west basin because the east basin images captured the downstream reaches of the study area where salinity is higher. While the overlapping section should be nearly identical between east and west basin images taken only days apart, disjointed images may affect the identification of salinity trends, so removing them from the west preserved continuity in the fields near Fort Morgan, CO where the overlap occurred.

All images were processed to remove cloud cover based on NDVI values. NDVI can range from -1 to 1 but different land covers tend to fall in specific ranges (United States Department of Agriculture, 2022). Clouds reflect nearly all energy from the electromagnetic spectrum and usually have negative NDVI values (United States Department of Agriculture, 2022). In contrast, agricultural areas typically have NDVI values between ~0.1 for bare soils to ~0.9 for dense green vegetation (United States Department of Agriculture, 2022). Clouds were removed from images by identifying areas with NDVI < 0.1 and setting these areas to null in all images of the same day. Once clouds were removed from the data, some images had virtually no data of interest left due to a high amount of cloud covering almost the entire image of the basin. The removal of images lacking data over the basin was decided on an image-to-image basis as an image with a high percent cloud cover may have usable data if the clouds were not over the basin while an image with a low percent cloud cover could be rendered useless if clouds were located over the basin.

CRSI was calculated for all LandSat images for use in an initial mapping attempt. Later mapping attempts focused on dates representative of the corn growing season which is the primary agricultural output of South Platte producers (Thorvaldson and Pritchett, 2005). These attempts assumed an initial planting date of May 15 and used the growth stages identified in Table 8.3 of Allen et al. (2007) to estimate the end of the growing season: 30 days for initial growth, 40 days for development growth, 50 days for midseason growth and 50 days for late growth.

The initial growth period of the plant was ignored due to images showing mostly bare soil. After the midseason growth phase, crops were assumed to reach maturity; thus, it was assumed crops would begin to senesce thereafter, and the lack of biomass would prevent the detection of salinity through impact on crop health. Because of this, the development growth crop phase and midseason growth crop phase (June 15-September 3) would provide data with the most above ground leafy growth to connect plant health to soil health. Of the LandSat images collected, 241 were between these dates – after removing images with high cloud cover over the basin, and 182 usable images remained for the 2000-2023 period. For these images, ET_c data were collected from local agricultural weather stations and utilized. A summary of the LandSat data collected can be found in Table 2.2.

Table 2.2 Summary of LandSat data collected and used throughout the study.

	Summary of LandSat Images Collected (March-October)			Summary of LandSat Images from Corn Growing Season (June 15-September 3)		
Year	**East Basin**	**West Basin**	**# of Images**	**# of Images**	**Images with High Cloud Cover Over Basin**	**Usable Images**
2000	8	11	19	8	1	7
2001	11	14	25	10	2	7
2002	10	11	21	9	1	8
2003	13	11	24	8	2	6
2004	14	12	26	9	2	7
2005	13	15	28	10	3	7
2006	12	13	25	10	4	6
2007	13	13	26	11	0	11
2008	12	15	27	9	3	6
2009	10	13	23	8	3	5
2010	15	15	30	10	2	8
2011	13	14	27	10	4	6
2012	1	0	1	0	0	0
2013	13	12	25	11	2	9
2014	15	15	30	10	3	7
2015	13	15	28	10	2	8
2016	15	14	29	9	2	7
2017	15	15	30	10	2	8
2018	13	12	25	10	2	8
2019	13	14	27	10	4	6
2020	14	15	29	10	1	9
2021	15	13	28	10	5	5
2022	28	30	58	20	2	18
2023	26	30	56	19	6	13
Total	**325**	**342**	**667**	**241**	**58**	**182**

Because soil salinity within the surveyed fields exhibited high spatial heterogeneity, finer spatial resolution data were needed to improve the calibration of the EC_e estimation equations. For 2020-2024, 3-meter pixel images were collected throughout the growing season (June 15-September 3), approximately one image per week per field, from Planet Labs' PlanetDove satellite constellation (Planet Team, 2025a). Planet Labs operates over 200 satellites collecting global remote sensing data at a high frequency and imaging every part of the world nearly every day (Planet Team, 2021). The collected PlanetDove data included bands in R, G, B, and NIR wave lengths which were harmonized with data from the Sentinel 2 satellite constellation to ensure surface reflectance data accuracy.

Images were only compiled on days with no cloud cover to avoid the need for cloud removal and prevent errors due to shadows. This resulted in 10-12 images per field per year which could be used to calibrate the equations (Table 2.3). PlanetScope images surface reflectance values were rescaled to obtain reflectance as decimal values by dividing the downloaded data values by 10,000 following Planet Lab guidelines (Collison and Curdoglo, 2025). The obtained data were then used to calculate NDVI, CRSI, and, in conjunction with agricultural weather station data, CWSI.

Table 2.3 Summary of Planet Labs' PlanetDove data collected and used throughout the study.

Year	# of Images	Average # of Images Per Field
2020	116	10
2021	130	11
2022	117	10
2023	129	11
2024	129	11

2.3.4 Weather Data

Weather station data were gathered from Colorado Agricultural Meteorological Network (CO Ag Met) and Northern Water weather stations (Colorado Climate Center, 2018). This network consists of more than 90 research-grade agricultural weather stations throughout the state of Colorado originally designed for estimating crop ET (Colorado Climate Center, 2024). Data were gathered from 33 weather stations that were operating for at least part of the duration of this study and were in fully or partially irrigated areas near the SPRB areas of interest. Data downloaded from these weather stations included location (longitude and latitude), daily grass and alfalfa reference ET, daily alfalfa and corn actual ET estimated using a reference ET and a crop coefficient originally developed from irrigated crop lysimeter studies conducted in Kimberly, ID (Colorado Climate Center, 2025; Wright 1982), daily precipitation, and daily minimum temperature.

The weather station data were used for multiple different EC_e mapping attempts in various ways, but the process of interpolating the data from points to usable spatial data was the same. First, information was tabulated by date and weather station longitude and latitude; any missing data points were removed. Extreme data outliers (more than two standard deviations from the mean) were also removed in later mapping attempts. Tabulated data were converted to CSV format and uploaded into Arc GIS Pro. The data were treated as an X and Y point table and points were created for each weather station.

2.4 Utilizing Remote Sensing Data to Estimate EC_e

In Scudiero et al. (2014, 2015), the authors used multi-year LandSat 7 data and vegetation indexes to estimate EC_e. Based in the rich agricultural area of the San Joaquin Valley of California, their study used NDVI, EVI, salinity index (SI), GARI, and CRSI in conjunction with 542 ha of ground truth data to develop an equation to estimate EC_e (Scudiero et al., 2014). LandSat 7 data from January 2007 through December 2013 were utilized with most data (~77%) spanning spring, summer, and early fall (Scudiero et al., 2014). Ground truth data was obtained in 2013 with EM-38-MK2 surveys and utilized nonmetallic sleds; ground sampling in locations chosen by ESAP was utilized to calibrate the data (Scudiero et al., 2014).

In Scudiero et al. (2014), a variety of crop and soil types were present in the fields surveyed producing a robust data set with salinity ranges from near 0 to around 35.2 dS/m with about 50% of data indicating salinity levels less than 8 dS/m. Weather data were obtained from monitoring stations, and annual averages were computed to determine regional annual values (Scudiero et al., 2014). The field-measured EC_a was calibrated to EC_e and the cumulative coefficient of determination (R^2) was about 0.93 which indicates a high level of correlation across the region not found in other studies (Scudiero et al., 2014). Surveys were then interpolated into 30-m pixels to match the images acquired from LandSat 7 (Scudiero et al., 2014).

Even between consecutive years, there was large variation in the correlation between soil salinity and the annual average value for the bands of LandSat 7 indicating that using data from any single year may cause poor results (Scudiero et al., 2014). CRSI showed a high level of correlation with salinity when compared to other vegetation indexes, and the usage of a multi-year value further increased correlation (Scudiero et al., 2014). Although CRSI had the best correlation in their study, Scudiero et al. (2014) emphasized other vegetation indexes may perform better in other areas.

Because of its' relatively high correlation with salinity, CRSI was used to formulate an equation to estimate EC_e (Scudiero et al., 2015). Yearly average CRSI values were calculated and the multi-year maximum average CRSI was found for each pixel (Scudiero et al., 2015). The maximum average CRSI value was used to prevent factors other than salinity, which is relatively stable from year to year, from impacting vegetation reflectance and therefore EC_e estimates (Scudiero et al., 2015). Salinity estimation equations were developed using only CRSI as well as CRSI in combination with other variables like percent silt, annual rainfall, annual average minimum temperature, and landcover characteristics – cropped or fallow (Scudiero et al., 2015).

The most accurate EC_e (dS/m) equation, with a R^2 of 0.73, utilized a coefficient to describe the field (cropped or fallow), CRSI, annual precipitation, and annual average minimum temperature (Scudiero et al., 2015). The most accurate model developed by Scudiero et al. (2015) for estimating EC_e is shown in Equation 8 below.

$$EC_e = 26.3 + \beta_{Crop} \times CRSI + 0.025 \times Rain\ (mm) + 3.35 \times Temperature\ (°C) \tag{8}$$

Where EC_e is measured in dS/m and β_{crop} is -100.76 for cropped land and -93.40 for fallow land. This model was adopted without modification to its coefficients to generate EC_e estimates in the SPRB. However, due to poor accuracy when estimated values were compared to ground truth measurements, the model was recalibrated. Adjustments included restricting weather variables to the local growing season as well as to the development and midseason plant growth phases. Additionally, model coefficients were re-estimated using nonlinear optimization in Microsoft Excel Solver to minimize the sum of squared errors (SSE) between estimated and observed values.

2.5 Alternative Remote Sensing-based Method to Estimate EC_e

In his MS thesis, Craig (2023) utilized LandSat 7 and 8 data from 2018 and 2019 to develop EC models to estimate soil salinity for maize fields in Colorado's Lower Arkansas River Valley. Low cloud cover images were collected between May 12 and October 27 of 2018 and between May 15 and October 22 of 2019 resulting in 31 images used for analysis. Ground truth data were collected using EM-38-MK2 surveys for 18 fields in the Fairmont Drainage District (Craig, 2023). CRSI and NDVI were calculated from the remote sensing data. Remote sensing data in conjunction with the Remote Sensing of Evapotranspiration-Raster (ReSET) package in Arc GIS were used to calculate ET_a. CWSI was then computed using weather station data. When values were outside of the 0 to 1 expected range for CWSI, values greater than 1 were set to 1 and values less than 0 were set to 0.

Each of these values, NDVI, CRSI, ET_a, and CWSI, were input into RStudio along with growth stages and multiple linear regressions were run (Craig, 2023). The best EC models were found using a combination of log transformed and non-log transformed variables. The best equation (Equation 9) for predicting EC_e (dS/m) combined CWSI, the natural log of CRSI and the natural log of NDVI:

$$\begin{aligned}\ln(EC_e) = -306.84 &+ 586.78 \times CWSI + 316.71 \times \ln(CRSI) + 327.60 \times \ln(NDVI) \\ &- 600.32 \times CWSI \times \ln(CRSI) - 616.07 \times CWSI \times \ln(NDVI) \\ &- 337.12 \times \ln(CRSI) \times \ln(NDVI) \\ &+ 630.64 \times CWSI \times \ln(CRSI) \times \ln(NDVI) \qquad (9)\end{aligned}$$

This equation had a RMSE of 0.84 dS/m and used only data from the corn midseason growth stage. Each of the index values in this equation were summed across the midseason growth stage for 2018 and 2019, and the maximum value for each pixel between these years was used. The summed indexes did not interpolate between days with LandSat data, instead, only days when data were available were used.

This model developed in Craig (2023) was initially applied directly to the SPRB to estimate EC_e. However, similar to Scudiero et al. (2015), adjustments were needed to improve model performance under local conditions. Weather variables and vegetation indexes were restricted to the local growing season as well as the development and midseason crop growth phases. Model coefficients were re-estimated using nonlinear optimization in Microsoft Excel Solver to minimize the SSE between predicted and observed values.

2.6 Performance Metrics for EC_e Estimation Models

Since this study aims to find a model that can be used to adequately estimate soil salinity in the SPRB, it is imperative to identify a method for comparing the performance of the developed models. One of the most common methods for comparing models is the coefficient of determination or R^2. This method was used in Scudiero et al. (2015) due to the linear structure of the equation. While R^2 should not be used alone, and is strictly suitable only for assessing linear relationships, it generally provides a reference for how well a model fits the data with 0 indicating no correlation and 1 indicating perfect correlation. R^2 is calculated as the square of the Pearson correlation coefficient (r). The Pearson correlation coefficient describes the strength and direction of a linear relationship (Montgomery and Runger, 2011) and is calculated as:

$$r = \frac{\sum_{i=1}^{n} y_i(x_i - \bar{x})}{\sqrt{\sum_{i=1}^{n}(y_i - \bar{y})^2 \times \sum_{i=1}^{n}(x_i - \bar{x})^2} \tag{10}$$

Where n is the number of values, y_i is the observed value, $\bar{y}$ is the average observed value, x_i is the model estimated value, and $\bar{x}$ is the average model estimated value (Montgomery and Runger, 2011). This metric produces a value between -1 and 1 with -1 indicating perfect correlation with a negative slope and 1 indicating a perfect correlation with a positive slope (Montgomery and Runger, 2011). When squared, the coefficient of determination is found which is a value between 0 and 1 with 0 indicating no correlation and 1 indicating perfect correlation. R^2 should be used with caution, however, as it can be increased by having a model with many values much higher and much lower than the observed values which results in the estimated values being correct on average (Montgomery and Runger, 2011). This metric also tends to indicate a better fit for more complex (many variable) models as more variables can capture more of the variation in the data even if the variation is small.

The R^2 metric should not be used on its' own as it simply indicates whether a model fits the data and not whether the model is unbiased, accurate, or appropriate for the set of data. Other performance metrics such as mean bias error (MBE), normalized mean bias error (NMBE), root mean square error (RMSE), and normalized root mean square error (NRMSE) can be evaluated to help indicate when a given model is appropriate. The MBE is used to assess whether a model is systematically under- or overestimating predicted values (Thieu, 2021a). It is calculated as:

$$MBE = \frac{1}{n}\sum_{i=1}^{n}(P_i - O_i) \tag{11}$$

Where n is the number of values, P_i is the predicted value, and O_i is the observed value (Thieu, 2021a). This metric can have a range of negative infinity to infinity with positive values indicating that the model is overpredicting values and negative indicating the model is underpredicting values (Thieu, 2021a). While MBE gives a general direction for bias in a model, it is easily impacted by outliers and is usually not appropriate for data that are not expected to have a normal distribution (Thieu, 2021a). While it is unnecessary for data that have the same number of samples, the normalized MBE (NMBE) can be compared across scales and is calculated as:

$$NMBE = \frac{1}{n\bar{O}}\sum_{i=1}^{n}(P_i - O_i) \times 100 \tag{12}$$

Where $\bar{O}$ is the average observed value. NMBE is expressed as a percentage of the average observed values, so the larger the percentage, the larger the difference between the average observed value and the predicted values. The percentage can be positive or negative with the sign indicating the direction of the bias. While useful for comparing across data with a different number of samples, NMBE generally provides the same information as MBE when using data with the same number of samples.

The RMSE (Equation 13) was designed to estimate the accuracy of a model and can range from 0 to infinity with values closer to 0 indicating higher accuracy in the model (Thieu, 2021b).

$$RMSE = \sqrt{\frac{1}{n}\sum_{i=1}^{n}(P_i - O_i)^2} \tag{13}$$

Where n is the number of values, P_i is the predicted value, and O_i is the observed value (Thieu, 2021b). The RMSE indicates the average size of the error between the predicted and observed values but like MBE it needs to be normalized (NRMSE) before it can be used to compare data sets with different sample sizes (Thieu, 2021b). The NRMSE is calculated as:

$$NRMSE = \frac{1}{\bar{O}}\sqrt{\frac{1}{n}\sum_{i=1}^{n}(P_i - O_i)^2} \times 100 \tag{14}$$

Where $\bar{O}$ is the average observed value. NRMSE is similar to NMBE in that it is expressed as a percentage of the average observed value. The lower the percentage of the average observed value, the better the model performs.

Unlike R^2, MBE, NMBE, RMSE, and NRMSE can be used with nonlinear equations as they were developed as general error metrics. However, issues can arise when using these metrics to rank models because models which score highly in one area may perform poorly in another. To compare and rank models, a performance metric that evaluates a model's fit was needed that could be used on both linear and nonlinear equations and could be evaluated in conjunction with these other metrics. The Corrected Akaike Information Criterion (AICc) was developed for use to evaluate both linear and nonlinear model fit while penalizing more complex (many variable) models (Zajic, 2025). Penalizing more complex models is beneficial for ensuring the model is not overfitted where it appears accurate on training data by capturing random noise rather than the underlying relationship in the data. The best model will have the lowest AICc score (Equation 15).

$$AIC_c = n \times \ln(\hat{\sigma}^2) + 2K + \frac{2K(K+1)}{(n-K-1)} \tag{15}$$

Where n is the sample size, $\hat{\sigma}^2$ is the residual sum of squares divided by the sample size, and K is the number of parameters including an error term (Zajic, 2025). AICc must also be reported with deltas (Δ), the difference between the lowest AICc and the next AICc, and with the weight (W), which is the likelihood that the model is the best among the models tested (Equation 16).

$$W = \frac{e^{-0.5\times\Delta_i}}{\sum e^{-0.5\times\Delta}} \tag{16}$$

The AICc can identify the best fitting equation with a corresponding W to indicate the likelihood that the model is the best and can be used in conjunction with MBE, NMBE, RMSE, and NRMSE to ensure the level of bias and error is acceptable. Just because a model appears to have a good fit does not mean it is not systematically under or over predicting values or predicting values with large errors that are on average accurate. Thus, a combination of performance measures were used herein to evaluate the EC_e models.

CHAPTER 3: RESULTS AND DISCUSSION

3.1 Ground Truth Data

Data from the EM-38-MK2 surveys were calibrated from EC_a to EC_e using measured data from the field soil samples analyzed for EC_e in the laboratory. The R^2 values for the linear regression model ranged from 0.72 to 1. Figure 3.1 displays the calibrated soil surveys.

Previous studies in the upper SPRB conducted by the Northern Water Conservation District found soil salinity ranging from 0 to 6.7 dS/m near Fort Collins, Colorado (Wilson et al., 2005). No previous soil salinity data could be found for areas of the SPRB closer to the Colorado-Nebraska border, but since salinity increased in surface water along the CO SPRB (NIERBO Hydrogeology, 2020), it was expected that soil salinity would increase downstream as well.

All values greater than 15 dS/m or less than 0 dS/m were removed from the data sets. After excluding outliers, the estimated EC_e range was 0.00–13.33 dS/m.

The data from the EM-38-MK2 surveys generally displays the trend of increasing salinity downstream. This is seen in the data depicted in Figure 3.2.

Variation in the accuracy of the EC_a-to-EC_e calibrations across fields likely reflects limitations of the EM-38-MK2 surveys such as changes in operator, sampling frequency, and GPS inaccuracies. Although calibration quality was consistently high (e.g. $R^2 > 0.9$), many fields showed relatively large standard errors (Table 3.1). This emphasizes the need for caution when interpreting the EC_e values, even when calibration statistics suggest strong performance.

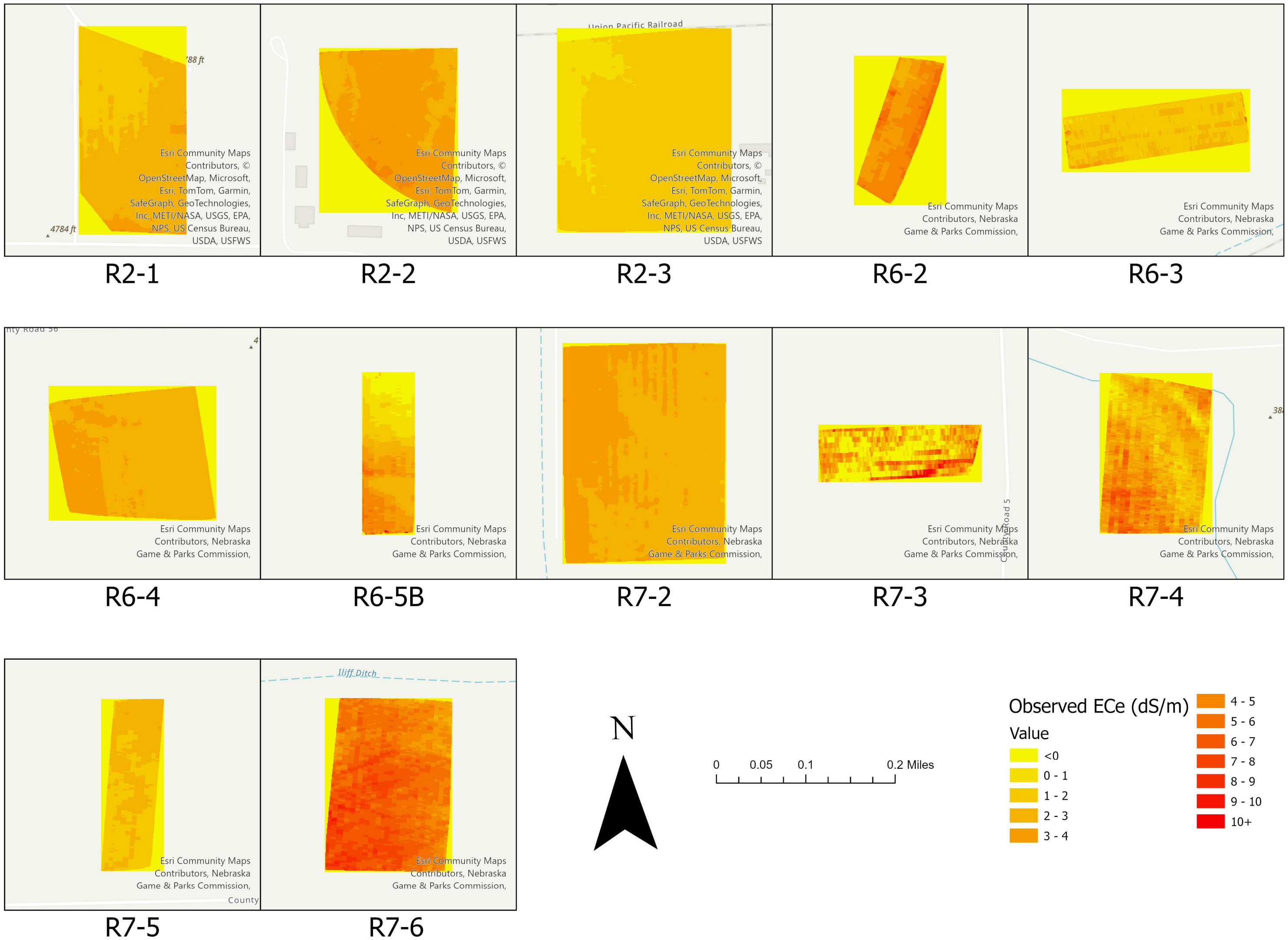

Figure 3.1 Soil EC_e (dS/m) from EM-38-MK2 surveys conducted during the summer of 2024 and calibrated with same day soil samples. The most upstream fields tend to have lower salinity levels than the fields downstream which was expected. Maps created in Arc GIS Pro.

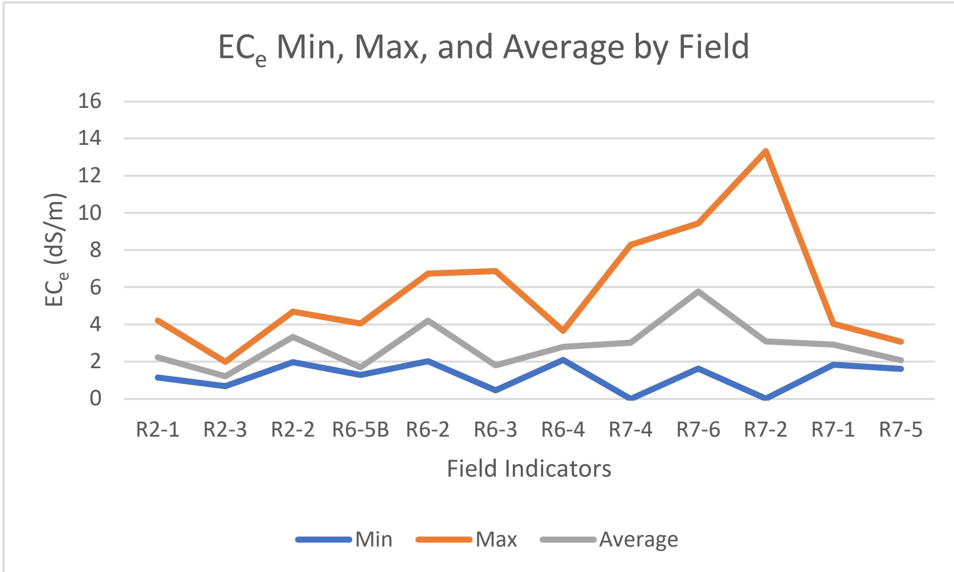

Figure 3.2 The fields are ordered from most upstream to most downstream field. Displayed in this way, the EC_e generally seems to increase downstream as expected. However, there is much variation present in the data indicating other factors may be influencing soil salinity.

Table 3.1 Summary of correlation statistics for EC_a to EC_e regression equations for each field.

Field	Multiple R	R^2	St Error
R2-1	0.88	0.77	79.4
R2-2	0.93	0.86	73.23
R2-3	1	1	3.79
R6-2	0.85	0.72	79.12
R6-3	1	0.99	6.79
R6-4	0.96	0.91980093	29.17
R6-5B	1	1	13.97
R7-1	0.99	0.98	82.76
R7-2	0.97	0.95	49.74
R7-4	0.97	0.94	91.61
R7-5	0.98	0.95	90.08
R7-6	0.99	0.98	25.11

A summary of the conditions at each field site used for EC_e model calibration is presented in Table 3.2. Soils at the sites were mostly loamy or sandy. These coarser soil types generally retain less water than clayey soils which can result in lower average EC_e values since salts can be more easily flushed from the soil column. Observed soil salinity typically ranged from 0 to 7 dS/m. Crop type and irrigation method can influence the distribution of salts within the soil profile, which affects the observed EC_e values used for model calibration. Shallow rooted plants like onions and cabbage tend to extract water primarily from the upper portions of the soil profile especially when combined with water conservative irrigation systems like drip irrigation (Liu et al., 2020). Deeper rooted plants like corn and alfalfa can redistribute soil moisture vertically facilitating deeper salt movement (Liu et al., 2020). While crop type and irrigation method may influence the distribution of salts, soil properties like texture and structure and the availability of sufficient leaching water have a much larger role. If restrictive soil layers or shallow water tables exist, even high volumes of water may not prevent salt build up.

Depth to groundwater can also influence the salt concentration in soils due to capillary rise which can result in the upward movement of salts from a shallow groundwater table while deeper groundwater tables will have a smaller effect on the soil salinity. Groundwater quality, as measured by pH and EC, will also affect the observed soil salinity level, especially in areas with shallow groundwater tables and high groundwater salinity levels. Although pH remained relatively stable through all the fields, groundwater testing revealed high electrical conductivity in the groundwater in some areas. Fields like R7-2 with a 1.45 m depth to groundwater and high salinity (EC of 4.41 dS/m) may be prone to large spikes in soil salinity within the root zone. Weather conditions on the day of the soil survey can also influence the EM-38-MK2 measurements. Generally, the field conditions were hot and dry, but surveys were timed to be completed when the soil was at or near field capacity as the EM-38-MK2 sensor works best when this condition is met. Soil moisture values are not included in the table; however, soil samples collected at each sampling location were used to measure soil moisture (as an estimate of field capacity) to be used when calibrating the EM-39-MK2 readings. The weather conditions on the day of the soil survey – especially on hotter, dryer days – could increase evaporation in the top part of the soil resulting in a concentration of salts, but soil samples were taken at depths up to 120-150cm to calibrate the EM-38-MK2 data which should reduce the influence of soil surface fluctuations and provide a more representative salinity estimate for the overall soil profile.

Table 3.2 Field conditions for surveyed fields used to calibrate EC_e models.

Field	**R2-1**	**R2-2**	**R2-3**	**R6-2**	**R6-3**	**R6-4**	**R6-5B**	**R7-1**	**R7-2**	**R7-4**	**R7-5**	**R7-6**
Soil Texture	Sandy loam and loam	Loamy sand, loam, and clay loam	Sandy loam	Sandy loam, sand, and loam	Sandy loam	Clay loam	Loamy sand	Loam	Clay loam and sandy loam	Loam	Loam	Clay loam
Min Observed EC_e (dS/m)	0.9	1.8	0.7	1.8	0.2	2.1	0.6	1.7	-7.4	-1.6	1.1	1.5
Max Observed EC_e (dS/m)	4.2	4.7	2.0	6.8	6.9	3.8	4.2	4.1	31.5	9.7	3.1	9.9
Avg Observed EC_e (dS/m)	2.2	3.3	1.2	4.2	1.8	2.8	1.7	2.9	1.8	2.6	2.1	5.8
2024 Crop	Onion	Alfalfa	Cabbage	Corn	Corn	Alfalfa	Corn	Soybean	Grass	Hay	Alfalfa	Alfalfa
Average Depth to Water Table (m)	8.5	3.5	8.7	3.2	3.4	3.9	1.6	4.2	1.5	2.5	4.4	2.8
Avg Ground Water EC (dS/m)	3.2	2.1		7.0	2.0	2.2	4.6	3.9	4.4	2.5	2.1	4.9
Irrigation Type	Drip	Sprinkler	Drip	Sprinkler	Sprinkler	Sprinkler	Flood	Sprinkler	Flood	Flood	Sprinkler	Sprinkler
Ground Water pH				7.5	7.9	7.7	7.6	7.8	7.5	7.6	7.7	7.5
Date of Survey	8/1/2024	9/6/2024	8/6/2024	6/13/2024	6/20/2024	8/14/2024	7/11/2024	7/24/2024	6/28/2024	7/17/2024	6/27/2024	7/23/2024

Closest Weather Station	lcn01	ksy01	pkh01	ftm02	ftm02	bru01	wig01	crk01	crk01	stg02	crk01	stg02
Avg Temp (C)	24.1	17.7	25.6	24.4	22.9	20.1	25.9	23.7	25.1	21.3	26.4	23.0
Max Temp (C)	36.1	28.5	35.7	31.7	33.3	32.2	37.1	34.1	34.0	31.6	36.2	33.0
Min Temp (C)	12.4	8.2	17.0	14.5	17.4	14.2	12.3	11.6	18.5	15.0	19.4	12.2
Liquid Precip (mm)	0	0	0.5	0.1	19.0	2.1	0	0	0	3.7	0.1	0

3.2 Weather Data

Thiessen polygons were drawn around weather station locations. Polygons were converted to raster images, maintaining one value for the area, to be used in calculations (Figure 3.3). The data from weather stations were assumed to be accurate over large areas – with some weather stations almost 40 km (25 miles) away from study fields. Because of the large area represented by each weather station, there may be considerable discrepancy between the estimated and actual weather data for study locations introducing uncertainty into the weather characterization.

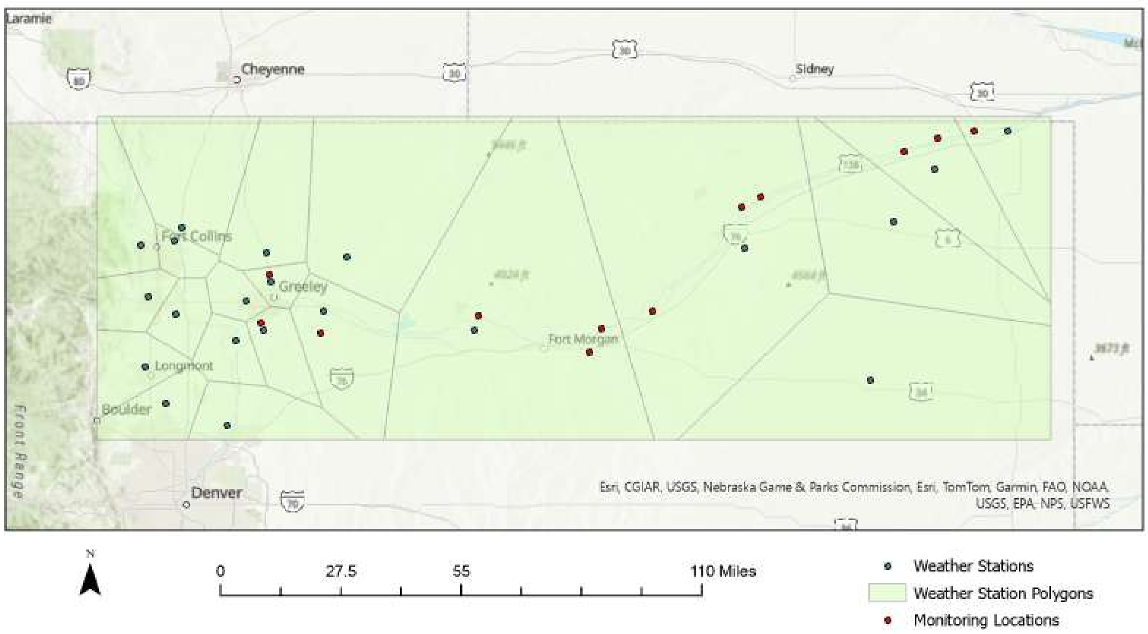

Figure 3.3 The weather stations in fully or partially irrigated areas from CO Ag Met's weather station network are shown in blue. A Thiessen polygon (shown in green) was drawn around each weather station and values from that station were used in EC_e estimation equations for monitoring locations (shown in red) within that polygon. Map created in Arc GIS Pro.

3.3 Vegetation Indexes

Figure 3.4 displays a scatter plot of the 2024 average NDVI vs 2024 average CRSI for the 12 irrigated agricultural fields included in this study located between Kersey and Sterling along the

SPRB. A positive correlation is present with an R^2 of 0.88. As expected, CRSI increases as NDVI increases over the range; however, there is localized scatter in the data. This indicates that dense green vegetation is usually found when stress from salinity is low. While the values are correlated, NDVI indicates the degree of dense green vegetation while CRSI indicates the degree of stress from salinity. The need for both indexes is highlighted in the areas where CRSI is low and NDVI is high. From the NDVI value alone, the crop may seem to be healthy – dense and green; however, when taken with the CRSI value, an underlying salinity problem may be suggested.

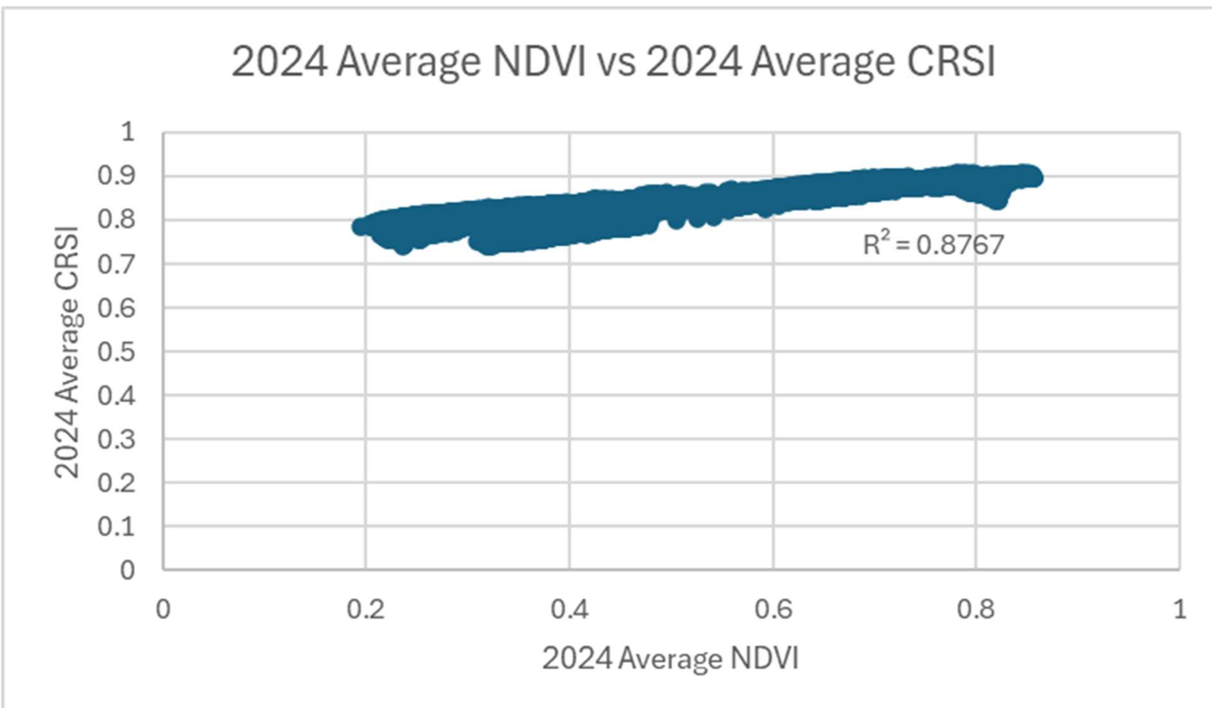

Figure 3.4 Avg NDVI vs Avg CRSI for 2024 for the fields used in this study. There is a slight positive correlation which indicates dense green vegetation is often seen in areas with lower stress from salinity.

Like Figure 3.4, Figure 3.5 shows 2024 average CWSI vs 2024 average CRSI for the fields in this study. The indexes are inversely correlated with a R^2 of 0.88. As CWSI decreases, CRSI increases as expected yet local scatter still exists. The correlation indicates that when plants are experiencing less water stress – low CWSI – they also tend to experience less stress due to salinity – high CRSI. Using both indexes together helps to differentiate stress caused by salinity from stress caused by lack of water since one can exist without the other.

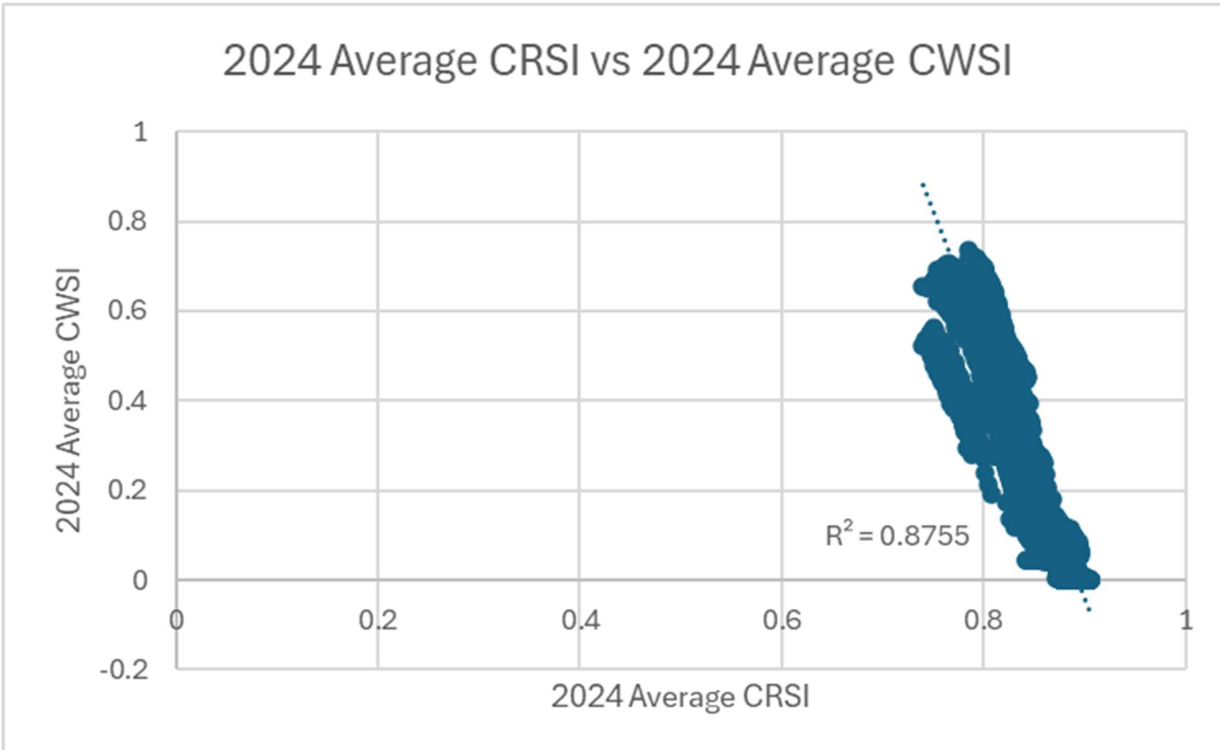

Figure 3.5 Avg CWSI vs Avg CRSI for 2024 for the fields used in this study. There is a slight negative correlation which indicates water stress is often seen in areas with higher stress from salinity.

Although NDVI and CWSI are both included as model variables, a direct comparison between the two is not presented because NDVI is used in the calculation of CWSI in this study. Due to this defined mathematical dependency (Equations 3-7), a strong negative correlation between the indexes is expected. However, both indexes were retained because they capture different aspects of crop condition: NDVI indicates biomass growth while CWSI isolates plant water stress. Including both indexes allows the model to distinguish between biomass reductions caused by water stress and biomass reductions resulting from other factors like salinity.

While NDVI, CRSI, and CWSI are indicative of specific aspects of plant health (e.g. NDVI reflects biomass production, CRSI provides a measure of response to salinity, and CWSI is indicative of water stress), many factors affect plant health, so no index can identify a plant's response to a single isolated factor. Since plant type and the factors affecting plant health vary by location, indexes deemed successful for estimating soil salinity in one location do not always work in other areas. However, once an equation is locally calibrated and shown to accurately estimate EC_e, it can be applied flexibly within that region using remote sensing data from different satellite platforms or historical imagery, as long as the necessary spectral bands are available to derive the indexes.

3.4 EC_e Modeling

3.4.1 Method I

The initial attempt at estimating EC_e utilized the data collected from the LandSat constellation and followed the method outlined in Scudiero et al. (2015). CRSI was calculated for each image and averaged by year then the multi-year maximum was taken. A summary of the CRSI and weather values used is shown in Table 3.3 below. Scudiero et al. (2014, 2015) do not explicitly state the range of multiyear maximum average CRSI nor specify the weather data used for model calibration; however, based on the figures in Scudiero et al. (2014), the range for multiyear maximum average CRSI is likely around 0.6-0.85. This is a much smaller range than the multiyear maximum CRSI values found in this study.

Table 3.3 Summary of the independent variables used for Scudiero et al. (2015) method.

Statistic	Multi-year Maximum Average CRSI	Precipitation 2023 (mm)	Temperature 2023 (°C)	Growing Season Precipitation 2023 (mm)	Growing Season Temperature 2023 (°C)
Min	0.48	322.33	-0.14	150.88	11.29

Max	1	594.61	1.51	375.41	13.15

The initial attempt at utilizing this method resulted in extreme negative values for estimated EC_e across the basin. The values estimated ranged from -1260.43 to -28.08 dS/m when the multiyear maximum CRSI was used in conjunction with 2023 precipitation and temperature data (Figure 3.6). The large range and extreme negative values indicate that the Scudiero et al. (2015) model is not directly transferable to the SPRB, and that local calibration is needed to transfer the approach from one river basin to another.

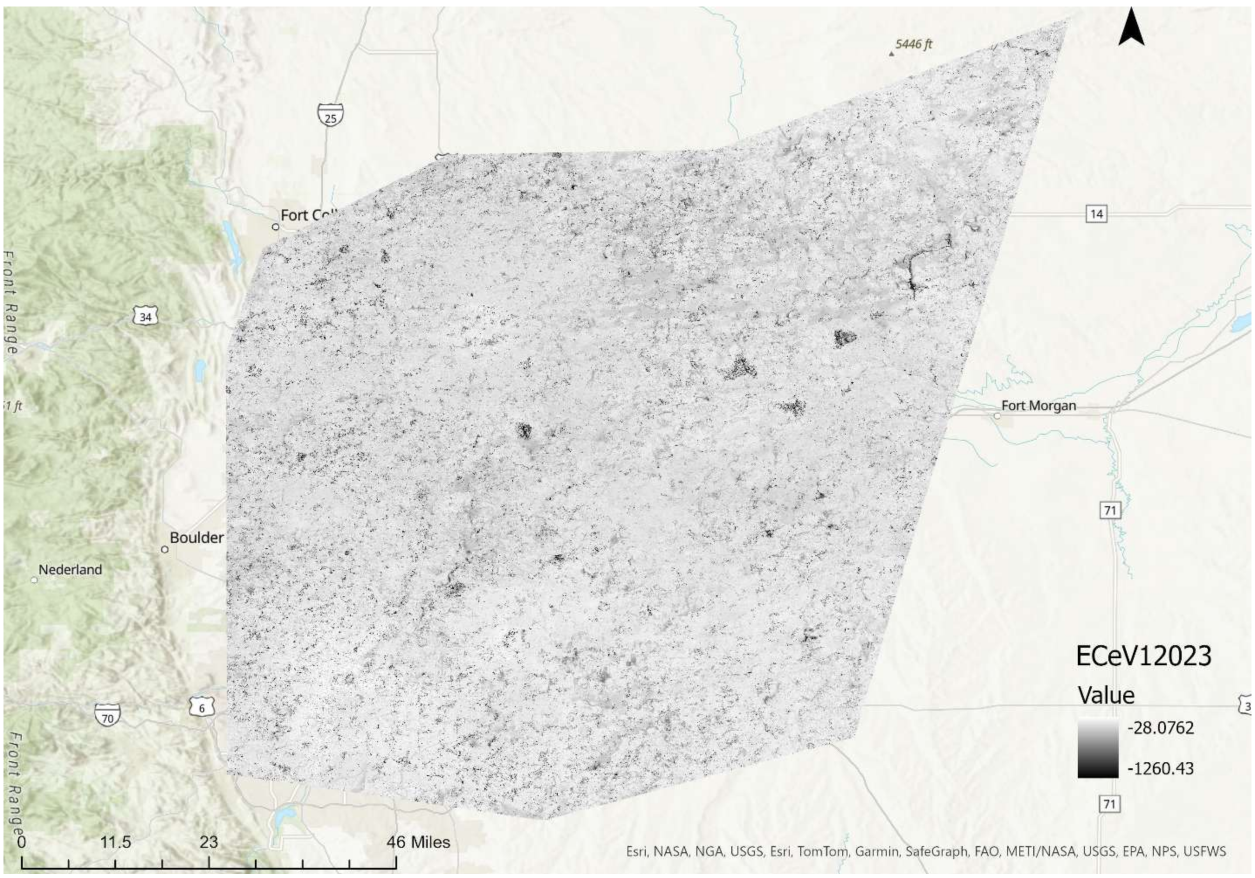

Figure 3.6 Initial attempt at applying the Scudiero, Skaggs, and Corwin (2014, 2015) method to data from the SPRB led to a large range of predicted values all of which are negative and do not match the ground truth data. Map created in Arc GIS Pro.

An attempt was made to calibrate the Scudiero et al. (2015) EC_e equation to the CO SPRB by adjusting the data retrieved from weather stations. While the range of values for weather station data was not provided by Scudiero et al. (2015), it is likely there are major differences between the calibration climate of the San Joaquin Valley, CA and the SPRB. It was thought that the EC_e equation would better fit the SPRB if variables relating to climate were restricted to the crop growing season only which might better match the climate values present in the San Joaquin Valley.

In the San Joaquin Valley, the growing season is nearly year-round (Le Strange and Jimenez, 2013). Additionally, the average annual precipitation ranges from 127-406 mm (5-16 inches) (Galloway and Riley, 1999), and the minimum temperature rarely falls below -1.7°C (29°F) (National Oceanic and Atmospheric Administration, 2025). This is a stark contrast to the SPRB, where the growing season is May at the earliest to early November at the latest (Colorado Department of Agriculture, 2025), average annual precipitation is 254-406 mm (10-16 inches) in agricultural areas (Ryan and Doesken, 2014), and the minimum temperature in agricultural areas is usually less than -6.7°C (20°F) in the winters but ranges up to around 10°C (50°F) in the summers (Natural Resources Conservation Service, 2025).

Since the largest difference in climate is the average minimum temperature, the temperature value was adjusted for the second EC_e modeling attempt. Instead of using an average annual minimum temperature, the average minimum temperature was only taken from the growing season data – May 15 to October 31. While the estimated EC_e values improved with this adjustment, they were still extremely negative with a range of -12228.69 to 2.80 dS/m using 2023 weather data (Figure 3.7).

Like the first attempt, the wide range of values and the lack of values in the expected range for EC_e indicate that the Scudiero et al. (2015) model is not directly transferable to the SPRB.

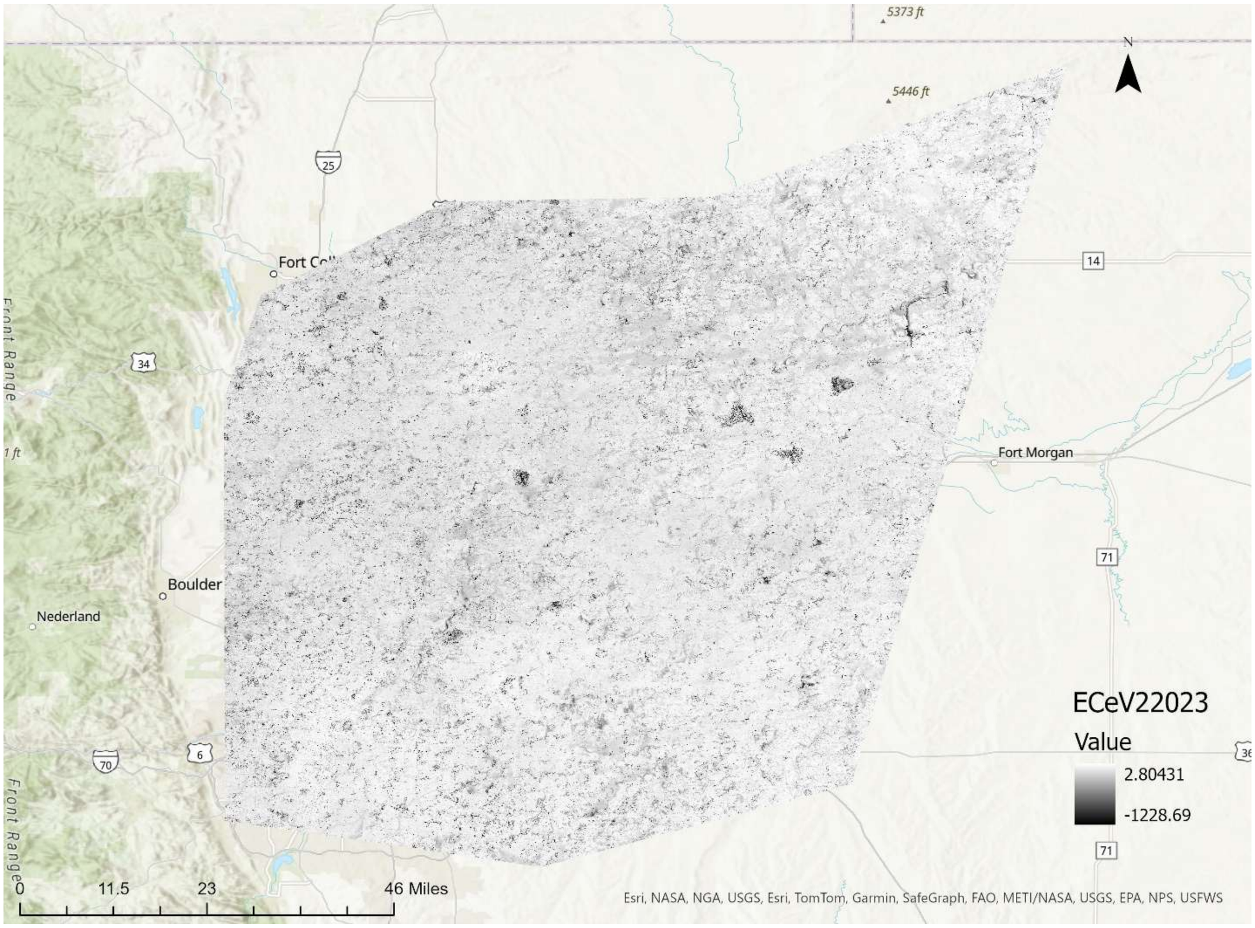

Figure 3.7 Second attempt at applying the Scudiero, Skaggs, and Corwin (2014, 2015) method to data from the SPRB also led to a large range of predicted values most of which are negative. The predicted values do not match the ground truth data. Map created in Arc GIS Pro.

3.4.2 Method II

Because the Lower Arkansas River Valley has a climate similar to that of the SPRB, the EC_e equation deemed most accurate by Craig (2023) was utilized to estimate salinity in the SPRB. While NDVI was downloaded from EEFLux and CRSI had previously been calculated, Craig's equation also required CWSI values. With weather station ET_c data and ET_a maps downloaded from EEFLux, CWSI was calculated for each image.

ET_c from weather stations was mapped using the same method as mapping weather data. Weather station data were interpolated across the basin using Theissen polygons which allowed for CWSI to be calculated for the entire basin, but like the weather data, ET_o from weather stations was assumed to be accurate over large areas.

When CWSI was calculated, there were many values outside of the expected 0 to 1 range which is caused when ET_a is larger than the ET_c. Since Craig (2023) used a summed CWSI, a summed CWSI map was created for the SPRB setting values outside the 0 to 1 range to null to see if there were enough images with better CWSI data to supplement missing information. As shown in Figure 3.8, even in the summed CWSI, CWSI data were missing from much of the SPRB as indicated in green. While the Craig (2023) method "fixed" the CWSI values to fall within the 0 to 1 range, in the SPRB images these out-of-range CWSI values were mainly found in agricultural fields. Therefore, "fixing" these values could potentially interfere with the EC_e calculation. Instead of fixing the out-of-range CWSI values this way, the cause of values falling outside the 0 to 1 range was explored, and other methods of calculating CWSI were tested.

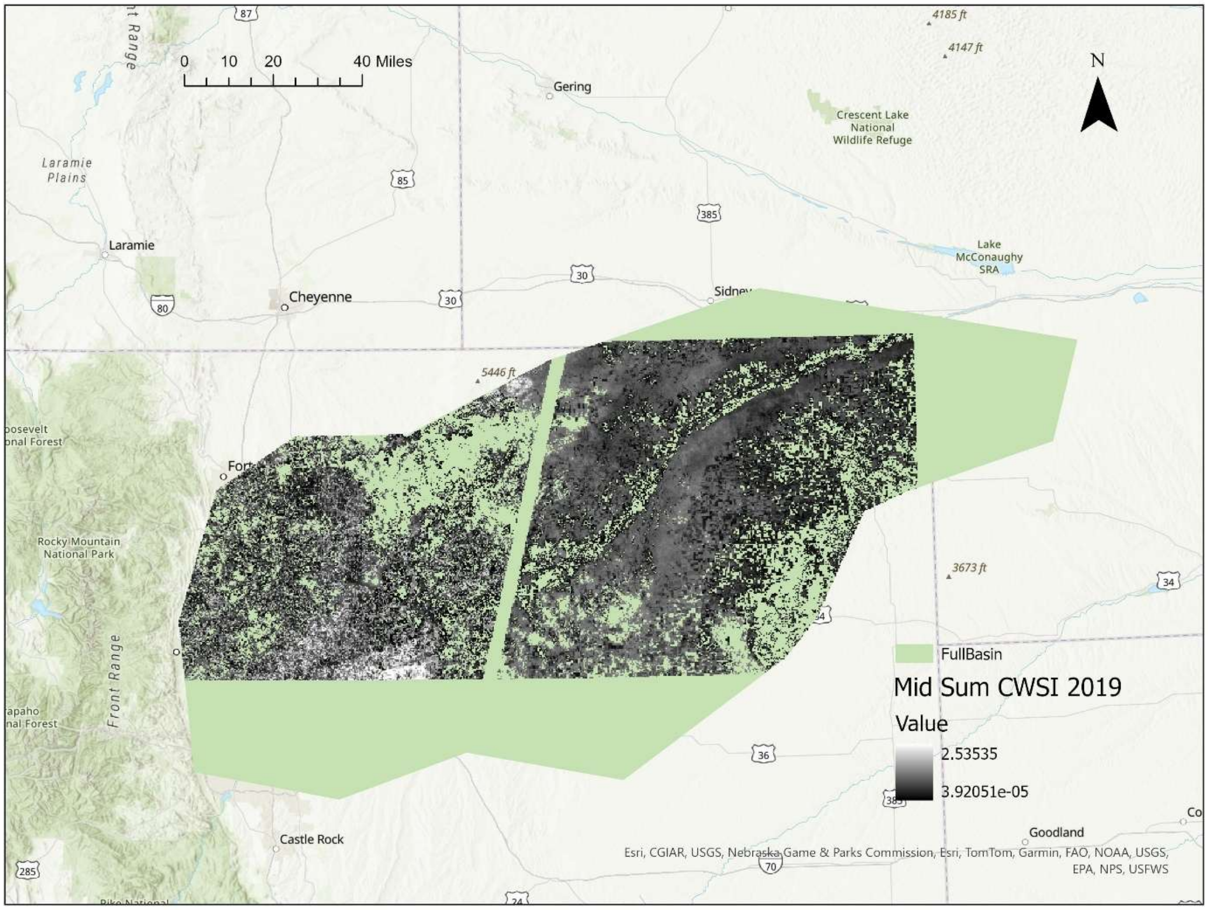

Figure 3.8 Initial attempt at calculating the CWSI summed index resulted in many cells being outside the 0 to 1 range. Even the summed index could not provide data to cover the entire basin as shown by the areas in green. Map created in Arc GIS Pro.

Upon further investigation into out-of-range CWSI values, it was discovered nearly half the ET_a values from EEFlux were 13 mm/day or higher which is nearly double the highest ET_c rate estimated from the weather station data. For this reason, ET_a values from EEFlux were not used. As indicated in Chapter 1, the Trout (2008) and Trout and DeJong (2018) method was followed to estimate K_c and was used with the K_c from weather station data to estimate CWSI. The values that existed outside the 0 to 1 range were closer to the acceptable CWSI range when compared to previous attempts, thus this method was deemed acceptable. Because there were fewer CWSI values outside the acceptable range and the values were closer to the acceptable range, “fixing” (limiting) the values outside the range to the [0, 1] limits using the Craig (2023) method was also deemed acceptable. The result of this method is shown in Figure 3.9.

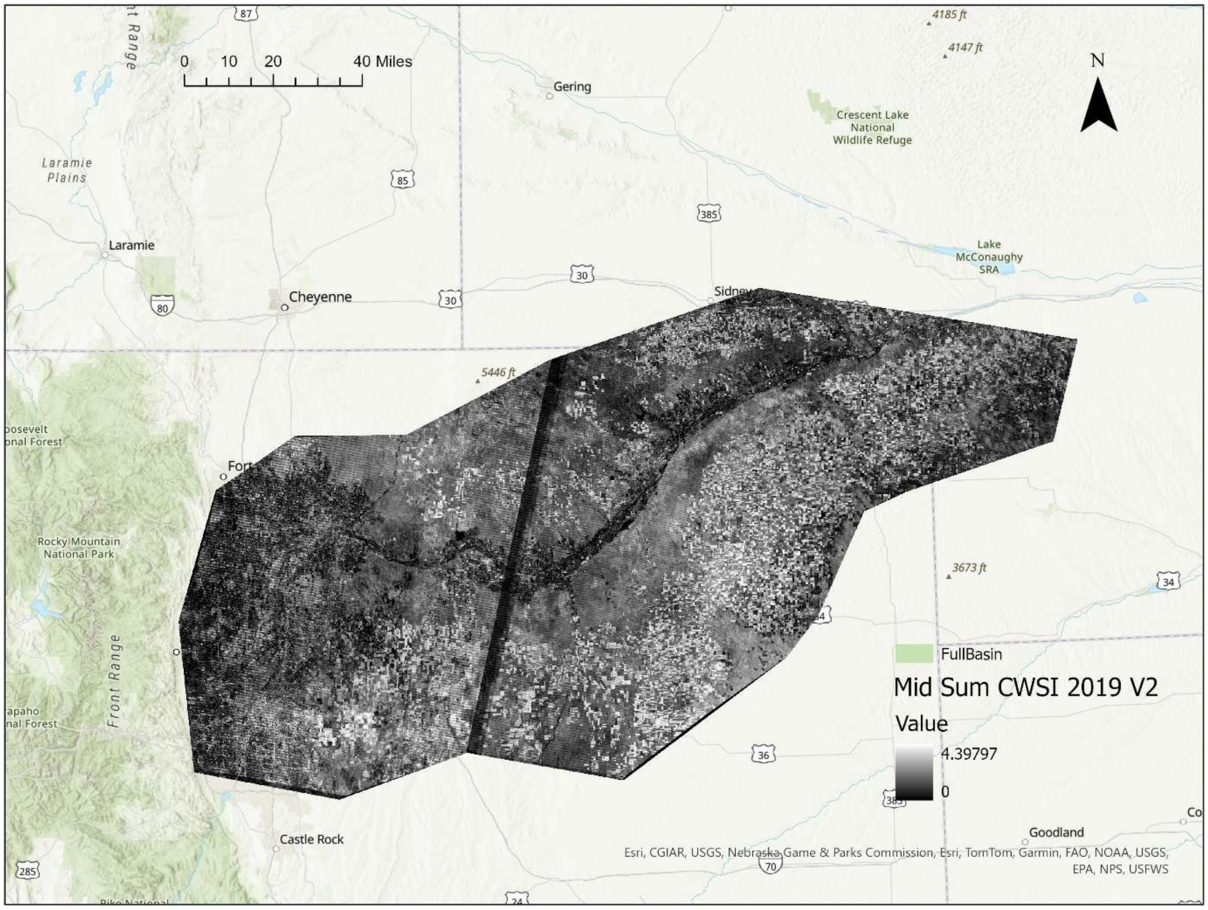

Figure 3.9 Second attempt at calculating CWSI resulted in far fewer cells being outside the 0 to 1 range for CWSI so for the cells that were outside of the 0 to 1 range, it was deemed acceptable to set them to 0 and 1 respectively allowing the summed index to cover the entire basin. Map created in Arc GIS Pro.

Values for CWSI, NDVI, and CRSI were summed across the midseason growth stage for each year and the multi-year maximum of each summed index was found following the methodology outlined in Craig (2023). While both the method presented in Scudiero et al. (2014, 2015) and Craig (2023) use multi-year maximum index values, Scudiero et al. (2014, 2015) uses annual meteorological data to produce yearly EC_e maps, whereas Craig's method does not, resulting in a single map over the entire study period. The ranges for the vegetation indexes are shown in Table 3.4. Craig (2023) does not explicitly provide the ranges of NDVI, CRSI, CWSI, and EC_e used for his model development, so comparison to the values in this study is not possible. Craig (2023) used 16 images from 2018 – two initial development phase images, two development phase images, five midseason images, and five late season images. He used 15 images from 2019 – two initial development phase images, three development phase images, five midseason images, and five late season images. Based on the number of images within the midseason phase, there is a possible summed index range of 0-5 for CRSI, NDVI, and CWSI. The SPRB, in contrast, has summed index values as high as 8.36 for CRSI and 7.87 for NDVI indicating that more images were available in the midseason phase for at least one year in this study. This suggests that summed index values may present challenges when the number of usable images differs from year to year. This is a possible explanation for why Craig's (2023) model did not transfer well to the SPRB.

Table 3.4 Summary of the vegetation index values used for mapping EC_e using the Craig (2023) method.

Statistic	Midseason Multiyear Maximum Sum CRSI	Midseason Multiyear Maximum Sum NDVI	Midseason Multiyear Maximum Sum CWSI
Min	0	0	3.9*10-5
Max	8.36	7.87	2.54

The map in Figure 3.10 shows the calculated EC_e using the Craig (2023) method. While the range for EC_e values was about 0 to 15 dS/m, which is not much larger than the expected EC_e range of 0 to about 13 dS/m, many areas of the map are empty. The rasters were checked to confirm pixel alignment was not the cause of the missing cells. When it was confirmed that it was not a raster issue, the value of a few empty cells was calculated in Excel. It was determined that in those cells the calculated value was undefined as the Craig (2023) equation uses the natural log of CRSI, NDVI, and CWSI and those cells contained a 0 for either NDVI or CRSI. In addition to having many blank areas, most of the cells with data had values near 0 which does not adequately display the range of EC_e values present in the SPRB. As in the case of the Scudiero et al, (2015) method, the Craig (2023) method requires a localized calibration.

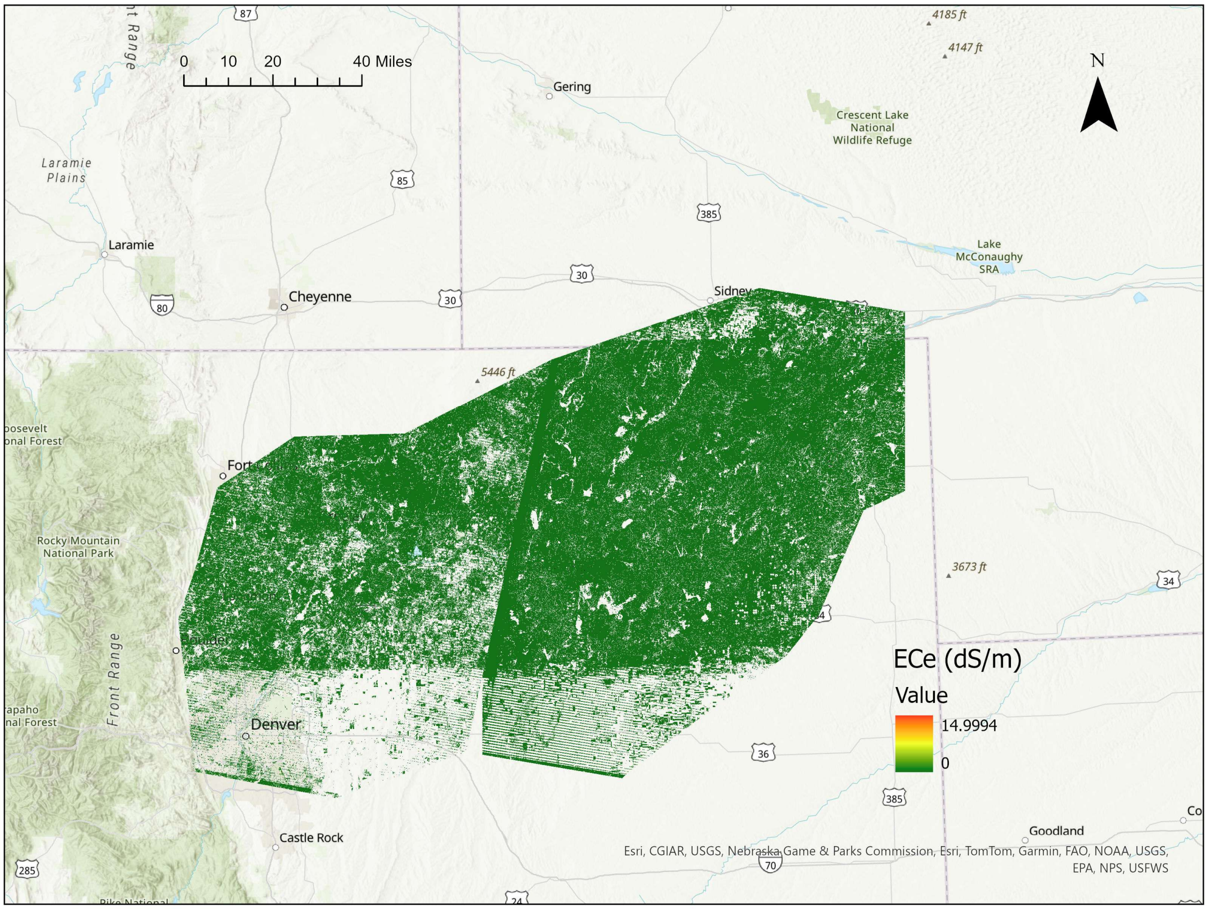

Figure 3.10 EC_e (dS/m) calculated using the Craig (2023) method and CWSI calculated from Trout (2008) and Trout and DeJong (2018) Kc reflectance. Map created in Arc GIS Pro.

3.5 EC_e Mapping Method I and II Optimization

Since neither existing EC_e mapping method yielded reasonable results, optimization of the EC_e model coefficients was attempted. EC_e values calibrated from measured EC_a were scaled up to match the 30-m pixel size of the LandSat satellites. The 30-m EC_e data were entered into excel along with annual average precipitation (mm), seasonal average precipitation (mm), annual average minimum temperature (°C), seasonal average minimum temperature (°C), and ET estimates for corn and alfalfa from the weather stations to prepare for subsequent model calibration using Excel's Solver function. Surface reflectance values from the R, G, B, and NIR bands for each pixel/image from the May 15 to September 3, 2023, time period for three fields (R6-2, R6-3, and R6-5B) were input into Excel as well. These fields were chosen for the analysis because of the wide range of salinity values they represent and provided data covering 87 30-m pixels.

After calculating NDVI, CRSI, and CWSI values for each pixel on each day, the values were averaged using the methods outlined by Scudiero et al. (2015) and summed according to Craig (2023) for the optimization of both the Scudiero (2015) and Craig (2023) models. The original EC_e equations from Scudiero (2015) and Craig (2023) were used to calculate a baseline EC_e estimate and the sum of square errors (SSE) was utilized to determine the goodness of fit for performance evaluation.

3.5.1 Optimization of ECe Mapping Method I

From the baseline Scudeiro et al. (2015) equation, changes were made using the Solver function in Excel which attempted to set the SSE to 0 by changing coefficients and intercepts in an effort to improve the goodness of fit. Three iterations were run to determine what adjustments led to the best outcome. The first iteration used annual weather data and only adjusted coefficients and intercepts, the second iteration used seasonal average minimum temperature instead of annual average minimum temperature and adjusted coefficients and intercepts, and the third iteration used seasonal data for both average minimum temperature and precipitation and adjusted coefficients and intercepts. From these iterations, it was found that the optimized EC_e equation with the lowest SSE utilized annual weather data with adjusted coefficients and intercept to better fit the observed data. The variable ranges used to calibrate this localized equation were EC_e between 1.18-6.13 (dS/m), CRSI between 0.84-0.89, precipitation between 501.9-594.11 mm, and temperature between 0.24-1.39 °C.

While these changes did improve the goodness of fit, the coefficient of determination remained low. Even when evaluating other statistics like MBE, NMBE, RMSE, and NRMSE, the effort to optimize the Scudiero et al. (2015) EC_e model resulted in unacceptable levels of accuracy. While there was virtually no bias in the optimized EC_e estimates (MBE = $-9.57*10^{-6}$ dS/m and NMBE=-0.0004%), the R^2 value was about 0.25, indicating very low correlation between the model and the observed values. The NRMSE of the optimized equation was 43.7%, with EC_e predicted values depicting a spread of about 1 dS/m (Table 3.5). Since the range of observed values used for optimization is 1.18 – 6.13 dS/m, a 1 dS/m error is large. Therefore, despite the lack of bias in the model, poor accuracy makes it unreliable.

Table 3.5 Summary of the statistical performance measures of the original Scudiero, Skaggs, and Corwin equation and the optimized equation.

	Original Scudiero, Skaggs, and Corwin	**Optimized Scudiero, Skaggs, and Corwin**
R-Squared	0.254	0.254
MBE (dS/m)	-46.321	-9.57E-06
NMBE (%)	-1949.840	-0.000403
RMSE (dS/m)	46.370	1.039
NRMSE (%)	1951.877	43.734

3.5.2 Optimization of ECe Mapping Method II

Optimization efforts for the Craig (2023) EC_e method involved relating NDVI, CRSI, and CWSI to measured EC_e values, maintaining the structure of the original EC_e equation. Further, midseason summed index values were utilized following the Craig (2023) method in addition to development season summed index values. Results indicate a limited improvement in EC_e estimates with the development phase summed index values performing better. The variable ranges used to calibrate this localized equation were EC_e between 1.18-6.13 (dS/m), CRSI between 0.77-3.55, NDVI between 0.24-3.06, and CWSI between 0.003-0.83. Even after the optimization attempt, the R^2 value of 0.25 indicates the EC_e equation does not fit the observed EC_e data (Table 3.6). Values of EC_e predicted by the model have a strong negative bias (MBE = -0.427 dS/m and NMBE = -17.986%), and there is an average error of about 1.3 dS/m. The improvement in the metrics was achieved primarily because the equation estimated approximately 1/3 of the EC_e values to be 0. Due to difficulties in maintaining non-zero values for salinity estimates using this equation, it was ultimately decided that Craig's method was non-transferable to the SPRB.

Table 3.6 Summary of statistical performance measures for the original Craig equation and the optimized equation.

	Original Craig	**Optimized Craig**
R-Squared	6.88E-05	0.254
MBE (dS/m)	-1.975	-0.427
NMBE (%)	-83.131	-17.986
RMSE (dS/m)	2.429	1.302
NRMSE (%)	102.244	54.816

3.6 New EC_e Model Development

Despite applying local weather data, aligning independent variables with the local growing season, and recalibrating the coefficients, neither Method I nor II produced models with reliable results, indicating these models fail to support the hypothesis of transferability with minimal local calibration. To produce a locally accurate model of EC_e, new regression equations were developed directly from the data collected for the SPRB, incorporating vegetation indexes and weather variables and evaluating new model performance. A key consideration in the development of new models was the spatial resolution of the imagery used to derive vegetation indexes.

Since the LandSat image has a pixel size of 30-m, each pixel holds an average surface reflectance value from a 900-m^2 area. Because of this large pixel area, different soil salinity levels will be averaged together when high spatial heterogeneity is present. Indeed, based on the EM-38-MK2 measured EC_a data, it was clear that a high EC_e heterogeneity was present in most surveyed fields. Dividing fields into areas based on the proposed divisions in Scudiero et al. (2014) [EC_e in dS/m of 0-2 (non-saline), 2-4 (slightly saline), 4-6 and 6-8 (moderately saline)], the area encompassed by each salinity level was on average about 16,000 km^2. However, often areas with different salinity levels were intermixed within a field; therefore, individual LandSat pixels frequently represented a mixture of multiple salinity levels.

Thus, it was thought that a smaller pixel size would reduce the areal averaging effect to improve the correlation between measured EC_e, the remote sensing-based vegetation indexes, and CWSI. For this purpose, raster images from the PlanetDove satellite constellation with a 3-m pixel size were collected for all fields surveyed for the 2020-2024 growing season. Approximately 10 images per field were collected from the development and midseason phases (June 15-September

3) of the growing season for each year. These images were used to calculate NDVI, CRSI, and CWSI values to be used for equation development alongside the previously collected minimum temperature and precipitation data.

3.6.1 Average EC_e Analysis

The first method applied for EC_e model development used only 2024 data. Instead of developing an EC_e equation using all the remote sensing pixels, fields were divided into sections (sub-areas) based on their salinity level. Measured EC_e values were interpolated to create a raster layer with the same cell size as the remote sensing imagery pixel size of 3 m. Values of EC_e outside of the 0-15 dS/m range were removed (0.0062% of values from R6-3, 0.51% of values from R7-4, 9% of values from R6-5B, and 19% of values from R7-2) since they are outside of the expected soil salinity range for the SPRB. Then sections were drawn based on the observed salinity level range by aggregating pixels within a given EC_e range (Figure 3.11). Panel A shows the observed EC_e in dS/m for field R7-6 with a range of 0 dS/m to nearly 10 dS/m. The map from Panel A is overlaid in Panel B with the salinity level polygons from ranges 0-2, 2.001-4, and 4.001-6 dS/m demonstrating the heterogeneity of salinity levels within the field.

While EC_e values existed outside the selected ranges, they were scattered across the field making their inclusion in this analysis difficult. Fields R6-3 and R7-2 had no identifiable soil salinity pattern and EC_e values in different ranges were scattered throughout the field; therefore, these fields were left out of this analysis. R6-5B was split into east and west sections as the NDVI indicated that half the field was vegetated, and the other half was likely bare soil. With fields R2-1, R2-2, R2-3, R6-2, R6-4, R6-5B, R7-1, R7-4, R7-5, and R7-6 split into sections based on salinity, the average value for EC_e, annual minimum temperature, seasonal minimum

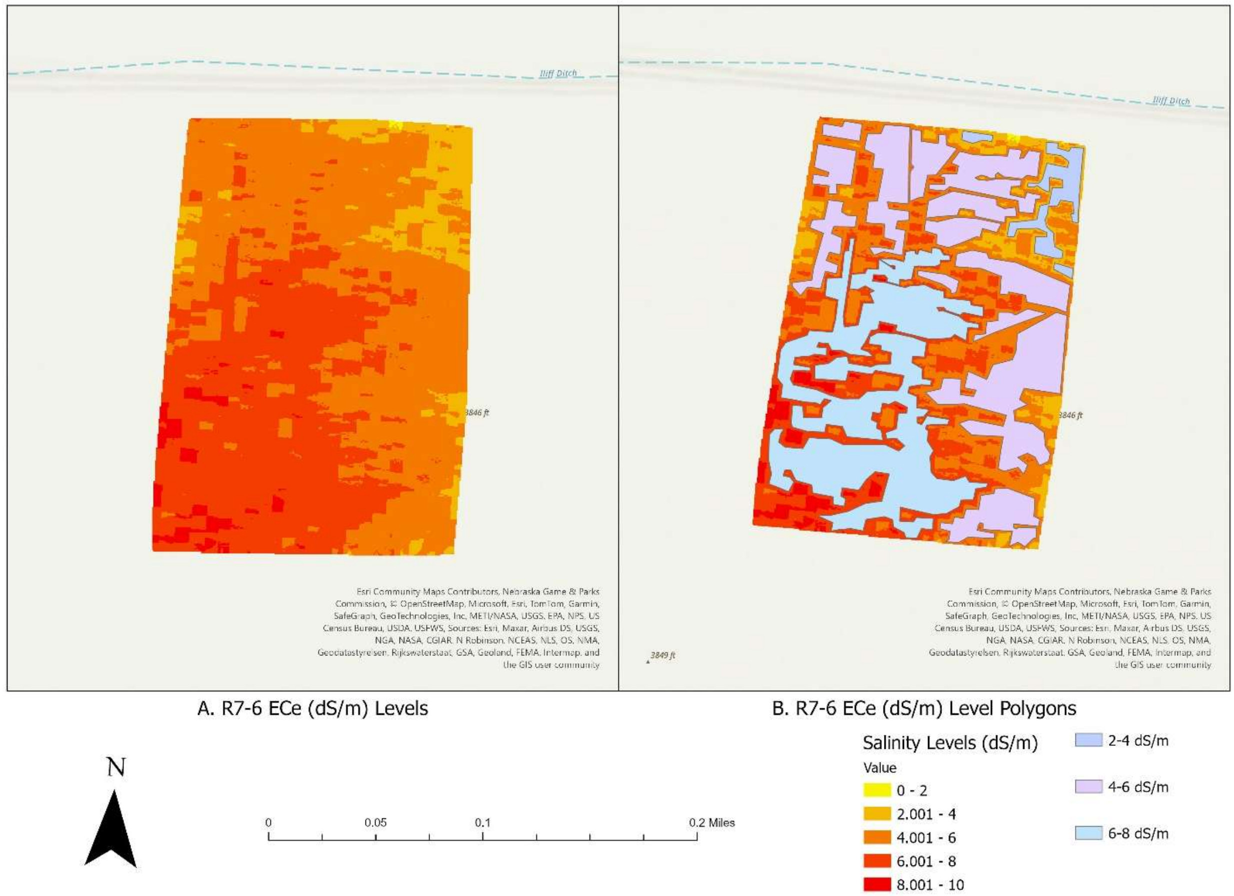

Figure 3.11 Panel A: Observed EC_e (dS/m) in Field R7-6. Panel B: Observed EC_e (dS/m) in Field R7-6 overlaid with salinity level polygons. The heterogeneity within the field leads to large-pixel remote sensing data blending distinct salinity levels, reducing the ability to distinguish fine-scale variability. Maps created in Arc GIS Pro.

temperature, annual precipitation, seasonal precipitation, CWSI, CRSI, and NDVI were collected for each section.

Multiple linear regression analysis was conducted in Excel using every combination of the available data to identify the best EC_e equations to estimate soil salinity. Combinations never included more than one value of the same type (i.e. if annual minimum temperature was used, seasonal minimum temperature was not). The new models were calibrated for EC_e values ranging between 0.75-7.01 dS/m, annual average minimum temperature between 0.44-2.48 °C, seasonal average minimum temperature between 10.89-12.17 °C, annual average precipitation between 185.42-452.12 mm, seasonal average precipitation between 53.84-233.43 mm, average

CWSI between 0.02-0.59, average CRSI between 0.82-0.90, and average NDVI between 0.34-0.82. The best-fitting regressions always included CWSI, temperature, and precipitation data; however, none of the regressions obtained a coefficient of determination greater than 0.3 (Table 3.7). Since none of the resulting EC_e functions from the regressions indicated a high level of correlation with the observed data, this method was not pursued further.

Table 3.7 Summary of the best soil salinity level regressions based on R-Squared values.

R-Squared	Variables Included
0.3	Seasonal Avg Min Temp, Annual Precipitation, Avg CWSI, Avg CRSI, Avg NDVI
0.3	Seasonal Avg Min Temp, Annual Precipitation, Avg CWSI, Avg NDVI
0.3	Seasonal Avg Min Temp, Annual Precipitation, Avg CWSI, Avg CRSI
0.29	Seasonal Avg Min Temp, Annual Precipitation, Avg CWSI
0.28	Annual Avg Min Temp, Annual Precipitation, Avg CWSI, Avg CRSI, Avg NDVI

3.6.2 2024 and Multiyear EC_e Modeling

Since none of the average EC_e values within a specified range yielded an adequate equation, a new regression analysis was performed without sectioning the data by EC_e range values. Data were organized into three datasets, one dataset included all fields surveyed (all-fields) and included fields R2-1, R2-2, R2-3, R6-2, R6-3, R6-4, R6-5B, R7-1, R7-2, R7-4, R7-5, and R7-6; one dataset included only the corn fields surveyed (corn fields) and included fields R6-2, R6-3, and R6-5B; and one dataset included only the non-corn fields surveyed (non-corn fields) and included fields R2-2, R2-3, R6-4, R7-1, R7-2, R7-4, R7-5, and R7-6. Field R2-1 was not included in the non-corn field analysis as it was an onion field with very low biomass presence rendering reflectance values primarily from bare soil rather than leafy growth. Figure 3.12 shows the general process for the creation of these new models.

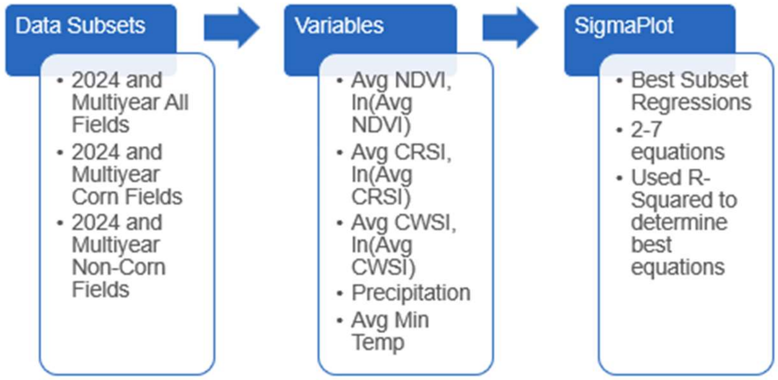

Figure 3.12. Flow chart representation of new model creation. Graphic created in PowerPoint.

For each dataset, EC_e (dS/m) and ln(EC_e) were used as dependent variables in the model development. Independent variables were calculated both for a single year (2024) and multiple years (2020-2024) data. For the single year data, independent variables included average NDVI, average CRSI, and average CWSI as well as the natural log of each of these variables calculated from the entire crop season considered, for the development phase, and for the midseason phase. Average minimum temperature and total precipitation were included for an annual time period as well as for each of the different crop growth periods. The multiyear independent variables were multiyear maximum average values – the average index value was calculated for each year and the maximum of these values was used. For NDVI, it was decided to also test a true multiyear average value as well as the multiyear maximum average value to see if the true average would be more representative of the conditions on the field. Multiyear weather station data were the average value across the time frames (annual, seasonal, development phase, midseason phase) for all the years considered (2020-2024). The ranges for the variables used in the different models are presented in Table 3.8.

Table 3.8. Summary of observed ranges for all independent variables across the six datasets used for model creation. The smallest and largest values from all years are displayed and values may not come from the same year.

Variable	Min	Max
EC_e (dS/m)	0	13.33
Avg NDVI	0.24	0.89
Avg CRSI	0.70	0.93
Avg CWSI	0.09	0.86
Dev Avg NDVI	0.25	0.85
Dev Avg CRSI	0.71	0.93
Dev Avg CWSI	0.12	0.87
Mid Avg NDVI	0.23	0.98
Mid Avg CRSI	0.69	0.94
Mid Avg CWSI	0.05	0.87
Annual Precipitation (mm)	346.71	543.31
Seasonal Precipitation (mm)	83.57	302.26
Dev Precipitation (mm)	17.27	78.74
Mid Precipitation (mm)	46.23	284.99
Annual Avg Min Temp (C°)	1.25	3.49
Seasonal Avg Min Temp (C°)	13.50	14.88
Dev Avg Min Temp (C°)	13.29	14.80
Mid Avg Min Temp (C°)	13.70	14.97

Once dependent variables were calculated, the data were organized into 6 groups: 2024 all field, 2024 corn field, 2024 non-corn field, multiyear all field, multiyear corn field, and multiyear non-corn field. These files were uploaded to Sigmaplot Version 16 (Systat Software, Inc., 2023) and best-subset multiple linear regressions were run offering the program 8 independent variables to choose from and one of the two dependent variables. Best-subset regressions are a statistical method used to identify the predictor variables that produce the best-fitting regression model by maximizing the R^2.

The multiple linear regression model structure was chosen since the Scudiero et al. (2015) and Craig (2023) models were similar in structure, generally following the pattern indicated in Equation 17.

$$y = \beta_0 + \beta_1 x_1 + \beta_2 x_2 + \cdots + \beta_n x_n \tag{17}$$

Where y is the dependent variable (e.g. EC_e), x are the independent variables (e.g. remote sensing indexes or weather data), and β are the estimated coefficients.

The major difference between the Scudiero et al. (2015) and Craig (2023) model structures was that in Craig (2023) some of the independent variables were multiplied together with a coefficient as opposed to the linear structure in Equation 17. Additionally, the Craig (2023) equations contained log-transformed variables which were analyzed using multiple linear regressions in RStudio. SigmaPlot was used in place of RStudio in this study due to its' accessible interface and built in regression options which allowed for model development without the need for advanced coding. However, as a result, only model structures supported by SigmaPlot's built in regression tools such as the structure described in Equation 17 could be produced. This model structure closely aligns with that of Scudiero et al. (2015).

While the independent variables used in the best-subset regression analysis always included NDVI, CRSI, CWSI, ln(NDVI), ln(CRSI), ln(CWSI), precipitation, and temperature value, it was not feasible, due to time and software constraints, to also consider the product of these independent variables as was done by Craig (2023). Regressions never included more than one variable of the same type (i.e. if annual minimum temperature was used, seasonal minimum temperature was not) and index variables were grouped by the time of the growing season they represented (i.e. full-season index values were not mixed with development-phase index values). Mixing of time frame was conducted only between index values and weather values (i.e. full-season index values were utilized in combination with annual, seasonal, development phase, and midseason phase weather data while development-phase index values were utilized in combination with annual, seasonal, and development phase weather data and midseason-phase index values were utilized in combination with annual, seasonal, and midseason phase weather data).

SigmaPlot Best-Subset Regressions processed between two and seven subsets for each set of eight variables. The output from the reports was compiled into Excel by dataset (all-field, corn field, or non-corn field) identifying the variables included in the regression, the R^2 value, and the report identifier. Due to time constraints, it was impossible to test all models developed, so regressions were sorted by R^2 value which was already calculated in SigmaPlot to determine which regressions would be selected for further testing.

From each of the three data sets (all-field, corn field, and non-corn field), the top 20 regressions (60 regressions total) were selected for further testing. For all field and non-corn field regressions, the top regressions all used $\ln(EC_e)$ as the dependent variable and utilized 2024 data while for the corn field regressions, the top regressions used EC_e as the dependent variable and utilized multiyear data.

The AICc was used to determine the best fitting models in conjunction with other performance metrics to determine which models performed the best. While the regression equations identified as the best by the AICc may not have the highest R^2 values, they consistently have the lowest RMSE values.

For the all-field data set, the best model (Equation 18) used data from only the 2024 crop development phase data for indexes and weather station data:

$$\ln(EC_e) = -0.727 - 3.215 \times NDVI + 1.679 \times CWSI + 2.4 \times \ln(NDVI) - 0.0163 \times \ln(CWSI) + 0.0382 \times Precipitation\ (mm) + 0.267 \times Temperature\ (°\mathrm{C}) \tag{18}$$

Similarly, the best non-corn field model (Equation 19) only used 2024 crop development phase data for indexes and weather station data:

$$\begin{aligned}\ln(EC_e) = 68.887 - 2.425 \times NDVI - 71.394 \times CRSI + 2.324 \times CWSI \\ + 2.436 \times \ln(NDVI) + 57.567 \times \ln(CRSI) - 0.0215 \times \ln(CWSI) \\ + 0.0506 \times Precipitation\ (mm) \\ + 0.235 \times Temperature\ (°C)\end{aligned} \tag{19}$$

The all-field and non-corn field models had very similar model statistics. For both data sets, the R^2 values ranged from 0.63 to 0.7, indicating a moderate level of correlation between the model and the observed EC_e data. Both had a very small negative bias (NMBE between -5.54 and -1.91%). Based on the NRMSE (33.34-40.83% error), the models would likely be classified as inaccurate: however, while the percent error is greater than desired, it translates to an average error of about 1 dS/m (RMSE between 0.93 and 1.19 dS/m) which indicates these models may be accurate enough for regional level EC_e mapping.

The corn field models deviated from the all-field and non-corn field models. All corn field models had a R^2 value around 0.84, demonstrating very strong correlation between observed EC_e data and model predicted EC_e. These models also indicate very small bias (NMBE between -0.25 and 1.5%), and the RMSE values indicate they are accurate to 0.48 dS/m with a NRMSE less than 20% (19.81-19.97%). The best corn field model (Equation 20) used multiyear data (instead of 2024 data only) and annual weather data, but like the all-field and non-corn field best regressions, it still utilized the development crop growth phase for index values. The best model also used the multiyear maximum average NDVI as opposed to the true average NDVI which was also tested:

$$EC_e = -325.19 + 83.523 \times NDVI + 246.425 \times CRSI + 2.544 \times CWSI - 57.253 \times \ln(NDVI) - 217.35 \times \ln(CRSI) - 1.8 \times \ln(CWSI) + 0.649 \times Temperature\ (°C) \quad (20)$$

Appendix B provides a summary of regression statistics for each equation tested, and Appendix C provides the reports from SigmaPlot with regression coefficients for each of the tested regressions. Table 3.9 shows the model performance statistics for the models developed in each data set, and Table 3.10 shows the performance statistics for the best model in each data set.

Table 3.9 Summary of performance metrics for each data set.

Data Set	**R^2**	**MBE (dS/m)**	**NMBE (%)**	**RMSE (dS/m)**	**NRMSE (%)**
All-Field	*0.63 - 0.68*	*-0.14 - -0.11*	*-5.19 - -3.97*	*0.93 - 1.12*	*33.34 - 40.4*
Corn Field	*0.83 - 0.84*	*-0.01 - 0.04*	*-0.25 - 1.5*	*0.47 - 0.48*	*19.81 - 19.97*
Non-Corn Field	*0.65 - 0.7*	*-0.16 - -0.06*	*-5.54 - -1.91*	*0.98 - 1.19*	*33.64 - 40.83*

Table 3.10 Summary of performance statistics for the best models in each data set as determined by AIC_c..

Dataset	***Best All-Field Model***	***Best Corn Field Model***	***Best Non-Corn Field***
Dependent Variable	ln(ECe)	ECe	ln (ECe)
AICc	-10750	-13002	-2343
Delta	0	0	0
Weight	1	0.073	1
R^2	0.68	0.84	0.7
MBE (dS/m)	-0.11	-0.0007	-0.13
NMBE (%)	-4.04	-0.03	-4.32
RMSE (dS/m)	0.93	0.47	0.98
NRMSE (%)	33.34	19.81	33.64
Variables	Dev Avg NDVI, Dev Avg CWSI, ln Dev Avg NDVI, ln Dev Avg CWSI, Dev Precip, Dev Avg Min Temp	Dev Max Avg NDVI, Dev Max Avg CRSI, Dev Max Avg CWSI, ln Dev Max Avg NDVI, ln Dev Avg CRSI, ln Dev Max Avg CWSI, Annual Avg Min Temp	Dev Avg NDVI, Dev Avg CRSI, Dev Avg CWSI, ln Dev Avg NDVI, ln Dev Avg CRSI, ln Dev Avg CWSI, Dev Precip, Dev Avg Min Temp

All 60 of the tested regressions included at least one form of weather data (average minimum temperature or precipitation), indicating that accurate weather data may lead to better prediction of soil salinity. Nearly all the best EC_e equations (58/60) included some form of NDVI or ln(NDVI). For the corn field regressions – the only dataset that utilized multiyear data in the best regressions – 14 of the 20 tested regressions used multiyear maximum average NDVI instead of multiyear true average NDVI, indicating that multiyear maximum average values may lead to better EC_e models. Additionally, all corn field regressions utilized some form of development phase data while the all-field and non-corn field datasets utilized a mix of crop development phase, midseason phase, and full season data. Moreover, 47 of the 60 models used at least one form of crop development phase data, while 12 EC_e models used at least one form of midseason crop growth data, and 25 used at least one form of full season data (Table 3.11).

Table 3.11 Summary of Types of Variables used in each the best regressions.

Variable	**Regressions Used (out of 60)**	**Time of Season**	**Regressions Used (out of 60)**
NDVI	58	Development Phase	47
CRSI	41	Midseason Phase	12
CWSI	42	Full Season	25
Precipitation	46		
Temperature	47		

For the 20 all-field and 20 non-corn field regressions tested, the fitted equation with the lowest AICc had a W value near 1, indicating it had the highest likelihood of being the best-performing EC_e model among those tested. This near-perfect W value implies these models capture the variation in EC_e across the fields substantially better than the alternatives. In contrast, all 20 corn field regressions had similar W values, with the highest ranked model having a W of approximately 0.07. The lack of a high W indicates that no corn field model was much more likely to be the best performing model than the others which was expected given the extremely small level of variation in the other statistics (R^2, MBE, NMBE, RMSE, NRMSE), demonstrating that these models are virtually identical in terms of accuracy and bias. This suggests that, unlike all-field and non-corn field models, any of the top models could be used without materially affecting the results.

One non-corn field and one corn field were mapped using the best regressions. Figure 3.13 shows the best all-field and non-corn field regressions mapped on field R2-2, an alfalfa field, as compared to the observed EC_e from the EM-38-MK2 survey while Figure 3.14 shows the best all-field and corn field regressions mapped on R6-2, a corn field as compared to the observed EC_e from the EM-38-MK2 survey. Both the non-corn field and corn field regressions capture the average salinity of the field more accurately than the all-field model. The corn field regression captures the variability of the EC_e in the field much better than the non-corn field or all-field regression. While the corn field model does not capture the full range of EC_e values present from the EM-38-MK2 survey, it is a better reflection of the ground-truth data when compared to the all-field and non-corn field regressions. The improved accuracy in the corn field models is likely due to a more uniform vegetation structure type and growing conditions (e.g., similar stages) across the fields used for calibration. Unlike the non-corn field and all field models, the corn field models were calibrated using datasets with only one crop which reduces variability in factors relating to the crop like root depth, stem and leaf structure, and water use. While other factors, such as irrigation method, depth to groundwater, and groundwater quality were different between the corn fields used, focusing the calibration on a single crop can avoid confounding effects from crop specific factors. As a result, the corn field regressions are better able to isolate the relationship between the reflectance indexes and soil salinity, leading to more consistent model performance.

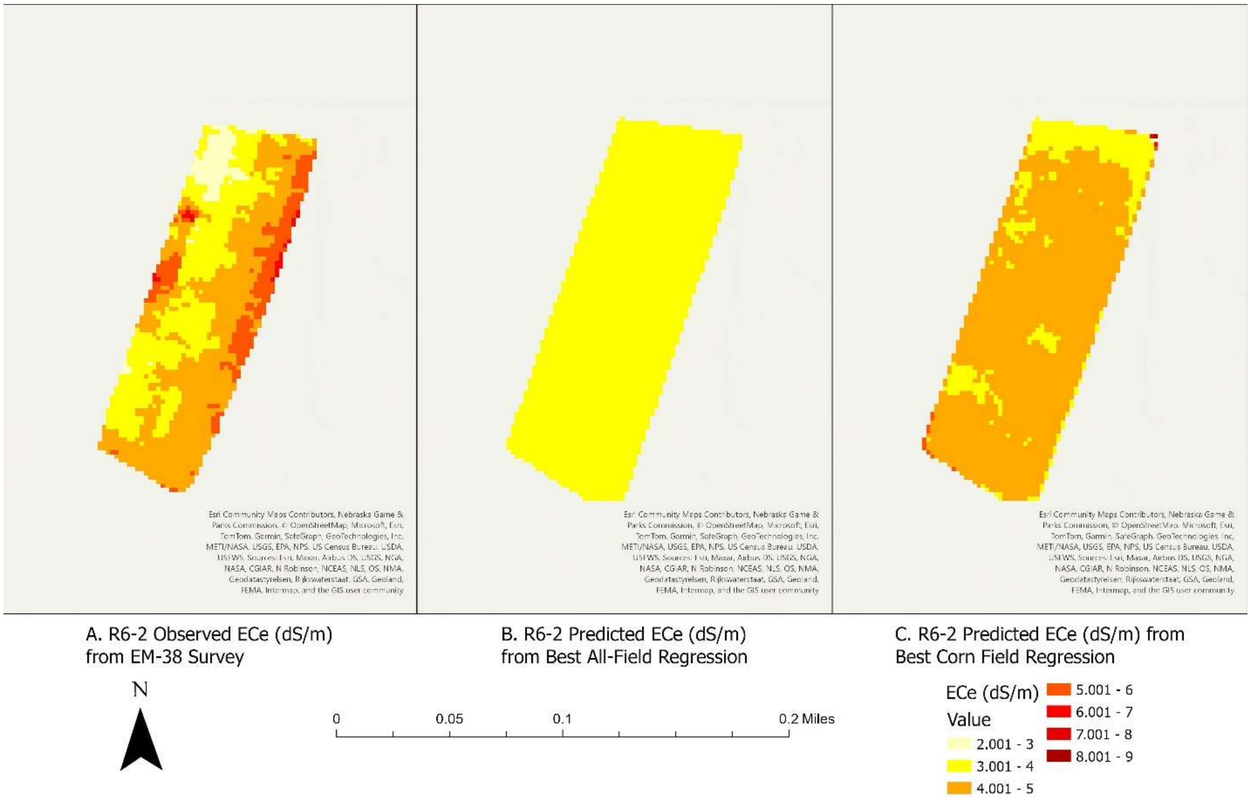

Figure 3.13 Comparison of observed and predicted soil electrical conductivity (EC_e, dS/m) for field R6-2. Panel A: Observed EC_e (dS/m) from the EM-38-MK2 survey. Panel B: Predicted EC_e (dS/m) from the best all field regression. Panel C: Predicted EC_e (dS/m) from the best corn field regression. The all field model underestimates spatial variability. The corn field only model better captures the observed salinity patterns across the field. Maps created in Arc GIS Pro.

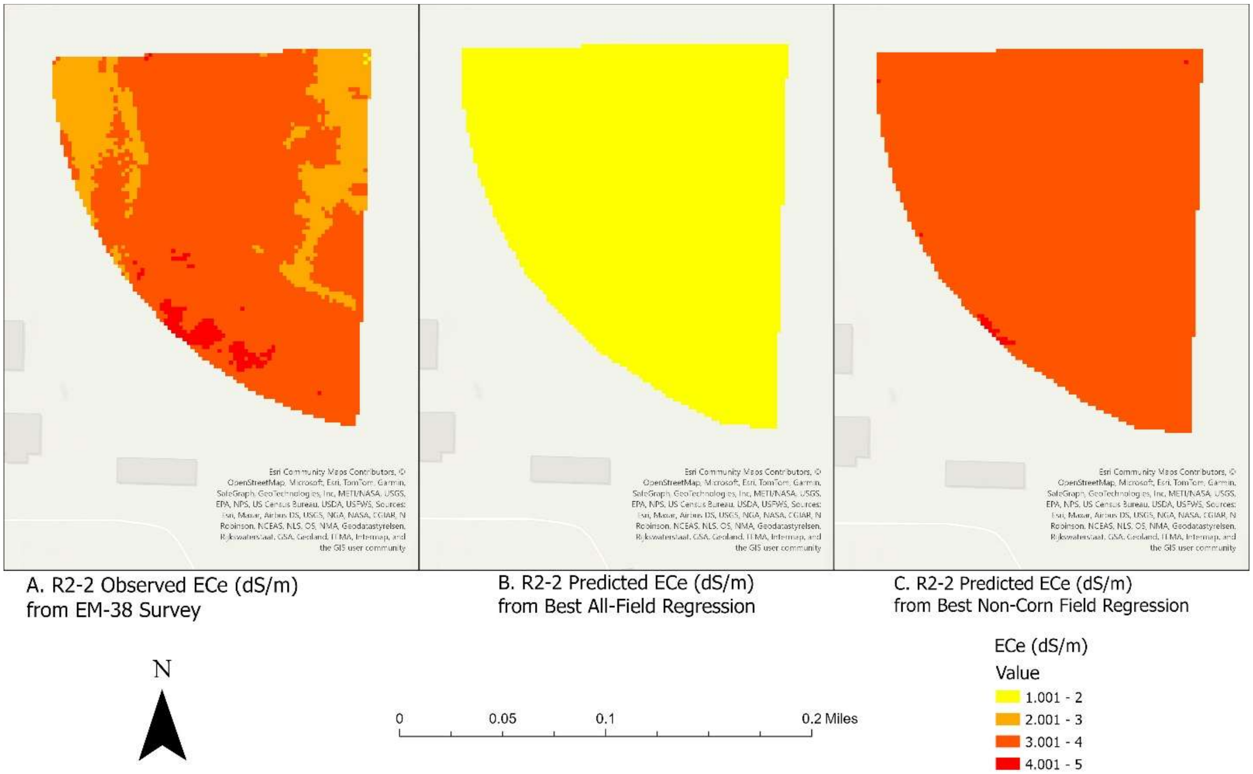

Figure 3.14 Comparison of observed and predicted soil electrical conductivity (EC_e, dS/m) for field R2-2. Panel A: Observed EC_e (dS/m) from the EM-38-MK2 survey. Panel B: Predicted EC_e (dS/m) from the best all field regression. Panel C: Predicted EC_e (dS/m) from the best non-corn field regression. The models cannot capture the variability in the field. The all field regression consistently underestimates EC_e. The non-corn field regression provides a closer estimation of soil salinity for the majority of the field but fails to capture the variability of lower and higher salinity areas. Maps created in Arc GIS Pro.

A key point of interest in the all-field regression was the consistent underestimation of EC_e in both corn and non-corn fields. Although the all-field regression does not have statistically significant bias, the mapped regression model consistently estimates EC_e to be 1-2 dS/m for these fields which does not match the observed EC_e range of 1-9 dS/m.

Another recurring pattern was the importance of the crop development phase (stage) on the accuracy of the EC_e models. Nearly 80% of fitted regression equations incorporated one or more variables tied to the development phase of crop growth. This trend likely exists because of the physiology of plants during this phase and the way remote sensing detects leaf canopy reflectance. Plant growth usually follows a sigmoidal curve (or S curve) where growth starts slowly before increasing exponentially then enters a linear phase of growth before reaching a plateau (Dambreville et al., 2014). The crop development phase corresponds to the linear phase where plants are rapidly expanding leaf area and adding biomass (Dambreville et al., 2014). In the early growth stages, plants tend to be more sensitive to environmental stresses like salinity (Atta et al., 2023). During the germination and development phase of growth, salts in soil can lead to poor root development which stunts the growth of the plant leading to visually smaller and sparser leaves and less dense canopies (Atta et al., 2023). At the same time, plant leaves tend to have higher chlorophyll content during this phase (Liu et al., 2019). Because chlorophyll strongly absorbs red and blue light while reflecting green and NIR wave lengths (Campbell and Wynne, 2011), changes in canopy expansion results in noticeable changes in indexes like NDVI, CRSI, and CWSI which rely on these wavelengths for their derivation. During other phases of growth, when the plant canopy is not changing as rapidly, plants become less sensitive to salinity, and a decrease in chlorophyll concentration leads to remote sensing indexes losing some of their sensitivity to crop stress caused by environmental stressors like salinity. Together, these factors provide insight into why models built from vegetation indexes consistently perform better when the development phase data is utilized.

Although development-phase data improved model performance, the accuracy of these models must also be evaluated. Figures 3.15 and 3.16 illustrate the error (difference) between the observed EC_e and the estimated EC_e from the best all fields model. These maps highlight the homogeneity of the model predictions relative to the substantial heterogeneity present in the observed data. The model-predicted EC_e values ranged between 1.15 and 1.30 dS/m for R2-2 and between 3.34 and 3.87 dS/m for R6-2, whereas the observed EC_e ranged from 1.86 to 4.68 dS/m in R2-2 and from 2.01 to 6.74 dS/m in R6-2. Both maps show that the model consistently underpredicts EC_e across these fields by as much as 3.5 dS/m. Even the average of the predicted EC_e values – 1.19 dS/m for R2-2 and 3.69 dS/m for R6-2 – show substantial error when compared to the average observed EC_e values of 3.33 dS/m for R2-2 and 4.2 dS/m for R6-2. The magnitude of error present in the all-field model renders it unsuitable for supporting field level soil salinity management decisions.

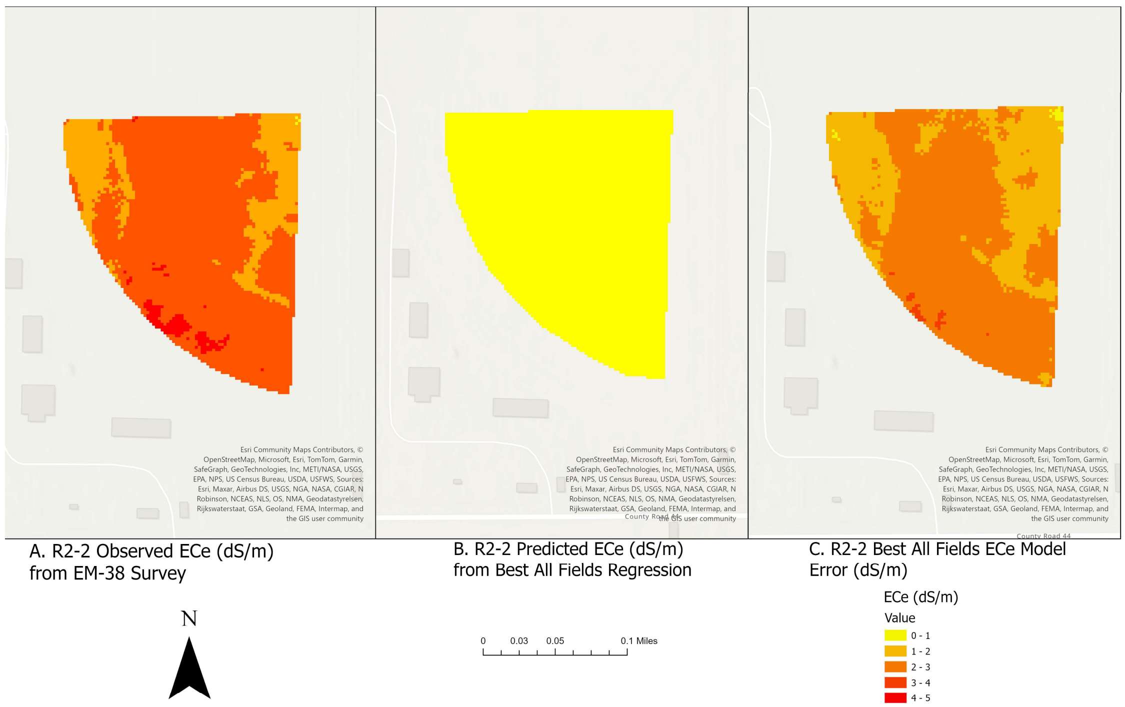

Figure 3.15 Comparison of observed and predicted soil electrical conductivity (EC_e, dS/m) for field R2-2. Panel A: Observed EC_e (dS/m) from the EM-38-MK2 survey. Panel B: Predicted EC_e (dS/m) from the best all field regression. Panel C: Error (observed-predicted EC_e) for Field R2-2. The error shown in the map highlights consistent underprediction across the field as predicted values lack the spatial variability present in the observed data. Map created in Arc GIS Pro.

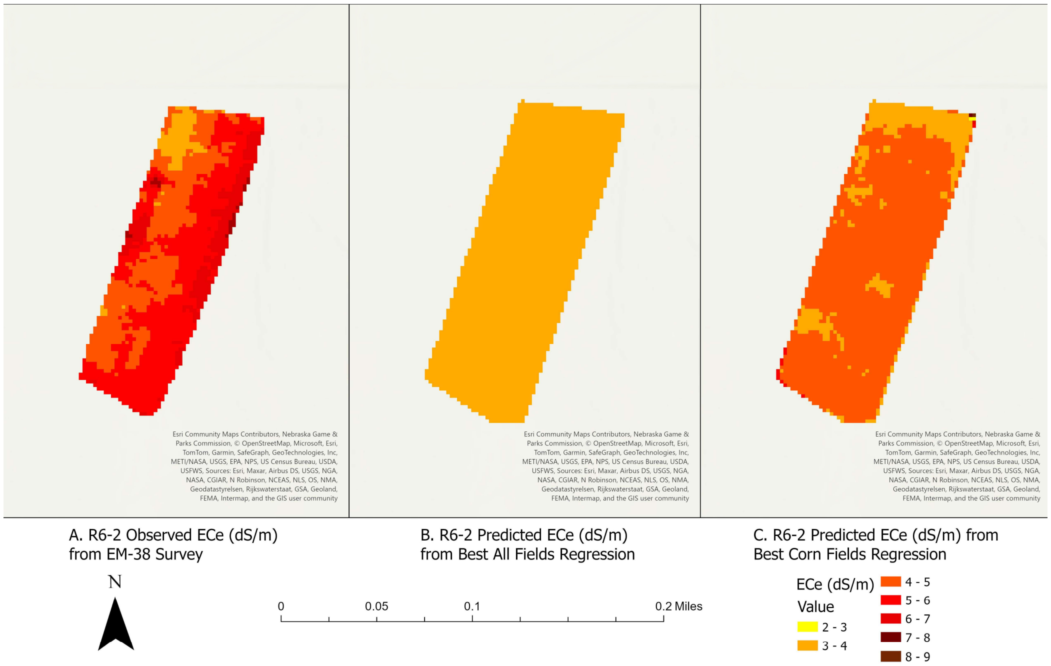

Figure 3.16 Comparison of observed and predicted soil electrical conductivity (EC_e, dS/m) for field R6-2. Panel A: Observed EC_e (dS/m) from the EM-38-MK2 survey. Panel B: Predicted EC_e (dS/m) from the best all field regression. Panel C: Error (observed-predicted EC_e) for Field R6-2. The error shown in the map highlights consistent underprediction across the field as predicted values lack the spatial variability present in the observed data. Map created in Arc GIS Pro.

To identify whether these specific fields are outliers, estimated EC_e was graphed against observed EC_e for the best model from each data set. The best all-field model plot shown in Figure 3.17 illustrates that for each field, the equation tends to estimate a constant value as opposed to varying with location in the field. While the predicted values generally align with the observed values, in areas where the observed data shows high variability the regression is inaccurate. The model from Equation 18 consistently underestimates or flattens out regions with higher salinity, leading to noticeable gaps between the orange and blue plots.

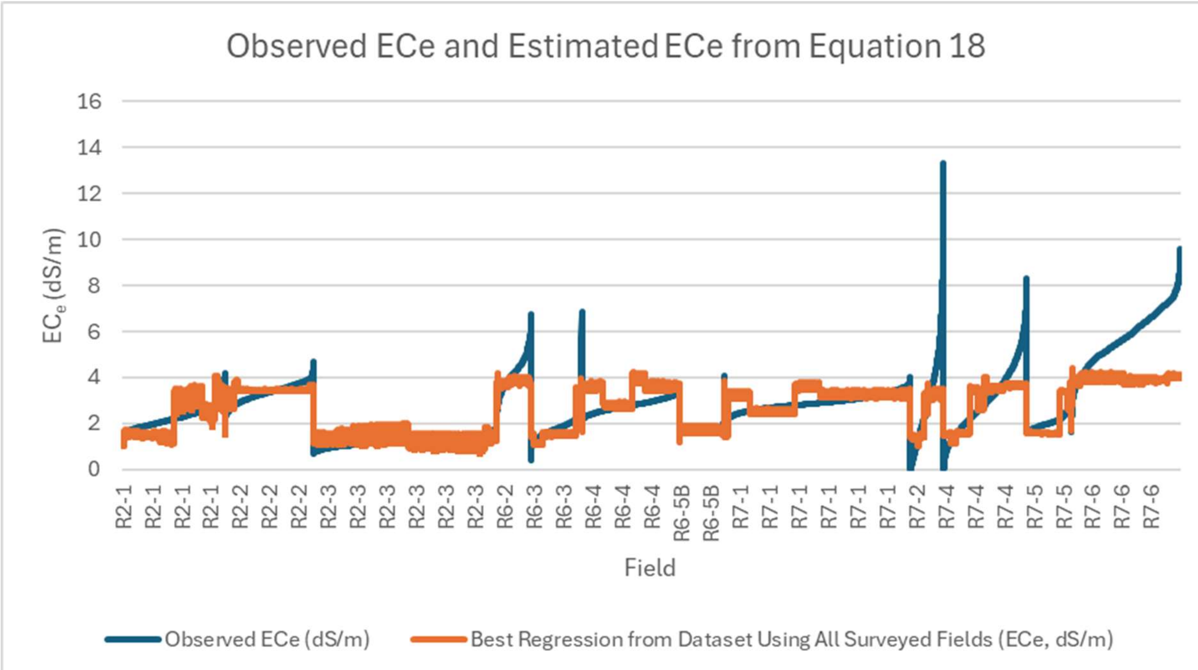

Figure 3.17 Observed ECe vs estimated ECe from the best all fields regression in dS/m. The estimated values consistently underestimate ECe within any given field.

Similar trends are shown in Figure 3.18, for the best non-corn field model (Equation 19). A little more variation can be seen with these estimates; however, even in moderate salinity areas, the model still fails to reflect the full range of variation seen in the observed data being especially pronounced in regions with high EC_e values. The best corn field model (Equation 20) – shown in Figure 3.19, like the best all-field and non-corn field models, tends to estimate the average for each field. While the con field model still fails to capture the observed variability within the fields, it shows much less error than the other models on average, with the largest errors occurring when the observed value is much lower or higher than the rest of the field. Based on these plots, the regressions perform best (error of about +/-1 dS/m) when the observed EC_e value is between 0 and 5 dS/m. Outside of this range, all best models show error that increases proportionally with the observed EC_e values.

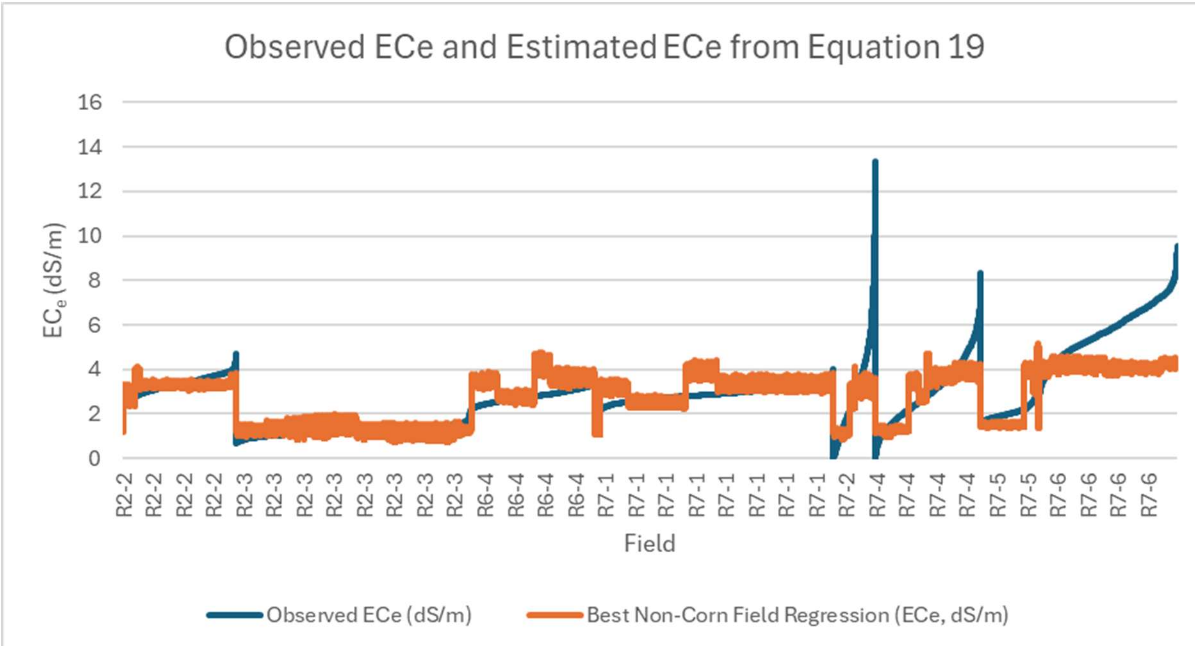

Figure 3.18 Observed EC_e vs estimated EC_e from the best non-corn fields regression in dS/m. The estimated values consistently underestimate EC_e within any given field.

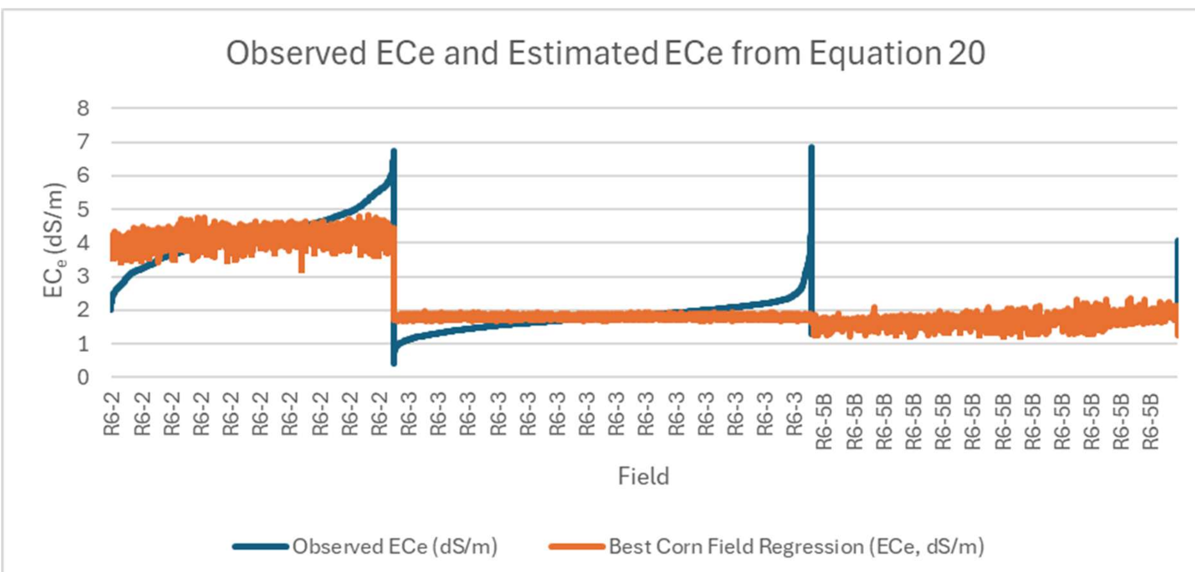

Figure 3.19 Observed EC_e vs estimated EC_e from the best corn fields regression in dS/m. The estimated values area about the average for the field unable to capture areas of high or low EC_e.

While the regression models exhibit limitations in utilizing remote sensing to estimate EC_e, applying a model across different remotely sensed data sets illustrates how the pixel size can influence variability. Figure 3.20 shows NDVI, CWSI, and the all-field EC_e model applied on LandSat's 30-meter pixel and PlanetScope's 5-meter pixel imagery as well as the EM-38-MK2 survey values interpolated through empirical Bayesian kriging. Generally, the two scales capture the same spatial trends with areas of high NDVI corresponding to low CWSI highlighting the relationship between dense healthy vegetation and low water stress. Although the trends are the same, the level of detail is noticeably different. The LandSat imagery shows a mostly homogenous field with a few localized spots of lower NDVI/high CWSI while the PlanetScope imagery shows considerable variation within those same areas. This indicates that within LandSat's 900 m^2 pixel, substantial heterogeneity may exist.

The calculated EC_e maps show a similar spatial distribution. The areas of higher calculated EC_e generally appear in similar locations at both scales; however, regardless of scale, the model (Equation 18) consistently underestimates salinity for the majority of the field when compared with the observed EC_e. Estimated EC_e values range from approximately 3.3-3.9 dS/m while observed values range from about 1-7 dS/m. LandSat's broader pixels show field scale trends but mask local zones of high salinity. PlanetScope's smaller pixel size can match the localized trends of the observed EC_e better than the LandSat data even if the model shows consistent underestimation. The contrast between the LandSat and PlanetScope estimated EC_e maps underscore how pixel size can mask or highlight spatial trends.

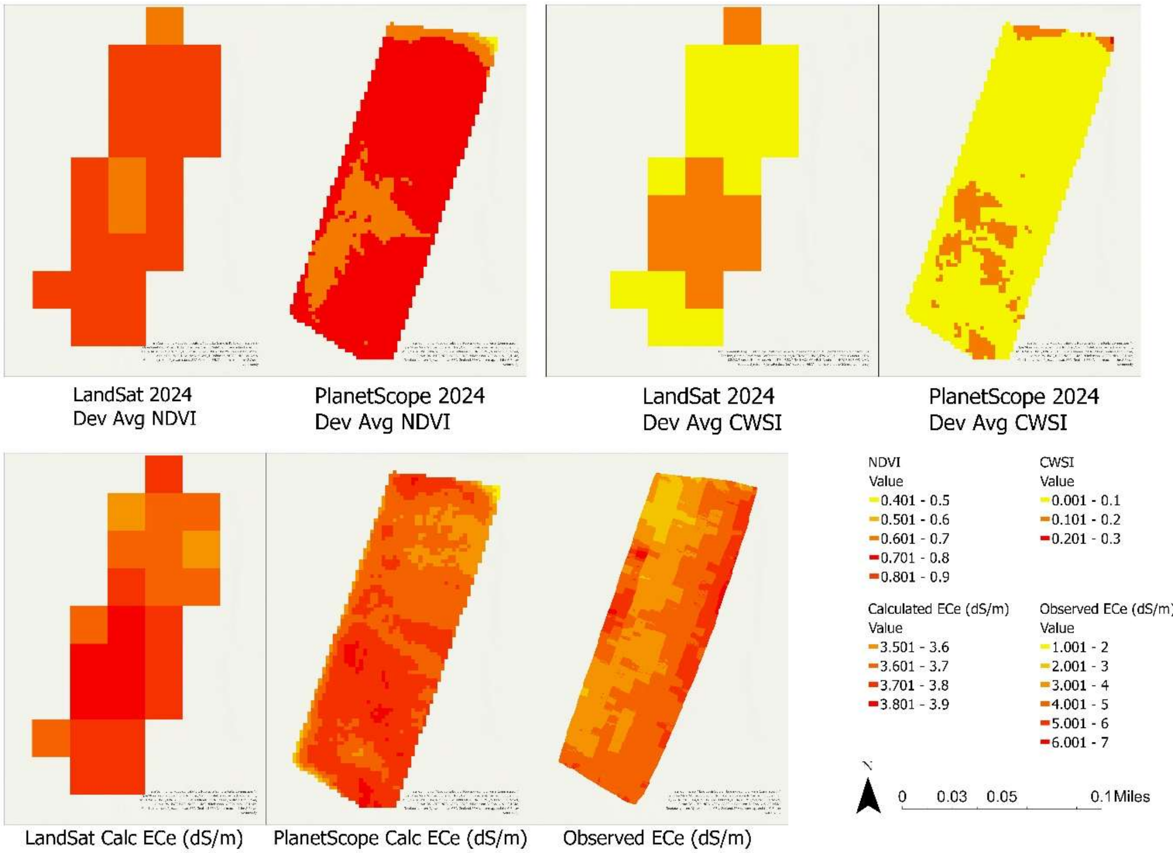

Figure 3.20 Comparison of vegetation indexes (NDVI and CWSI) and estimated soil salinity (EC_e) using 2024 LandSat (30-m) and PlanetScope (5-m) imagery as well as observed ECe from EM-38-MK2 surveys. LandSat maps (left panels) show field scale trends but mask sub field scale variability. PlanetScope (right panels) capture fine details within the field and more closely resemble the EM-38-MK2 data. Both calculated EC_e maps show similar spatial distribution but consistently underestimate the range of observed salinity values. Note the difference in the range of observed ECe and predicted ECe in the legend. Map created in ArcGIS Pro.

CHAPTER 4: CONCLUSIONS AND SUGGESTIONS FOR FURTHER WORK

Developing a model for mapping soil salinity in irrigated agricultural settings using remote sensing is necessary to monitor the temporal and spatial salinity changes over large regions. Soil salinity maps will aid decision makers in their understanding of the salinity problem as they develop management strategies to control the soil salinization process.

The objectives of this study were to:

1) evaluate selected remote sensing-based EC_e models in Colorado's South Platte River Basin (SPRB); and
2) calibrate selected EC_e models and/or develop new EC_e models for use in the SPRB.

These objectives tested the hypothesis that established remote sensing-based soil salinity models could be transferred to a new region with minimal local calibration.

Evaluating the EC_e methods presented in Scudiero et al. (2014, 2015) and Craig (2023) revealed they are not transferable to the CO SPRB region, even with local calibration efforts. The results do not support the adopted hypothesis. Within the Scudiero et al. (2014, 2015) method, the inability to produce accurate EC_e results in this study may be attributable to major climactic differences in the climate between California and Colorado as well as the different ranges of EC_e encountered in both locations. The Scudiero et al. (2014, 2015) model was developed using a very large and diverse dataset collected across extensive agricultural areas, whereas this study used fewer fields and smaller spatial extents. These differences in scale may reduce the transferability of the original model. To improve transferability, weather variables with the largest variation between the regions (average minimum temperature and total precipitation) were limited to the growing season and the EC_e model coefficients were calibrated using measured EC_e values, yet a relatively accurate EC_e equation could not be produced. As for the method presented in Craig (2023), it was not possible to improve the EC_e model for the SPRB. Additionally, the large pixel size of LandSat smoothed the variability present in the soil salinity which may explain why EC_e equations utilizing these remote sensing data were inaccurate. However, it was learned that the best EC_e estimates tended to utilize region-specific and growing-season-specific weather data.

New EC_e models were developed using both single year and multiyear datasets, as well as non-linear transformations of dependent and independent variables. The similarities between EC_e models developed using the all-field and non-corn field datasets suggest that the explanatory variables used (i.e., NDVI, CRSI, and CWSI) resulted in similar EC_e model performance across different crop types. While the best EC_e models developed using the all-field and non-corn field datasets showed acceptable levels of accuracy for regional mapping, they revealed important limitations. Specifically, using such diverse datasets limited the models' ability to capture the spatial variability of soil salinity.

In contrast, the corn fields EC_e models calibrated on fields with observed EC_e ranging from 1.23-4.81 dS/m consistently outperformed the all-field and non-corn field EC_e models across all regression statistics. Not only did the corn field models achieve higher predictive accuracy, but the mapped results also demonstrated their ability to better capture field-level variability in soil salinity. Among the three, the all-field model performed the poorest, consistently underestimating salinity and failing to represent variability across the field. The non-corn field model performed moderately better, capturing the average salinity levels but still missing much of the variability. The best model from each dataset performed most accurately when observed EC_e values were between 0 and 5 dS/m. At higher observed salinity levels, the models exhibited a proportional increase in error. However, this apparent increase in model error may be misleading, as it can be influenced by the EC_a-to-EC_e calibration. Consequently, it is unclear whether model performance truly declines at high salinity levels or if the apparent performance decline calibration related error.

Challenges encountered in finding a transferable model for predicting soil salinity using remote sensing data in the SPRB highlight the importance of region-specific adjustments when applying existing models to new areas. This study identified NDVI and weather data as important variables for improving model performance, highlighting how crop health can provide insight on underlying soil conditions. Additionally, incorporating data from the crop growth development phase has been shown to further enhance model accuracy, indicating crop growth phase is an influential factor in model accuracy.

The findings of this study align with the extensive early work on vegetation index-based soil EC estimation. Like Scudiero et al. (2014, 2015), this study found CRSI and NDVI are reliable indicators of soil EC especially when multiyear data are used. CWSI, a water stress variable, also helped enhance the accuracy of the models consistent with Craig (2023) and emphasizes the difficulty in separating crop response to each stressor present (water and salinity). Compared to studies like Peng et al. (2019) and Ramos et al. (2020), this study indicates that although vegetation indexes provide great predictive power, additional covariates improve model accuracy. In contrast to Wang et al. (2024), localized calibration is emphasized as spectral responses vary by crop type, growth stage, climate, etc. which will influence the accuracy of the soil EC model. This work adds to the growing body of evidence that vegetation indexes are powerful tools for estimating soil EC but underscores the need for localized models and for not assuming model transferability even across small geographic regions (i.e. Colorado's Arkansas River Basin to Colorado's South Platte River Basin).

Future research should refine both the input variables and modeling approaches used. For example, adjusting the ET estimates used in calculating CWSI to account for crop type may enhance the accuracy of salinity models as it accounts for differences in crop water use and root depth. Additionally, depth to ground water can heavily influence observed salinity and using it as an independent variable may improve model accuracy. Furthermore, consideration should be given to farm management practices like irrigation system type and irrigation water quality which can influence soil salinity. While these factors cannot be directly captured through remote sensing, they could be incorporated as categorical variables similar to the β in the Scudiero et al. (2014, 2015) model which adjusted predictions based on management practices (e.g. cropped or fallow fields). However, integrating management practices into a model would require reliable field level records which are often unavailable at large scales.

Since non-linear transformations of variables generally improved model accuracy, further exploration of advanced modeling techniques such as machine learning models may develop EC_e models which better capture the relationships between remotely sensed variables and soil salinity. While the multiple linear regression model structure has been used in this study and in many preceding studies, other model structures which are more time-consuming to experiment with in programs like RStudio and SigmaPlot may produce better models. Additionally, this study was conducted using multispectral data with specific bands in the red, green, blue and near infrared ranges. Because multispectral sensors average reflectance values over a somewhat broad range of wavelengths, hyperspectral imagery with continuous imaging via narrow-band measurements in the visible and near infrared spectrum may improve modeling as certain wavelengths may be able to detect minor changes in crops that the multispectral imagery does not capture. Future research should consider utilizing hyperspectral data to capture crop changes that may not be discernable with multispectral data.

Ultimately, this study underscores the complexity of modeling soil salinity in irrigated agricultural regions and highlights the need for locally-calibrated approaches. Further research is necessary to develop transferable models which can support long-term monitoring and management of soil salinity at regional and field scales.

REFERENCE LIST

Allen, R. G., Wright, J. L., Pruitt, W. O., Pereira, L. S., & Jensen, M. E. (2007). Chapter 8. Water Requirements. *Design and Operation of Farm Irrigation Systems, 2nd Edition*, 208–288. https://doi.org/10.13031/2013.23691

Allen, R., Morton, C., Kamble, B., Kilic, A., Huntington, J., Thau, D., Gorelick, N., Erickson, T., Moore, R., Trezza, R., Ratcliff, I. C., & Robison, C. (2015). EEFlux: A Landsat-based Evapotranspiration mapping tool on the Google Earth Engine. *ASABE Irrigation Symposium Paper* , *152143511*. https://digitalcommons.unl.edu/cgi/viewcontent.cgi?article=2465&context=natrespapers

Atta, K., Mondal, S., Shouvik Gorai, Singh, A., Kumari, A., Ghosh, T. K., Roy, A., Suryakant Hembram, Gaikwad, D. J., Mondal, S. S., Bhattacharya, S., Uday Chand Jha, & Jespersen, D. (2023). Impacts of salinity stress on crop plants: improving salt tolerance through genetic and molecular dissection. *Frontiers in Plant Science*, *14*. https://doi.org/10.3389/fpls.2023.1241736

Bandak, S., Movahedi-Naeini, S. A., Mehri, S., & Lotfata, A. (2024). A longitudinal analysis of soil salinity changes using remotely sensed imageries. *Scientific Reports*, *14*(1), 10383. https://doi.org/10.1038/s41598-024-60033-6

Barkerer, J. B., Neale, C. M. U., Heeren, D. M., & Suyker, A. E. (2018). Evaluation of a Hybrid Reflectance-Based Crop Coefficient and Energy Balance Evapotranspiration Model for Irrigation Management. *Transactions of the ASABE*, *61*(2), 533–548. https://doi.org/10.13031/trans.12311

Bennett, D., George, R., & Ryder, A. (1995). Soil salinity assessment using the EM38: Field operating instructions and data interpretation. In *Soil salinity assessment using the EM38:*

Field operating instructions and data interpretation. Department of Agriculture, Government of Western Australia. https://library.dpird.wa.gov.au/cgi/viewcontent.cgi?article=1152&context=misc_pbns

Bouaziz, M., Matschullat, J., & Gloaguen, R. (2011). Improved remote sensing detection of soil salinity from a semi-arid climate in Northeast Brazil. *Comptes Rendus Geoscience*, *343*(11-12), 795–803. https://doi.org/10.1016/j.crte.2011.09.003

Brown, A. (2023). *Electromagnetic Sampling Analysis and Prediction (ESAP V. 2.35) for Signal Processing Data Collected with EMI Instrumentation* [Powerpoint to Lucas Lenoch & Mike Ryan].

Campbell, J. B., & Wynne, R. H. (2011). *Introduction to Remote Sensing, Fifth Edition*. Guilford Press.

Collison, A., & Curdoglo, M. (2025). Planet Surface Reflectance. In *Surface Reflectance White Paper*. Planet Labs. https://assets.planet.com/marketing/PDF/Planet_Surface_Reflectance_Technical_White_Paper.pdf

Colorado Climate Center. (2018). *CoAgMET Crop ET Access*. CoAgMET Crop et Access; Colorado State University. https://coagmet.colostate.edu/cgi-bin/extended_etr_form.pl

Colorado Climate Center. (2024). *Homepage - CoAgMET*. Homepage; Colorado State University. https://coagmet.colostate.edu/

Colorado Climate Center. (2025). *CoAgMET Crop ET Coefficients*. Colostate.edu. https://coagmet.colostate.edu/crop_et_coefficients.html?utm_source=chatgpt.com

Colorado Department of Agriculture. (2025). *Colorado Produce Calendar* . Colorado Produce Calendar | Department of Agriculture; Colorado Department of Agriculture. https://ag.colorado.gov/markets/colorado-proud/colorado-produce-calendar

Colorado Division of Water Resources. (2019, November 19). *Division 1 Canals - Irrigation canals, ditches, and ditch service areas.* Division 1 - South Platte; Colorado Decision Support System. https://cdss.colorado.gov/gis-data/division-1-south-platte

Colorado Water Center. (2019). *Water Rights*. Water Rights | Colorado Water Knowledge | Colorado State University; Colorado State University. https://waterknowledge.colostate.edu/water-management-administration/water-rights/

Colorado Water Center. (2020). *Water Uses*. Water Uses | Colorado Water Knowledge | Colorado State University; Colorado State University. https://waterknowledge.colostate.edu/water-management-administration/water-uses/#1525208065430-1ccb9fc1-47bf

Colorado Water Center. (2025). *South Platte Salinity Stakeholder Group*. South Platte Salinity Stakeholder Group; Colorado State University. https://watercenter.colostate.edu/water-quality-and-access/south-platte-salinity-stakeholders/

Colorado Water Conservation Board. (2022). *Climate*. Climate | DNR CWCB; Colorado Department of Natural Resources. https://cwcb.colorado.gov/focus-areas/hazards/climate

Colorado Water Science Center. (2012, June 1). *South Platte Alluvial Aquifer Water-Level Monitoring*. South Platte Alluvial Aquifer Water-Level Monitoring; United States Geological Survey. https://www.usgs.gov/centers/colorado-water-science-center/science/south-platte-alluvial-aquifer-water-level-monitoring#overview

Conran, M. (2013, October 23). *Buy & Dry: Selling Agricultural Water to Growing Cities*. Buy & Dry: Selling Agricultural Water to Growing Cities; Colorado Public Radio. https://www.cpr.org/2013/10/23/buy-dry-selling-agricultural-water-to-growing-cities/

Corwin, D. L. (2003). Soil Salinity Measurement. *Encyclopedia of Water Science*, 852–857. https://www.ars.usda.gov/arsuserfiles/20361500/pdf_pubs/P1747.pdf

Corwin, D. L., & Lesch, S. M. (2005). Apparent soil electrical conductivity measurements in agriculture. *Computers and Electronics in Agriculture*, *46*(1-3), 11–43. https://doi.org/10.1016/j.compag.2004.10.005

Corwin, D. L., & Scudiero, E. (2019). Review of soil salinity assessment for agriculture across multiple scales using proximal and/or remote sensors. *Advances in Agronomy*, *158*, 1–130. https://doi.org/10.1016/bs.agron.2019.07.001

Corwin, D. L., & Scudiero, E. (2020). Field-scale apparent soil electrical conductivity. *Soil Science Society of America Journal*, *84*(5), 1405–1441. https://doi.org/10.1002/saj2.20153

Corwin, D. L., & Yemoto, K. (2017). Salinity: Electrical Conductivity and Total Dissolved Solids. *Methods of Soil Analysis*, *2*(1), 0. https://doi.org/10.2136/msa2015.0039

Craig, B. D. (2023). *Exploring the Contribution of Crop Water Use to Remotely Sensed Estimates of Soil Salinity in Irrigated Agriculture* [Thesis]. https://www.proquest.com/openview/119f6d182e67698ec73c56d968705df3/1?cbl=18750&diss=y&pq-origsite=gscholar

Cui, X., Han, W., Zhang, H., Dong, Y., Ma, W., Zhai, X., Zhang, L., & Li, G. (2023). Estimating and mapping the dynamics of soil salinity under different crop types using Sentinel-2 satellite imagery. *Geoderma*, *440*, 116738–116738. https://doi.org/10.1016/j.geoderma.2023.116738

Dambreville, A., Lauri, P.-É., Normand, F., & Guédon, Y. (2014). Analysing growth and development of plants jointly using developmental growth stages. *Annals of Botany*, *115*(1), 93–105. https://doi.org/10.1093/aob/mcu227

Dell US. (2024). Latitude 7230 Rugged Extreme Tablet Setup and Specifications. In *Latitude 7230 Rugged Extreme Tablet Setup and Specifications* (pp. 18–19). Dell US. https://dl.dell.com/content/manual20602438-latitude-7230-rugged-extreme-tablet-setup-and-specifications.pdf?language=en-us

Dennehy, K. F., Litke, D. W., Tate, C. M., Qi, S. L., McMahon, P. B., Bruce, B. W., Kimbrough, R. A., & Heiny, J. S. (1998). *Water Quality in the South Platte River Basin, Colorado, Nebraska, and Wyoming, 1992–95* (U.S. Geological Survey Circular 1167). United States Department of the Interior. https://pubs.usgs.gov/circ/circ1167/circ1167.pdf

Douaoui, A. E. K., Nicolas, H., & Walter, C. (2006). Detecting salinity hazards within a semiarid context by means of combining soil and remote-sensing data. *Geoderma*, *134*(1-2), 217–230. https://doi.org/10.1016/j.geoderma.2005.10.009

Environmental Equipment and Supply. (2025). *EM-38 MK2 with Archer Field PC and Hemisphere GPS - Environmental Equipment & Supply*. Environmental Equipment & Supply. https://www.envisupply.com/product/em-38-mk2-with-archer-field-pc-hemisphere-gps/

Eswar, D., Karuppusamy, R., & Chellamuthu, S. (2021). Drivers of soil salinity and their correlation with climate change. *Current Opinion in Environmental Sustainability*, *50*, 310–318. https://doi.org/10.1016/j.cosust.2020.10.015

Food and Agriculture Organization of the United Nations. (2015). *Status of the World's Soil Resources: Main Report*. United Nations. https://openknowledge.fao.org/items/f16010ce-1874-4108-bd03-a6a592e2e53a

Food and Agriculture Organization of the United Nations. (2017). *Water Scarcity*. Water Scarcity | Land & Water | Food and Agriculture Organization of the United Nations; United Nations. https://www.fao.org/land-water/water/water-scarcity/en/

Food and Agriculture Organization of the United Nations. (2020). *Global Soil Information System*. FAO GloSIS; United Nations. https://data.apps.fao.org/glosis/?lang=en

Food and Agriculture Organization of the United Nations. (2021). *The State of the World's Land and Water Resources for Food and Agriculture 2021 – Systems at breaking point*. United Nations. https://digitallibrary.un.org/record/3954263?v=pdf

Food and Agriculture Organization of the United Nations. (2025). *Annex 1. Crop salt tolerance data*. Www.fao.org. https://www.fao.org/4/y4263e/y4263e0e.htm

Galloway, D., & Riley, F. S. (1999). Mining Ground Water. In *Land Subsidence in the United States U.S. Geological Survey Circular 1182* (pp. 23–34). United States Department of the Interior. https://pubs.usgs.gov/circ/circ1182/

Geonics Limited. (2016). EM38-MK2 Ground Conductivity Meter Operating Manual. In *EM38*. Geonics Limited. https://geophysicalequipmentrental.com/files/2020/01/EM38-MK2-Operating-Manual.pdf

Ghada Sahbeni, Ngabire, M., Musyimi, P. K., & Balázs Székely. (2023). Challenges and Opportunities in Remote Sensing for Soil Salinization Mapping and Monitoring: A Review. *Remote Sensing*, *15*(10), 2540–2540. https://doi.org/10.3390/rs15102540

Giordano, M., Barron, J., & Ünver, O. (2019). Water Scarcity and Challenges for Smallholder Agriculture. *Sustainable Food and Agriculture*, 75–94. https://doi.org/10.1016/b978-0-12-812134-4.00005-4

Gowda, P. H., Chávez, J. L., Colaizzi, P. D., Evett, S. R., Howell, T. A., & Tolk, J. A. (2008). ET mapping for agricultural water management: present status and challenges. *Irrigation Science*, *26*(3), 223–237. https://doi.org/10.1007/s00271-007-0088-6

Hanson, C., Mazur, E., Stolle, F., Davis, C., & Searchinger, T. (2022, February 24). *5 Takeaways on Cropland Expansion and What It Means for People and the Planet*. 5 Takeaways on Cropland Expansion and What It Means for People and the Planet; World Resources Insitute. https://www.wri.org/insights/cropland-expansion-impacts-people-planet

Heggie, J. (2019, March 18). *How Can We Farm Our Unfarmable Land?* How Can We Farm Our Unfarmable Land?; National Geographic. https://www.nationalgeographic.com/science/article/partner-content-how-farm-our-unfarmable-land

Hoffman, G. J., & Evan, R. G. (2007). Chapter 1. Introduction. *Design and Operation of Farm Irrigation Systems, 2nd Edition*, 1–32. https://doi.org/10.13031/2013.23684

Idrisa, H., Kadam, S. A., & Gorantiwar, S. D. (2022). Estimation of Crop Coefficients Based on Normalize Difference Vegetation Index. *Journal of Agriculture Research and Technology*, *47*(03), 381–388. https://doi.org/10.56228/jart.2022.47320

Ingrao, C., Strippoli, R., Lagioia, G., & Huisingh, D. (2023). Water scarcity in agriculture: An overview of causes, impacts and approaches for reducing the risks. *Heliyon*, *9*(8). https://doi.org/10.1016/j.heliyon.2023.e18507

Ismayilov, A. I., Mamedov, A. I., Fujimaki, H., Tsunekawa, A., & Levy, G. J. (2021). Soil Salinity Type Effects on the Relationship between the Electrical Conductivity and Salt Content for 1:5 Soil-to-Water Extract. *Sustainability*, *13*(6), 3395. https://doi.org/10.3390/su13063395

Jia, K., Hasan, U., Jiang, H., Qin, B., Chen, S., Li, D., Wang, C., Deng, Y., & Shen, J. (2024). How frequent the Landsat 8/9-Sentinel 2A/B virtual constellation observed the earth for continuous time series monitoring. *International Journal of Applied Earth Observation and Geoinformation*, *130*, 103899–103899. https://doi.org/10.1016/j.jag.2024.103899

Kelly, A. (2024, March 9). *A Snapshot of Colorado Agriculture*. A Snapshot of Colorado Agriculture | Colorado General Assembly; Legislative Council. https://leg.colorado.gov/publications/snapshot-colorado-agriculture

Khorram, S., van der Wiele, C. F., Koch, F. H., Nelson, S. A. C., & Potts, M. D. (2016). *Principles of Applied Remote Sensing* (1st ed.). Springer. https://link.springer.com/book/10.1007/978-3-319-22560-9

Kumar, D. N., & Reshmidevi, T. V. (2013). Remote Sensing Applications in Water Resources. *Journal of the Indian Institute of Science*, *93*(2), 163–188. https://www.researchgate.net/publication/245538996_Remote_Sensing_Applications_in_Water_Resources

Kuzma, S., Bierkens, M. F. P., Lakshman, S., Luo, T., Saccoccia, L., Sutanudjaja, E. H., & Beek, R. V. (2023). Aqueduct 4.0: Updated Decision-Relevant Global Water Risk Indicators. *Aqueduct 4.0: Updated Decision-Relevant Global Water Risk Indicators*. https://doi.org/10.46830/writn.23.00061

Le Strange, M., & Jimenez, M. (2013). Vegetable Planting Guide for San Joaquin Valley Gardens [Online Image]. In *84716*. https://ucanr.edu/sites/default/files/2013-03/84716.pdf

Liu, A., Qu, Z., & Nachshon, U. (2020). On the potential impact of root system size and density on salt distribution in the root zone. *Agricultural Water Management*, *234*, 106118. https://doi.org/10.1016/j.agwat.2020.106118

Liu, C., Liu, Y., Lu, Y., Liao, Y., Nie, J., Yuan, X., & Chen, F. (2019). Use of a leaf chlorophyll content index to improve the prediction of above-ground biomass and productivity. *PeerJ*, *6*, e6240. https://doi.org/10.7717/peerj.6240

Liu, X., Liu, W., Tang, Q., Liu, B., Wada, Y., & Yang, H. (2022). Global Agricultural Water Scarcity Assessment Incorporating Blue and Green Water Availability Under Future Climate Change. *Earth's Future*, *10*(4). https://doi.org/10.1029/2021ef002567

Metternicht, G. I., & Zinck, J. A. (2003). Remote sensing of soil salinity: potentials and constraints. *Remote Sensing of Environment*, *85*(1), 1–20. https://doi.org/10.1016/S0034-4257(02)00188-8

Michel, D. (2023, October 16). Water and Food: How, When, and Why Water Imperils Global Food Security. *Center for Strategic and International Studies*. https://www.csis.org/analysis/water-and-food-how-when-and-why-water-imperils-global-food-security

Montgomery, D. C., & Runger, G. C. (2011). *Applied statistics and probability for engineers*. Wiley.

Nachtergaele, F., van Velthuizen, H., Verelst , L., Batjes, N., Dijkshoorn, K., van Engelen, V., Fischer , G., Jones, A., Montanarella, L., Petri, M., Prieler, S., Teixeira, E., Wiberg, D., &

Shi, X. (2009). Harmonized World Soil Database Version 1.1 . In *Harmonized World Soil Database - Version 1.1* . United Nations. https://www.fao.org/4/aq361e/aq361e.pdf

National Aeronautics and Space Administration. (2021a, May 18). *Remote Sensing*. Remote Sensing | NASA Earthdata; NASA. https://www.earthdata.nasa.gov/learn/earth-observation-data-basics/remote-sensing

National Aeronautics and Space Administration. (2021b, November 30). *History* . History | Landsat Science; National Aeronautics and Space Administration. https://landsat.gsfc.nasa.gov/satellites/history/

National Oceanic and Atmospheric Administration. (2025). *Central and Southern San Joaquin Valley Climate Graphs*. Central and Southern San Joaquin Valley Climate Graphs; National Weather Service. https://www.weather.gov/hnx/Cliplot

Natural Resources Conservation Service. (1997). Irrigation Guide. In *National Engineering Handbook*. United States Department of Agriculture. https://www.nrcs.usda.gov/sites/default/files/2023-01/7385.pdf

Natural Resources Conservation Service. (2011). Soil Quality Indicators Soil Electrical Conductivity. In *Soil Quality Indicators Soil Electrical Conductivity*. United State Department of Agriculture. https://www.nrcs.usda.gov/sites/default/files/2022-10/Soil%20Electrical%20Conductivity.pdf

Natural Resources Conservation Service. (2019). *Web Soil Survey*. Web Soil Survey - Home; United States Department of Agriculture. https://websoilsurvey.nrcs.usda.gov/app/

Natural Resources Conservation Service. (2022). Small Scale Solutions for your Farm Do You Have Problems With. In *Small Scale Solutions for Your Farm: Soil Testing*. United States

Department of Agriculture. https://www.farmers.gov/sites/default/files/2022-09/farmersgov-small-scale-factsheet-soil-testing-9-2022.pdf

Natural Resources Conservation Service. (2025). *AWS Plot*. AWS Plot; United States Department of Agriculture. https://nwcc-apps.sc.egov.usda.gov/awdb/basin-plots/POR/TAVG/assocHUC6/101900_South_Platte.html?hucFilter=10

NEIRBO Hydrogeology. (2020). *South Platte River Salinity*. Colorado State University. https://watercenter.colostate.edu/wp-content/uploads/sites/91/2023/10/South-Platte-CCAC-SalinityStudy_FinalDeliverable-Part-1.pdf

O'Connell, J. (2024, September 24). *Lecture 03 - Open Source Remote Sensing Image Products and Reflectance Indices* [Lecture to GR 503 Class].

ONSET. (2025a). HOBO® U20L Water Level Logger (U20L-0x) Manual. In *HOBO U20L Water Level Logger (U20L-0x) Manual*. ONSET. https://www.onsetcomp.com/sites/default/files/resources-documents/17153-G%20U20L%20Manual.pdf?srsltid=AfmBOoqG4zCl9WquG1OcUNzIh0_AtYicG2WlQXHLexfm5lfEe1RzyxUm

ONSET. (2025b). HOBO® U24 Conductivity Logger (U24-001) Manual. In *HOBO U23 Conductivity Logger (U24-001) Manual*. ONSET. https://www.onsetcomp.com/sites/default/files/resources-documents/15070-J%20U24-001%20Manual.pdf

Peng, J., Biswas, A., Jiang, Q., Zhao, R., Hu, J., Hu, B., & Shi, Z. (2019). Estimating soil salinity from remote sensing and terrain data in southern Xinjiang Province, China. *Geoderma*, *337*, 1309–1319. https://doi.org/10.1016/j.geoderma.2018.08.006

Philadelphia Water Department. (2024). Home Water Use. In *Home Water Use*. Philadelphia Water Department. https://water.phila.gov/wp-content/uploads/files/home-water-use-ig5.pdf

Planet Team. (2021). *Company*. Company | Planet; Planet Labs. https://www.planet.com/company/

Planet Team. (2025a). *Planet Application Program Interface: In Space for Life on Earth.* San Francisco, CA. https://api.planet.com

Planet Team. (2025b, March 17). *PlanetScope*. PlanetScope | Planet Documentation; Planet Labs. https://docs.planet.com/data/imagery/planetscope/

Ramos, T. B., Castanheira, N. L., Carolina, A., Ana Luísa Paz, Hanaa Darouich, Lucian Simionesei, Farzamian, M., & Jacirema, M. (2020). Soil salinity assessment using vegetation indices derived from Sentinel-2 multispectral data. application to Lezíria Grande, Portugal. *Agricultural Water Management*, *241*, 106387–106387. https://doi.org/10.1016/j.agwat.2020.106387

Ranganathan, J., Waite, R., Searchinger, T., & Hanson, C. (2018, December 5). *How to Sustainably Feed 10 Billion People by 2050, in 21 Charts*. How to Sustainably Feed 10 Billion People by 2050, in 21 Charts; World Resources Institute. https://www.wri.org/insights/how-sustainably-feed-10-billion-people-2050-21-charts

Romić, M., Zahalan, R., & Al-Zoubi, M. (2021). Standard operating procedure for saturated soil paste extract. In *Standard operating procedure for saturated soil paste extract*. United Nations. https://www.fao.org/fileadmin/user_upload/GSP/GLOSOLAN/Capacity_development/SOP-Saturated_Soil_Paste_Extract_GLOSOLAN_training_final.pdf

Roy, D., Huang, H., Houborg, R., & Martins, V. (2021). A global analysis of the temporal availability of PlanetScope high spatial resolution multi-spectral imagery. *Remote Sensing of Environment*, *264*, 112586. https://doi.org/10.1016/j.rse.2021.112586

Ryan, W., & Doesken, N. (2014). The Climate of the South Platte Basin. In *Microsoft PowerPoint - The Climate of the South Platte Basin*. Colorado State University. https://climate.colostate.edu/presentations/TheClimateoftheSouthPlatteBasin.pdf

Scudiero, E., Skaggs, T. H., & Corwin, D. L. (2014). Regional scale soil salinity evaluation using Landsat 7, western San Joaquin Valley, California, USA. *Geoderma Regional*, *2-3*, 82–90. https://doi.org/10.1016/j.geodrs.2014.10.004

Scudiero, E., Skaggs, T. H., & Corwin, D. L. (2015). Regional-scale soil salinity assessment using Landsat ETM + canopy reflectance. *Remote Sensing of Environment*, *169*, 335–343. https://doi.org/10.1016/j.rse.2015.08.026

Scudiero, E., Skaggs, T. H., & Corwin, D. L. (2016). Comparative regional-scale soil salinity assessment with near-ground apparent electrical conductivity and remote sensing canopy reflectance. *Ecological Indicators*, *70*, 276–284. https://doi.org/10.1016/j.ecolind.2016.06.015

Shahid, S. A., Zaman, M., & Heng, L. (2018). Soil Salinity: Historical Perspectives and a World Overview of the Problem. *Guideline for Salinity Assessment, Mitigation and Adaptation Using Nuclear and Related Techniques*, 43–53. https://doi.org/10.1007/978-3-319-96190-3_2

Shrestha, R. P. (2006). Relating soil electrical conductivity to remote sensing and other soil properties for assessing soil salinity in northeast Thailand. *Land Degradation & Development*, *17*(6), 677–689. https://doi.org/10.1002/ldr.752

Singh, A. (2021). Soil salinity: A global threat to sustainable development. *Soil Use and Management*, *38*(1). https://doi.org/10.1111/sum.12772

South Platte River Basin Stakeholders Group. (2025). *SPRB-Salinity Dashboard*. SPRB-Salinity; Colorado State University. https://southplattesalinity.erams.com/docs/?token=tIVkEh3PUy

Stavi, I., Thevs, N., & Priori, S. (2021). Soil Salinity and Sodicity in Drylands: A Review of Causes, Effects, Monitoring, and Restoration Measures. *Frontiers in Environmental Science*, *9*. https://doi.org/10.3389/fenvs.2021.712831

Svaldi, A. (2017, November 7). *What Colorado regions will grow fastest through 2050?* What Colorado Regions Will Grow Fastest through 2050?; Summit Daily. https://www.summitdaily.com/news/what-colorado-regions-will-grow-fastest-through-2050-the-answer-is-not-the-high-country/

Systat Software, Inc. (2023). SigmaPlot (Version 16) [Computer software]. https://systatsoftware.com/products/sigmaplot/

Thieu, N. V. (2021a). *BE - Mean Bias Error — Permetrics 2.0.0 documentation*. Readthedocs.io. https://permetrics.readthedocs.io/en/latest/pages/regression/MBE.html

Thieu, N. V. (2021b). *RMSE - Root Mean Square Error — Permetrics 2.0.0 documentation*. Readthedocs.io. https://permetrics.readthedocs.io/en/latest/pages/regression/RMSE.html

Thorvaldson, J., & Pritchett, J. (2005). Profile of the South Platte River Basin. In *Cooperative Extension, Colorado State University*. Colorado State University. https://pro15.org/wp-content/uploads/2017/03/CSUSouthPlatteRiverStudy-1.pdf

Tjur, T. (2009). Coefficients of Determination in Logistic Regression Models—A New Proposal: The Coefficient of Discrimination. *The American Statistician*, *63*(4), 366–372. https://doi.org/10.1198/tast.2009.08210

Trout, T. (2008). New Developments in Irrigation Scheduling. In *Microsoft Word - Trout08* (pp. 143–152). United States Department of Agriculture. https://www.k-state.edu/irrigate/oow/p08/Trout08.pdf

Trout, T. J., & DeJonge, K. C. (2018). Crop Water Use and Crop Coefficients of Maize in the Great Plains. *Journal of Irrigation and Drainage Engineering-Asce*, *144*(6). https://doi.org/10.1061/(asce)ir.1943-4774.0001309

Trout, T. J., & Johnson, L. F. (2007). Estimating crop water use from remotely sensed NDVI, crop models, and reference ET. *USCID Fourth International Conference*, 275–285. https://www.ars.usda.gov/ARSUserFiles/30121500/Publications/Trout07-ET-CC-NDVIICID.pdf

United Nations Water. (2022). *Water Scarcity*. Water Scarcity | UN-Water; United Nations. https://www.unwater.org/water-facts/water-scarcity

United States Bureau of Reclamation. (2020, November 4). *Water facts - worldwide water supply*. Water Facts - World Wide Water Supply; United States Bureau of Reclamation. https://www.usbr.gov/mp/arwec/water-facts-ww-water-sup.html

United States Department of Agriculture. (2022). *Normalized Difference Vegetation Index (NDVI)*. Ipad.fas.usda.gov/Cropexplorer/Definitions/Spotveg.htm; United States Department of Agriculture. https://ipad.fas.usda.gov/cropexplorer/Definitions/spotveg.htm

United States Department of Agriculture. (2025, January 8). *Irrigation & Water Use*. Irrigation & Water Use; United States Department of Agriculture. https://www.ers.usda.gov/topics/farm-practices-management/irrigation-water-use

United States Environmental Protection Agency. (2015a, September 2). *Secondary Drinking Water Standards: Guidance for Nuisance Chemicals*. Secondary Drinking Water Standards: Guidance for Nuisance Chemicals; United States Environmental Protection Agency. https://www.epa.gov/sdwa/secondary-drinking-water-standards-guidance-nuisance-chemicals

United States Environmental Protection Agency. (2015b). Standard Operating Procedure for the Standard/Well Volume Method for Collecting a Ground-Water Sample from Monitoring Wells for Site Characterization. In *finalgwsamp_sop.pdf*. United States Environmental Protection Agency. https://www.epa.gov/sites/default/files/2015-06/documents/finalgwsamp_sop.pdf

United States Geological Survey. (2000, June 19). *NAWQA South Platte River Basin Study*. NAWQA South Platte River Basin Study | U.S. Geological Survey; Colorado Water Science Center. https://www.usgs.gov/centers/colorado-water-science-center/science/nawqa-south-platte-river-basin-study

United States Geological Survey. (2024, May 31). *What are the band designations for the Landsat satellites?* What Are the Band Designations for the Landsat Satellites? | U.S. Geological Survey; United States Geological Survey. https://www.usgs.gov/faqs/what-are-band-designations-landsat-satellites

United States Geological Survey. (2025, June 5). *What are the acquisition schedules for the Landsat satellites? | U.S. Geological Survey*. Www.usgs.gov. https://www.usgs.gov/faqs/what-are-acquisition-schedules-landsat-satellites

Wang, N., Chen, S., Huang, J., Frappart, F., Taghizadeh, R., Zhang, X., Wigneron, J.-P., Xue, J., Xiao, Y., Peng, J., & Shi, Z. (2024). Global Soil Salinity Estimation at 10 m Using Multi-Source Remote Sensing. *Journal of Remote Sensing*, *4*. https://doi.org/10.34133/remotesensing.0130

Waskom, R. M. (2013). HB12-1278 Study of the South Platte River Alluvial Aquifer . In *Microsoft Word - HB1278 Final Report*. Colorado Water Institute. https://southplatte.colostate.edu/files/report/HB1278%20Final%20Report.pdf

Water Education Colorado. (2023a, April 5). *Agricultural Conservation & Efficiency*. Agricultural Conservation & Efficiency - Water Education Colorado; Water Education Colorado. https://watereducationcolorado.org/water-101/water-use-conservation-efficiency/agricultural-conservation-efficiency/#/

Water Education Colorado. (2023b, April 10). *South Platte River Basin*. South Platte River Basin - Water Education Colorado; Water Education Colorado. https://watereducationcolorado.org/water-101/hydrology-water-resources/major-river-basins/south-platte-river-basin/#/

Wilson, C. L., Fiedor, T. H., Anderson, D. L., Halley, A. A., & Crookston, M. A. (2005). A Study of Salinity in the Lower South Platte Basin . In *2004 Salinity Annual Summary*. Northern Colorado Water Conservancy District . https://www.northernwater.org/getattachment/e80a7f9d-43f0-4110-b130-911fc67ef64a/2004_Salinity_Annual_Summary.pdf

World Bank Group. (2024, October 9). *Agriculture and Food*. Agriculture Overview: Development News, Research, Data; World Bank. https://www.worldbank.org/en/topic/agriculture/overview

Wright, J. L. (1982). New Evapotranspiration Crop Coefficients. *Journal of the Irrigation and Drainage Division*, *108*(1), 57–74. https://doi.org/10.1061/jrcea4.0001372

Zajic, A. (2025, April 17). *What Is Akaike Information Criterion (AIC)?* What Is Akaike Information Criterion (AIC)? | Built In; Built In. https://builtin.com/data-science/what-is-aic

APPENDIX A: FIELD WORK PROCEDURES

GIDDINGS RIG PROCEDURE

Model: #25-SCS HDGSRPS

Inspection and Safety

1) First and foremost, inspect the machine and truck. Ensure you have all necessary fluids (gas for the engine, hydraulic fluid, motor oil), and confirm everything is secure. Inspect hydraulic lines for damage.
2) Hard hats, safety glasses, eye protection, ear protection, gloves, and steel-toe boots are critical. This is a powerful and loud machine. 2 people are needed to run this machine. Solo operation is not only dangerous but inefficient.
3) After your drill site is confirmed, be sure the area around it is level and compacted. This can be tricky in recently tilled or otherwise disturbed land. It is essential that the site where the hydraulic stabilizing foot drops down is compacted. You can use the hydraulic foot to compact the soil prior to drilling.
4) It is convenient to have all tools easily accessible before beginning to drill. A metal hammer, 9/16" wrenches or sockets, and a wire brush are needed. Have the red foot easily accessible.
5) Inspect Kelly bars and augers for damage, and set them in a convenient location next to the drill site. Pick the auger of choice or a soil sampler.
6) Be familiar with the hydraulic levers on the machine. There are 2 on each side of the mast. On the driver's side of the vehicle, one lever operates the mast, another operates the stabilizing foot. On the passenger side of the vehicle, one lever operates the height of the drill head, another operates the rotational speed and direction of the drill head.

Setup

7) With all tools ready and accessible, start the machine using the ignition. Choke is often needed upon starting. Turn the choke off (push in) after the engine has warmed up for a few seconds.

8) The push-pull lever next to the ignition is the throttle control. Leave the machine at idle while setting up, and only throttle up when needed. You may hear the machine struggle as you are drilling, this is an indication that more throttle is needed. Pull the lever out to throttle up and twist clockwise to lock the throttle in place.

9) Using the hydraulic lever, lift the mast into place. There is a small level located next to the hydraulic levers. Use these levels to ensure plumb drilling. There are 2 bolts for mast adjustment on the axis perpendicular to the hydraulic adjustment.

10) Once the mast is plumb, lower the foot using the lower driver's side lever to stabilize the machine. This may throw the mast out of plumb. Adjust accordingly. Always lift the foot before raising and lowering the mast.

Drilling

11) Once the machine is secure, install a Kelly bar and auger. Insert a Kelly bar into the drill head. Kelly bars only fit in the machine one way, the skinnier end goes on the bottom to attach to the auger. Use two people to install the Kelly bar. A clockwise twist on the barrel shape locking mechanism on the top of the head will lock the Kelly bar into place. Be sure you hear a ‘click’ and look under the small barrel to confirm the bar is locked.

12) With a Kelly bar installed, the auger will be installed next. Use the provided ⅜” x 2 ½” bolts to secure the auger to the Kelly bar. The hydraulic head may need lowered or raised to fit the auger below it.

13) Drilling may now commence. Communication is key while drilling. Have one person operate the hydraulic controls. The other prepares hardware and Kelly bars for adjustment. One hydraulic lever controls head height (up and down) and another controls rotational speed. Depending on the soil, it is usually advised to have a higher rotational speed and drop the head height slowly.

14) If soil does not automatically clear itself away from the hole, the auger will need to be lifted and cleaned every 4’ so buildup does not occur.

15) It is advised to use the 4’ marks on each Kelly bar for ease of operation and to know how far you have drilled. When you bottom out the drilling head, unlock it from the Kelly bar by twisting the top of the barrel clockwise. Watch for pinch points while doing this. Move the drilling head up 4’ so the head attaches to a blue mark on the Kelly bar. Continue drilling.

16) When you bottom out the Kelly bar after more drilling, attach another. Use 2 people to place the next bar into the one attached to the auger. Use the hydraulics to lift the drilling head above the connection point between the 2 Kelly bars. Have one person hold the top Kelly bar while moving the drilling head. Communication is important in these steps. There are many possible pinch points during these steps.

17) Use a provided ⅜” x 1 ¾” bolt and nut to secure the Kelly bars to one another. You may now continue drilling.

18) If soil is not clearing and you are having to clear the auger every 4', there is a lot of attaching and detaching of Kelly bars involved. This is the most dangerous and frequent step in the whole operation. Communication and watching out for one another are vital steps.

19) While the auger is in the hole but not at its lowest point, it is extremely critical to use the red foot on the Kelly bars at the ground surface while adding, subtracting, or moving the head. Failure to do so could result in a lost auger or Kelly bar which would be extremely difficult to remove.

20) Drill as far as needed. There is a 30' max depth with this machine, limited by the Kelly bars.

Cleanup and moving the auger for transportation

21) After your hole is complete, remove and clean all Kelly bars and augers. It is safe and polite to the other users of this drill rig to thoroughly clean and inspect everything after use.

22) Lift the stabilizing foot all the way up, and lower the mast back to the driving (lowest) position. Return all augers and soil sampling tools back to the box, and return the Kelly bars neatly stacked within their respective slot. Lock the augers and replace the pin that holds the Kelly bars in place.

23) Return all tools to the toolbox, and return the key for the drilling rig to the bag within the truck. Record the hours on the machine at this time.

MONITORING WELL CONSTRUCTION PROCEDURE

Materials & tools for well construction

- Concrete mix (1-2 80 lb bag/well)
- Bentonite chips (1 50 lb bag/well)
- Well cover (1/well)
- Grout basket (1/well)
- 2” Screen PVC (1-2 10’ sticks/well)
- 2” Solid PVC (1-3 10’ stick/well)
- 2” Threaded cap (1/well)
- 2” Slip cap (1-2/well)
- Water level meter
- Water (large barrel suggested, 50+ gallons)
- Wheelbarrow or bucket to mix concrete
- Tools for mixing and finishing concrete (hoe, shovel, trowel)
- Flathead screwdriver
- Hacksaw or similar to cut PVC pipe
- 9/16” wrench or socket for well cover
- Torpedo level
- T-post and driver
- Orange spray paint

Materials and tools for HOBO sensor installation

- HOBO sensors

    - Electrical Conductivity (EC) sensor- U24-001
    - 30' Water Level (30' WL) sensor- U20L-01
    - 13' Water Level (13' WL) sensor- U20L-04
- 1/16" stainless steel cable
- 1/16" ferrules and stops for stainless steel cable (4-6 each/well)
- ¼" x 3" eye hook and nut (1/well)
- Cutting tools for cable, such as lineman pliers
- Large crimping tool
- Drill with ¼" bit
- Long (30'+) soft tape measure

Well Construction Procedure

1) After drilling a 4 ¼" hole, clear out the well area of all loose soil.
2) Find your well depth using the water level meter. Lower the meter slowly until you hear it beep. Record depth from the soil surface.
3) Continue to lower the meter until you feel the line start to slack. Find the point where the line begins to tension slightly. This is the bottom of the well. Record this depth.
4) Carefully dig a 3' diameter x 8" deep hole concentric with the well. Be sure to not drop any loose soil into the well hole. This larger hole is for the well cover and concrete.
5) Using the depth to the bottom of the well (step 3), figure out your PVC needs. There will always be a section of solid PVC on top and screen PVC on the bottom.
6) Examples of PVC lengths:
    a) Well R2-1: total depth (TD) 29.5'

i) Used 2 x 10’ screen & 1 x 10’ solid (30’ total)

b) Well R2-2: TD 13’

i) Used 7.5’ screen & 5.5’ solid

7) Common sense is to be used in this step, rather than a precise set of guidelines. Consider that the water table may drop or rise and that we still want to collect measurements when that occurs. Also, consider that several feet (5’+, ideally 10’) of solid pipe is needed to keep out surface contaminants.

8) Cut your pipe. Be sure to only cut one end of each pipe, as they are threaded into one another. The top (solid) will always use a 2” slip cap. The bottom (screen) will use a 2” threaded cap if unaltered, or a 2” slip cap if the bottom is cut off.

9) It is recommended to fit the pipe lengths into the ground to mark the cut for the top piece, rather than rely on measurements. To do so, cap the bottom piece, carefully lower it (do not drop it), and add the second and third pieces (if needed). Push with moderate force as you feel the bottom.

10) Consider your final grade at this step. In the end, the top of the well cover will sit 2-3” above the ground surface. The top of the pipe will sit 3-4” below the top of the well cover, which is slightly below the grade. Mark the top piece of pipe, pull all pipe out, disconnect joints, and cut.

11) The grout basket needs to be installed near or on the joint of the screened and solid PVC. With the joint disconnected, slide the grout basket on the bottom of the solid pipe with the larger diameter facing up (like a funnel). Tighten the grout basket securely with a flathead screwdriver.

12) Lower the capped screen pipe back into the hole, holding it securely. Attach a second piece of screen pipe if needed, then the solid pipe with the grout basket already installed. When threading the pipe together, be sure you cannot see the black o-ring in the joint. If you can see the black o-ring, it is not threaded completely. Water is a good lubricant for these threads. Be careful not to cross-thread.

13) Continue to lower the pipe. The grout basket will keep the pipe centered within the hole.

14) When the bottom is reached, push the pipe down with moderate force.

15) Confirm the top is cut at an appropriate height. Trim if needed.

16) Fill the annulus with alternating layers roughly 6” tall of bentonite chips and water, until you reach the bottom of the well cover. Add water to assure all the bentonite is hydrated.

17) Gently place a 2” slip cap on the top of the pipe to prevent debris from falling in.

18) Set the well cover in place. Be sure the top of the cover is about 2” above grade, and centered over the 2” pipe. Put the boltholes for the cover facing east and west, with the triangle on the lid facing north. Level the cover. Be sure the cover is secured with some soil while concrete is being poured.

19) Mix one 80 lb bag of concrete. A drier mix is preferred for this application, as it will be easier to form by hand and reduces set time.

20) Carefully pour or scoop concrete around the well cover. The diameter of the concrete should be 3’, and pitching away from the well.

21) Clean off all concrete tools immediately after use to prevent drying.

22) Paint the top 2’ of a T-post orange and install it within 2’ of the well.

23) Grade the surrounding area that was disturbed by the drilling and construction operations.

Figure A.1 Example of finished well.

HOBO Sensor Installation

Note: This installation guide assumes all sensors are already launched with the proper identification, logging intervals, and logging parameters.

1) With the well construction complete, remove the cover with a 9/16” wrench or socket.
2) Remove the 2” PVC slip cap and drill a centered ¼” hole on the top of the slip cap.
3) Install the eye hook so that the bottom of the slip cap is in line with the top of the stainless cable. See the picture below.

Figure A.2 Example of eyehook attachment to 2" slip cap.

4) Using the water level meter and a straight edge, find the depth of the water table from the top of the well cover. Record this depth.
5) Use the water level meter to find the bottom of the well by measuring the depth till the line starts to go slack, from the top of the well cover.
6) The difference between these two is the water table depth.
   a) Example: Well R2-1
      i) Top of water table: 27.2'
      ii) Bottom of well: 29.8'
      iii) Water table depth: 2.6'
7) This measurement will be used to calculate the length of the stainless steel cable that suspends the sensors in place.

8) Measure the distance from the top of the well cover to the bottom of the slip cap. It should be roughly 4”.

9) Using the ferrule and stop kit, crimp one end of the stainless cable to the eye hook (see the above picture).

    a) Start by inserting the end of the cable through the ferrule

    b) Loop the cable through the eye hook then insert it back into the ferrule, leaving a 1” tail out of the ferrule. Crimp the ferrule

    c) Insert the tail end into the small stop. Crimp the stop. This stop is a safety in case the ferrule ever becomes loose, which is unlikely if crimped properly

10) On flat ground, lay the soft measuring tape and stainless cable next to each other.

11) Offset the PVC slip cap on the distance between the top of the well cover and the bottom of the slip cap (from step 8). This is critical as the well depth was measured from the top of the well cover.

12) If installing a 13’ WL sensor for barometric pressure, install this approximately 1’ below the bottom of the slip cap. Crimp. Install the other end of the stainless cable to the bottom of this sensor to continue.

13) If the barometric pressure is not needed at this well, skip step 12.

14) Use the water table depth from step 6 for the proper placement of the 30’ WL and EC sensors. The midpoint of the water table depth will be the midpoint between the 30’ WL and EC sensors.

    a) Example: Well R2-1

        i) Water table depth: 2.6’

        ii) Midpoint: 1.3’

iii) Depth to water (step 4): 27.2’

iv) Midpoint of EC and 30’ WL sensors: 27.2’ + 1.3’ = 28.5’

15) The calculated midpoint from step 14.a.iv is the midpoint of the EC and 30’ WL sensors. The sensors should be 2-3” apart from each other.

16) The EC sensor must always go on the bottom, as it only has one attachment point. The 30’ WL sensor has attachment points on the top and bottom.

17) With the sensors laid out next to the cable and measuring tape, assure everything is parallel and flat, and that the PVC cap is offset the amount measured in step 8.

18) Cut the stainless steel cable 4” longer than the top point of the 30’ WL sensor. Crimp the water level sensor on the cable.

19) Cut a 6-8” section of cable, loop through the top of the EC sensor and bottom of the 30’ WL sensor, and crimp. Put these sensors as close together as possible (2-3” is reasonable). See the picture below:

Figure A.3 Example of EC and 30’ WL sensor chained together.

20) At this point, double-check all your measurements and assure all ferrules and stops are properly crimped. Re-do any crimps if needed.

21) Carefully lower the chain of sensors into the hole. The PVC cap and eyehook assure that the sensors cannot be dropped into the well.

22) Gently install the PVC cap. Do not push it down all the way as this makes it difficult to remove later.

23) Replace the well cover and clean up the well site.

Low-flow Ground Water Sampling Procedure

Supplies

- In-Situ Aquatroll 500, calibrated and charged
- In-Situ low-flow apparatus
- ⅜" I.D. tubing
- In-line filter
- Clean sampling bottles
- Water level meter

Procedure

- Assuming all equipment has been cleaned, follow these steps
- Take initial water level and In-Situ readings
- Purge 3x well volumes (water height in deet x 0.163 = well volume in gallons)
    - The mini-typhoon pump at full rate usually pumps roughly 1.5gal/min
    - Do not purge more than 6 well volumes

- The top of pump should be placed at the middle of the water column.
    - Well depth - water level = water column height
    - Water column height/2 + Water level = pump depth from manhole cover
    - Add 2 feet to reach the In-Situ low flow apparatus
- Connect the In-Situ device to the Vu-Situ app on you phone or tablet.
- Set up a low flow test in the Vu-Situ app, adding the correct well location, parameters, and tolerances:
    - pH: Refer to sheet in grey notebook
    - Conductivity: Refer to sheet in grey notebook
    - Flow rate: 75 mL/min
- Begin the test AFTER starting the pump to prime the system.
- Once desired parameters stabalize, divert the flow into the filter and collect sample.
- Mark location, time and date on sample bottle
- Put sample on ice immediately, ship ASAP

Procedure for HOBO data collection and analysis

After files have been offloaded from the shuttle onto a computer, follow these steps. Each numerical step should be completed for EVERY site before moving onto the next step.

1) Export data to a .csv

- Open files in HOBOware Pro
- Export Table Data (Ctrl + E)
    - Confirm every row is selected
    - Save as .csv

- Organize sequentially in saved folder (R2-1_WL.1, R2-1_WL.2, etc)
    - This part can be tedious. Slow down & take care.

2) Crop and add to existing data

- I do this step in Google Sheets, simply to have a cohesive, cloud-based set of data.
- Do this step one site at a time
- Open .csv files for the site
- Find the earliest (at the beginning) and latest (at the end) occurrences of consistent data. ALWAYS delete the first and last complete rows for consistency (i.e. the “logged” rows)
- Copy data and add to the respective datasheet.
    - Confirm timestamps line up!
- Add barometric data from the closest site
    - Region 2: R2-
    - Region 6: R6-
    - Region 7: 1, 2, 3, 5 use R7-5
    - 4, 6 use R7-6

3) Analysis

- I usually complete these steps in Excel rather than Google Sheets.
- Complete columns N-T in the spreadsheet. The following equations are used to calculate water table depth from water and barometric pressure:

N: (C-K)

O: N*144

P: (Avg. D&H)

Q: Chart

R: O5/(Q5*32.2) hw

S: From notes Lc-Lr

T: (S-R)

U: EC (dS/m)= G/1000

V: Date, from J, formatted date only (NO timestamps)

W: Manual Water table depth readings

X: Manual Electrical Conductivity readings

4) Graphing

- Alas! You can graph.
- Highlight column J, T, and V
- Insert-> Recommended Charts -> First option

Title: Electrical Conductivity & Water Table Depth Vs. Time, SITE

Left Column Title: Electrical Conductivity (dS/cm)

Right Column Title: Water Table Depth (ft)

Horizontal Axis Title: Date

Legend: Blue: Water Table Depth (ft) Red: Electrical Conductivity (dS/cm)

SOIL METADATA PROCEDURE

Data Description:

Type - Soil Moisture, Bulk Density, Salinity, ECe

Source - Soil Samples and EM-38

Key Characteristics - Volumetric Soil Moisture, Bulk Density, Salinity

Procedures:

Soil Moisture, Bulk Density, and Salinity

- Navigate to GPS points designated by ESAP-RSSD
- Use bucket auger to take samples every 30cm starting at surface to 150cm
    - Divide samples in two parts; one part to be oven dried and measured for moisture and one part to be shipped to lab for salinity analysis
- Simultaneously use Modera Probe to take bulk density samples from undisturbed soil

ECe

- Determine survey area in field, centered on irrigation source and minimum of 20 acres
- Walk survey area with EM-38 device using 10m spacing transects
- Process data using ESAP-SigDPA and ESAP-RSSD to determine 6 soil sampling locations

Purpose:

To calibrate ECe data and determine field characteristics

File Type:

Excel and CSV files

APPENDIX B: SUMMARY OF BEST REGRESSIONS BASED ON AICc

Table B.1 Summary of the 20 best regressions from the all-field, corn field, and non-corn field datasets.

Dependent Variable	Report	AICc	Delta	Weight	R-Squared	MBE	NMBE	RMSE	NRMSE	Variables
ln(ECe)	2024 All Field Report 7	-10750.3	0	0.999741635	0.683	-0.1125	-4.04382	0.927427	33.33519	Dev Avg NDVI, Dev Avg CWSI, ln Dev Avg NDVI, ln Dev Avg CWSI, Dev Precip, Dev Avg Min Temp
ln(ECe)	2024 All Field Report 7	-10319.1	431.2301	2.28798E-94	0.683	-0.12769	-4.58959	0.930217	33.43547	Dev Avg NDVI, Dev Avg CRSI, Dev Avg CWSI, ln Dev Avg NDVI, ln Dev Avg CWSI, Dev Precip, Dev Avg Min Temp

ln(ECe)	2024 All Field Report 7	-10220.6	98.50312	4.07574E-22	0.683	-0.12383	-4.45099	0.930846	33.45805	Dev Avg NDVI, Dev Avg CRSI, Dev Avg CWSI, ln Dev Avg NDVI, ln Dev Avg CRSI, ln Dev Avg CWSI, Dev Precip, Dev Avg Min Temp
ln(ECe)	2024 All Field Report 7	-9145.23	1075.376	3.0545E-234	0.68	-0.11336	-4.07467	0.937916	33.7122	Dev Avg NDVI, Dev Avg CWSI, ln Dev Avg NDVI, Dev Precip, Dev Avg Min Temp
ln(ECe)	2024 All Field Report 3	-4106.3	5038.932	0	0.675	-0.11915	-4.28272	0.971565	34.92166	Avg NDVI, Avg CRSI, Avg CWSI, ln Avg

										CRSI, Dev Precip, Dev Avg Min Temp
ln(ECe)	2024 All Field Report 3	-3928.62	177.6732	2.62204E-39	0.676	-0.11054	-3.97338	0.972747	34.96413	Avg NDVI, Avg CRSI, Avg CWSI, ln Avg NDVI, ln Avg CRSI, ln Avg CWSI, Dev Precip, Dev Avg Min Temp
ln(ECe)	2024 All Field Report 3	-3587.33	341.2972	7.72942E-75	0.676	-0.12778	-4.5928	0.975086	35.04822	Avg NDVI, Avg CRSI, Avg CWSI, ln Avg NDVI, ln Avg CRSI, Dev Precip,

										Dev Avg Min Temp
ln(ECe)	2024 All Field Report 3	-3209.73	377.5958	1.01393E-82	0.673	-0.13792	-4.95742	0.977694	35.14194	Avg NDVI, Avg CRSI, ln Avg CRSI, Dev Precip, Dev Avg Min Temp
ln(ECe)	2024 All Field Report 7	-1511.76	1697.973	0	0.669	-0.13577	-4.88004	0.989394	35.56249	Dev Avg CWSI, ln Dev Avg NDVI, Dev Precip, Dev Avg Min Temp
ln(ECe)	2024 All Field Report 3	-1182.48	329.2805	3.14443E-72	0.667	-0.13812	-4.96443	0.991676	35.64453	Avg CWSI, ln Avg NDVI, Dev Precip, Dev Avg Min Temp
ln(ECe)	2024 All Field Report 7	2294.935	3477.41	0	0.661	-0.12768	-4.58924	1.016118	36.52306	ln Dev Avg NDVI, Dev Precip,

										Dev Avg Min Temp
ln(ECe)	2024 All Field Report 3	2895.42	600.4856	4.0373E-131	0.66	-0.14434	-5.18812	1.020397	36.67685	Avg NDVI, Dev Precip, Dev Avg Min Temp
ln(ECe)	2024 All Field Report 7	3614.917	719.4972	5.795E-157	0.647	-0.13741	-4.93887	1.025562	36.8625	Dev Precip, Dev Avg Min Temp
ln(ECe)	2024 All Field Report 8	5327.013	1712.095	0	0.66	-0.12942	-4.65189	1.037879	37.30524	Mid Avg NDVI, Mid Avg CRSI, ln Mid Avg CRSI, Annual Precip, Annual Avg Min Temp
ln(ECe)	2024 All Field Report 8	5489.395	162.3826	5.48207E-36	0.664	-0.12909	-4.64004	1.039016	37.34608	Mid Avg NDVI, Mid Avg CRSI, Mid Avg CWSI, ln Mid Avg NDVI, ln Mid Avg CRSI, ln

										Mid Avg CWSI, Annual Precip, Annual Avg Min Temp
ln(ECe)	2024 All Field Report 8	5505.917	16.52176	0.000258365	0.664	-0.13105	-4.71034	1.03915	37.35092	Mid Avg NDVI, Mid Avg CRSI, ln Mid Avg NDVI, ln Mid Avg CRSI, ln Mid Avg CWSI, Annual Precip, Annual Avg Min Temp
ln(ECe)	2024 All Field Report 8	5667.827	161.9104	6.94226E-36	0.662	-0.12967	-4.66076	1.040343	37.39379	Mid Avg NDVI, Mid Avg CRSI, ln Mid Avg NDVI, ln Mid Avg CRSI, Annual Precip, Annual

										Avg Min Temp
ln(ECe)	2024 All Field Report 8	9958.113	4290.285	0	0.65	-0.13978	-5.02431	1.07208	38.53455	Mid Avg NDVI, Mid Avg CRSI, ln Mid Avg CRSI, Annual Precip
ln(ECe)	2024 All Field Report 8	12016.72	2058.605	0	0.638	-0.14168	-5.09233	1.087651	39.09423	Mid Avg NDVI, Mid Avg CRSI, Annual Precip
ln(ECe)	2024 All Field Report 1	16711.52	4694.804	0	0.629	-0.13828	-4.97035	1.123899	40.39711	Avg NDVI, Avg CRSI, Avg CWSI, ln Avg NDVI, ln Avg CRSI, ln Avg CWSI, Annual Precip, Annual Avg Min Temp

ECe	Multiyear Corn Field Report 12	-13001.8	0	0.07325581	0.84	-0.00074	-0.03083	0.474487	19.80504	Dev Max Avg NDVI, Dev Max Avg CRSI, Dev Max Avg CWSI, ln Dev Max Avg NDVI, ln Dev Avg CRSI, ln Dev Max Avg CWSI, Annual Avg Min Temp
ECe	Multiyear Corn Field Report 14	-13001	0.779402	0.049613173	0.84	0.004547	0.189802	0.474508	19.80592	Dev Max Avg NDVI, Dev Max Avg CRSI, Dev Max Avg CWSI, ln Dev Max Avg NDVI, ln Dev Avg

										CRSI, ln Dev Max Avg CWSI, Dev Avg Min Temp
ECe	Multiyear Corn Field Report 12	-12999.6	1.403336	0.036317128	0.84	-0.00031	-0.01308	0.474655	19.81206	Dev Max Avg NDVI, Dev Max Avg CWSI, ln Dev Max Avg NDVI, , ln Dev Max Avg CWSI, Annual Avg Min Temp
ECe	Multiyear Corn Field Report 14	-12998.7	0.845356	0.048003773	0.84	-0.00468	-0.19531	0.474678	19.81302	Dev Max Avg NDVI, Dev Max Avg CWSI, ln Dev Max Avg NDVI, ln Dev Max Avg CWSI,

										Dev Avg Min Temp
ECe	Multiyear Corn Field Report 14	-12996.7	2.003799	0.02689816	0.84	0.005637	0.23528	0.474678	19.81302	Dev Max Avg NDVI, Dev Max Avg CWSI, ln Dev Max Avg NDVI, ln Dev Avg CRSI, ln Dev Max Avg CWSI, Dev Avg Min Temp
ECe	Multiyear Corn Field Report 12	-12972.9	23.8549	4.83967E-07	0.84	-0.0001	-0.00421	0.475436	19.84466	Dev Max Avg NDVI, ln Dev Max Avg NDVI, ln Dev Max Avg CWSI, Annual Avg Min Temp
ECe	Testing Report 13.1	-12972.8	0.071735	0.070674885	0.84	-0.00136	-0.05659	0.475438	19.84474	Dev Max Avg NDVI, ln

	Report 78									Dev Max Avg NDVI, ln Dev Max Avg CWSI, Seasonal Precip
ECe	Multiyear Corn Field Report 14	-12972.7	0.152336	0.067883252	0.84	-0.00241	-0.10059	0.475442	19.84491	Dev Max Avg NDVI, ln Dev Max Avg NDVI, ln Dev Max Avg CWSI, Dev Avg Min Temp
ECe	Testing Report 13.2 Report 22	-12971.7	0.989914	0.044656539	0.84	-0.00232	-0.09702	0.475414	19.84376	Dev Max Avg NDVI, Dev Max Avg CRSI, ln Dev Max Avg NDVI, ln Dev Max Avg CWSI, Seasonal

										Avg Min Temp
ECe	Testing Report 13.1 Report 79	-12971.5	0.147716	0.06804025	0.84	-0.00594	-0.24774	0.475473	19.8462	Dev Max Avg NDVI, ln Dev Max Avg NDVI, ln Dev Max Avg CWSI, Seasonal Avg Min Temp
ECe	Testing Report 13.2 Report 39	-12971.5	0.028982	0.072201909	0.84	-0.0034	-0.14211	0.475419	19.84396	Dev Max Avg NDVI, ln Dev Max Avg NDVI, ln Dev Max Avg CRSI, ln Dev Max Avg CWSI, Seasonal Avg Min Temp
ECe	Testing Report 13.2	-12971.3	0.232324	0.065221906	0.84	0.004149	0.17318	0.475425	19.84422	Dev Max Avg NDVI, ln Dev Max

	Report 38									Avg NDVI, ln Dev Max Avg CRSI, ln Dev Max Avg CWSI, Seasonal Precip
ECe	Testing Report 13.2 Report 21	-12970.8	0.457396	0.058280033	0.84	0.005229	0.218274	0.475438	19.84474	Dev Max Avg NDVI, Dev Max Avg CRSI, ln Dev Max Avg NDVI, ln Dev Max Avg CWSI, Seasonal Precip
ECe	Multiyear Corn Field Report 12	-12948.4	22.43598	9.83855E-07	0.84	0.035825	1.495325	0.475994	19.86797	Dev Max Avg NDVI, Dev Max Avg CWSI, ln Dev Max Avg NDVI, ln

										Dev Avg CRSI, ln Dev Max Avg CWSI, Annual Avg Min Temp
ECe	Testing Report 10.2 Report 55	-12861.2	87.17622	8.60529E-21	0.838	0.000487	0.020344	0.478431	19.96969	Dev Avg NDVI, Dev Max Avg CWSI, ln Dev Avg NDVI, ln Dev Max Avg CWSI, Seasonal Precip
ECe	Testing Report 10.2 Report 103	-12860.2	0.967047	0.045170035	0.838	0.001259	0.052557	0.478403	19.9685	Dev Avg NDVI, Dev Max Avg CWSI, ln Dev Avg NDVI, ln Dev Max Avg CRSI, ln Dev Max Avg CWSI,

										Seasonal Precip
ECe	Testing Report 10.2 Report 91	-12860.2	0.014547	0.072724923	0.838	-0.00022	-0.00902	0.478403	19.96852	Dev Avg NDVI, Dev Max Avg CRSI, Dev Max Avg CWSI, ln Dev Avg NDVI, ln Dev Max Avg CWSI, Seasonal Precip
ECe	Testing Report 10.2 Report 56	-12860	0.202668	0.066196235	0.838	0.005592	0.233399	0.478464	19.97104	Dev Avg NDVI, Dev Max Avg CWSI, ln Dev Avg NDVI, ln Dev Max Avg CWSI, Seasonal Avg Min Temp
ECe	Testing Report 10.2	-12859.8	0.220368	0.065612985	0.838	0.003613	0.150798	0.478415	19.969	Dev Avg NDVI, Dev Max

	Report 104									Avg CWSI, ln Dev Avg NDVI, ln Dev Max Avg CRSI, ln Dev Max Avg CWSI, Seasonal Avg Min Temp
ECe	Testing Report 10.2 Report 92	-12859.7	0.11254	0.069247537	0.838	-0.00375	-0.15656	0.478418	19.96913	Dev Avg NDVI, Dev Max Avg CRSI, Dev Max Avg CWSI, ln Dev Avg NDVI, ln Dev Max Avg CWSI, Seasonal Avg Min Temp
ln (ECe)	2024 Non Corn Report 7	-2343.02	0	1	0.7	-0.12562	-4.31613	0.979046	33.63749	Dev Avg NDVI, Dev Avg CRSI,

										Dev Avg CWSI, ln Dev Avg NDVI, ln Dev Avg CRSI, ln Dev Avg CWSI, Dev Precip, Dev Avg Min Temp
ln (ECe)	2024 Non Corn Report 7	-536.227	1806.795	0	0.697	-0.11268	-3.8714	0.995045	34.18719	Dev Avg NDVI, Dev Avg CRSI, Dev Avg CWSI, ln Dev Avg NDVI, ln Dev Avg CRSI, Dev Precip, Dev Avg Min Temp
ln (ECe)	2024 Non Corn Report 7	505.6827	1041.91	5.652E-227	0.692	-0.15046	-5.16951	1.004416	34.50914	Dev Avg NDVI, Dev Avg CWSI, ln Dev Avg NDVI, Dev

										Precip, Dev Avg Min Temp
ln (ECe)	2024 Non Corn Report 7	2338.798	1833.116	0	0.694	-0.05552	-1.9076	1.021034	35.0801	Dev Avg CRSI, Dev Avg CWSI, ln Dev Avg NDVI, ln Dev Avg CRSI, Dev Precip, Dev Avg Min Temp
ln (ECe)	2024 Non Corn Report 3	4924.281	2585.482	0	0.698	-0.1109	-3.81024	1.044968	35.90241	Avg NDVI, Avg CRSI, ln Avg NDVI, ln Avg CRSI, Dev Precip, Dev Avg Min Temp
ln (ECe)	2024 Non Corn Report 3	5054.502	130.2211	5.28271E-29	0.699	-0.1133	-3.89266	1.046151	35.94304	Avg NDVI, Avg CRSI, Avg CWSI, ln

										Avg NDVI, ln Avg CRSI, ln Avg CWSI, Dev Precip, Dev Avg Min Temp
ln (ECe)	2024 Non Corn Report 3	5312.13	257.6281	1.13965E-56	0.684	-0.13649	-4.68931	1.048644	36.02871	Avg NDVI, Avg CRSI, ln Avg CRSI, Dev Precip
ln (ECe)	2024 Non Corn Report 3	5435.635	123.5058	1.51727E-27	0.699	-0.13669	-4.69627	1.049749	36.06667	Avg NDVI, Avg CRSI, ln Avg NDVI, ln Avg CRSI, ln Avg CWSI, Dev Precip, Dev Avg Min Temp

ln (ECe)	2024 Non Corn Report 3	6593.426	1157.79	3.8822E-252	0.692	-0.13473	-4.62899	1.060736	36.44414	Avg NDVI, Avg CRSI, ln Avg NDVI, ln Avg CRSI, Dev Precip
ln (ECe)	2024 Non Corn Report 7	6701.642	108.2162	3.17073E-24	0.683	-0.15206	-5.22444	1.061784	36.48016	Dev Avg CWSI, ln Dev Avg NDVI, Dev Precip, Dev Avg Min Temp
ln (ECe)	2024 Non Corn Report 3	9320.845	2619.203	0	0.671	-0.14359	-4.93343	1.087021	37.34723	Avg NDVI, Avg CRSI, Dev Precip
ln (ECe)	2024 Non Corn Report 3	10819.87	1499.024	0	0.659	-0.14002	-4.8106	1.101742	37.85301	Dev Precip, Dev Avg Min Temp
ln (ECe)	2024 Non Corn Report 7	12003.67	1183.803	8.7175E-258	0.671	-0.16124	-5.5398	1.113473	38.25604	ln Dev Avg NDVI, Dev Precip,

										Dev Avg Min Temp
ln (ECe)	2024 Non Corn Report 8	12212.74	209.0684	3.99374E-46	0.68	-0.13769	-4.73051	1.115461	38.32435	Mid Avg NDVI, Mid Avg CRSI, Mid Avg CWSI, ln Mid Avg NDVI, ln Mid Avg CRSI, ln Mid Avg CWSI, Annual Precip, Annual Avg Min Temp
ln (ECe)	2024 Non Corn Report 8	13193.06	980.3203	1.337E-213	0.67	-0.15172	-5.21254	1.125364	38.66461	Mid Avg NDVI, Mid Avg CRSI, ln Mid Avg CRSI, Annual Precip, Annual Avg Min Temp
ln (ECe)	2024 Non	13266.52	73.45877	1.11849E-16	0.678	-0.14443	-4.96217	1.126065	38.68868	Mid Avg NDVI, Mid Avg

	Corn Report 8									CRSI, ln Mid Avg NDVI, ln Mid Avg CRSI, ln Mid Avg CWSI, Annual Precip, Annual Avg Min Temp
ln (ECe)	2024 Non Corn Report 8	13553.37	286.8469	5.15218E-63	0.676	-0.14988	-5.14936	1.128984	38.78896	Mid Avg NDVI, Mid Avg CRSI, ln Mid Avg NDVI, ln Mid Avg CRSI, Annual Precip, Annual Avg Min Temp
ln (ECe)	2024 Non Corn Report 8	14954.46	1401.091	5.7152E-305	0.66	-0.15096	-5.18654	1.14329	39.28048	Mid Avg NDVI, Mid Avg CRSI, Annual Precip, Annual

										Avg Min Temp
ln (ECe)	2024 Non Corn Report 8	18630.65	3676.191	0	0.649	-0.15721	-5.40129	1.181604	40.59685	Mid Avg NDVI, Mid Avg CRSI, Annual Precip
ln (ECe)	2024 Non Corn Report 5	19265.47	634.8268	1.4096E-138	0.646	-0.15454	-5.30963	1.18826	40.82554	Dev Avg NDVI, Dev Avg CRSI, Dev Avg CWSI, ln Dev Avg NDVI, ln Dev Avg CRSI, ln Dev Avg CWSI, Annual Precip

APPENDIX C: RELEVANT SIGMAPLOT REPORTS

2024 All Field Report 1 Dependent Variable ln(ECe)
Best Subsets Regression Friday, April 25, 2025 5:45:18 PM

Data source: Data 1 in 2024 All Field Optimization Data

Using R squared as best criterion.

Table C.1 2024 All-Field Report 1 Variable Definitions.

Variable	Symbol
Avg NDVI	A
Avg CRSI	B
Avg CWSI	C
ln Avg NDVI	D
ln Avg CRSI	E
ln Avg CWSI	F
Annual Precipitation	G
Annual Avg Min Temp	H

Table C.2 2024 All-Field Report 1 Model Summary.

Model #	Variable	Cp	Rsqr	Adj Rsqr	MSerr	A	B	C	D	E	F	G	H
1	1	8108.039	0.587	0.587	0.118							*	
2	2	3862.748	0.609	0.609	0.111				*			*	
3	3	2173.145	0.618	0.618	0.109	*					*	*	
4	4	1430.072	0.622	0.621	0.108	*	*			*		*	
5	5	526.233	0.626	0.626	0.107	*	*			*		*	*
6	6	104.477	0.628	0.628	0.106	*	*			*	*	*	*
7	7	23.973	0.629	0.629	0.106	*	*	*		*	*	*	*
8	8	9.000	0.629	0.629	0.106	*	*	*	*	*	*	*	*

Table C.3 2024 All-Field Report 1 Model 1 Coefficients.

Model # 1	**R squared**	**0.587**			
Variable	**Coef.**	**Std. Error**	**t**	**P**	**VIF**
Constant	-0.720	0.00522	-138.038	<0.001	0.000
Annual Precipitation	0.00495	0.0000155	318.533	<0.001	1.000

Table C.4 2024 All-Field Report 1 Model 2 Coefficients.

Model # 2 **R squared** **0.609**

Variable	Coef.	Std. Error	t	P	VIF
Constant	-0.380	0.00738	-51.521	<0.001	0.000
ln Avg NDVI	0.263	0.00414	63.479	<0.001	1.383
Annual Precipitation	0.00436	0.0000178	245.034	<0.001	1.383

Table C.5 2024 All-Field Report 1 Model 3 Coefficients.

Model # 3	R squared	0.618			
Variable	**Coef.**	**Std. Error**	**t**	**P**	**VIF**
Constant	-0.890	0.00550	-161.817	<0.001	0.000
Avg NDVI	0.847	0.0114	74.492	<0.001	2.712
ln Avg CWSI	0.0297	0.000696	42.664	<0.001	2.071
Annual Precipitation	0.00417	0.0000182	229.256	<0.001	1.478

Table C.6 2024 All-Field Report 1 Model 4 Coefficients.

Model # 4	R squared	0.622			
Variable	**Coef.**	**Std. Error**	**t**	**P**	**VIF**
Constant	88.995	2.230	39.916	<0.001	0.000
Avg NDVI	1.501	0.0224	66.970	<0.001	10.651 <
Avg CRSI	-92.348	2.273	-40.625	<0.001	3999.896 <
ln Avg CRSI	73.090	1.864	39.211	<0.001	3801.100 <
Annual Precipitation	0.00455	0.0000175	260.465	<0.001	1.377

Table C.7 2024 All-Field Report 1 Model 5 Coefficients.

Model # 5	R squared	0.626			
Variable	**Coef.**	**Std. Error**	**t**	**P**	**VIF**
Constant	96.539	2.230	43.293	<0.001	0.000
Avg NDVI	1.661	0.0229	72.517	<0.001	11.260 <
Avg CRSI	-100.029	2.273	-43.998	<0.001	4051.311 <
ln Avg CRSI	78.969	1.863	42.394	<0.001	3843.683 <
Annual Precipitation	0.00445	0.0000176	252.215	<0.001	1.424
Annual Avg Min Temp	-0.0648	0.00216	-29.988	<0.001	1.090

Table C.8 2024 All-Field Report 1 Model 6 Coefficients.

Model # 6	R squared	0.628

Variable	Coef.	Std. Error	t	P	VIF
Constant	69.580	2.581	26.961	<0.001	0.000
Avg NDVI	1.661	0.0228	72.751	<0.001	11.260 <
Avg CRSI	-72.503	2.632	-27.544	<0.001	5462.933 <
ln Avg CRSI	56.661	2.151	26.345	<0.001	5154.092 <
ln Avg CWSI	0.0165	0.000801	20.571	<0.001	2.827
Annual Precipitation	0.00429	0.0000192	223.575	<0.001	1.696
Annual Avg Min Temp	-0.0619	0.00216	-28.630	<0.001	1.095

Table C.9 2024 All-Field Report 1 Model 7 Coefficients.

Model # 7	R squared	0.629			
Variable	Coef.	Std. Error	t	P	VIF
Constant	68.578	2.582	26.563	<0.001	0.000
Avg NDVI	1.850	0.0309	59.888	<0.001	20.640 <
Avg CRSI	-71.628	2.633	-27.209	<0.001	5470.259 <
Avg CWSI	0.233	0.0256	9.082	<0.001	19.662 <
ln Avg CRSI	56.197	2.150	26.137	<0.001	5156.998 <
ln Avg CWSI	0.0157	0.000805	19.535	<0.001	2.858
Annual Precipitation	0.00434	0.0000198	219.150	<0.001	1.804
Annual Avg Min Temp	-0.0600	0.00217	-27.633	<0.001	1.105

Table C.10 2024 All-Field Report 1 Model 8 Coefficients.

Model # 8	R squared	0.629			
Variable	Coef.	Std. Error	t	P	VIF
Constant	64.362	2.777	23.178	<0.001	0.000
Avg NDVI	1.579	0.0728	21.704	<0.001	114.457 <
Avg CRSI	-67.091	2.853	-23.513	<0.001	6427.787 <
Avg CWSI	0.319	0.0330	9.644	<0.001	32.711 <
ln Avg NDVI	0.165	0.0401	4.120	<0.001	137.118 <
ln Avg CRSI	52.540	2.326	22.589	<0.001	6036.100 <
ln Avg CWSI	0.0148	0.000836	17.705	<0.001	3.081

Annual Precipitation	0.00433	0.0000199	217.715	<0.001	1.821
Annual Avg Min Temp	-0.0599	0.00217	-27.616	<0.001	1.105

2024 All Field Report 3 Dependent Variable ln(ECe)
Best Subsets Regression Friday, April 25, 2025 5:45:56 PM

Data source: Data 1 in 2024 All Field Optimization Data

Using R squared as best criterion.

Table C.11 2024 All-Field Report 3 Variable Definitions.

Variable	Symbol
Avg NDVI	A
Avg CRSI	B
Avg CWSI	C
ln Avg NDVI	D
ln Avg CRSI	E
ln Avg CWSI	F
Dev Precipitation	G
Dev Avg Min Temp	H

Table C.12 2024 All-Field Report 3 Model Summary.

Model #	Variable	Cp	Rsqr	Adj Rsqr	MSerr	A	B	C	D	E	F	G	H
1	1	18961.161	0.590	0.590	0.117							*	
2	2	6385.662	0.647	0.647	0.101							*	*
3	3	3486.802	0.660	0.660	0.097	*						*	*
4	4	1932.920	0.667	0.667	0.095			*	*			*	*
5	5	532.128	0.673	0.673	0.093	*	*			*		*	*
6	6	68.257	0.675	0.675	0.092	*	*	*		*		*	*
7	7	35.682	0.676	0.676	0.092	*	*	*	*	*		*	*
8	8	9.000	0.676	0.676	0.092	*	*	*	*	*	*	*	*

Table C.13 2024 All-Field Report 3 Model 1 Coefficients.

Model # 1	**R squared**	**0.590**			
Variable	**Coef.**	**Std. Error**	**t**	**P**	**VIF**
Constant	-0.380	0.00417	-91.296	<0.001	0.000
Dev Precipitation	0.0483	0.000151	320.442	<0.001	1.000

Table C.14 2024 All-Field Report 3 Model 2 Coefficients.

Model # 2	**R squared**	**0.647**			
Variable	**Coef.**	**Std. Error**	**t**	**P**	**VIF**
Constant	-3.622	0.0304	-119.088	<0.001	0.000
Dev Precipitation	0.0394	0.000163	242.217	<0.001	1.352

Dev Avg Min Temp	0.257	0.00239	107.453	<0.001	1.352

Table C.15 2024 All-Field Report 3 Model 3 Coefficients.

Model # 3	**R squared**	**0.660**			
Variable	**Coef.**	**Std. Error**	**t**	**P**	**VIF**
Constant	-3.227	0.0308	-104.863	<0.001	0.000
Avg NDVI	0.406	0.00771	52.593	<0.001	1.403
Dev Precipitation	0.0370	0.000166	223.454	<0.001	1.458
Dev Avg Min Temp	0.214	0.00249	86.266	<0.001	1.514

Table C.16 2024 All-Field Report 3 Model 4 Coefficients.

Model # 4	**R squared**	**0.667**			
Variable	**Coef.**	**Std. Error**	**t**	**P**	**VIF**
Constant	-2.753	0.0331	-83.094	<0.001	0.000
Avg CWSI	1.035	0.0262	39.460	<0.001	22.989 <
ln Avg NDVI	0.798	0.0155	51.533	<0.001	22.731 <
Dev Precipitation	0.0376	0.000166	226.134	<0.001	1.497
Dev Avg Min Temp	0.214	0.00247	86.708	<0.001	1.531

Table C.17 2024 All-Field Report 3 Model 5 Coefficients.

Model # 5	**R squared**	**0.673**			
Variable	**Coef.**	**Std. Error**	**t**	**P**	**VIF**
Constant	94.197	2.099	44.884	<0.001	0.000
Avg NDVI	1.416	0.0219	64.538	<0.001	11.829 <
Avg CRSI	-99.686	2.137	-46.653	<0.001	4095.217 <
ln Avg CRSI	79.332	1.750	45.340	<0.001	3880.844 <
Dev Precipitation	0.0395	0.000169	233.650	<0.001	1.578
Dev Avg Min Temp	0.188	0.00250	75.487	<0.001	1.590

Table C.18 2024 All-Field Report 3 Model 6 Coefficients.

Model # 6	**R squared**	**0.675**			
Variable	**Coef.**	**Std. Error**	**t**	**P**	**VIF**
Constant	89.022	2.106	42.279	<0.001	0.000
Avg NDVI	1.829	0.0291	62.942	<0.001	20.874 <

Avg CRSI	-94.818	2.142	-44.271	<0.001	4141.177 <
Avg CWSI	0.515	0.0239	21.575	<0.001	19.529 <
ln Avg CRSI	75.946	1.751	43.370	<0.001	3912.265 <
Dev Precipitation	0.0399	0.000169	235.384	<0.001	1.595
Dev Avg Min Temp	0.197	0.00252	78.194	<0.001	1.631

Table C.19 2024 All-Field Report 3 Model 7 Coefficients.

Model # 7	**R squared**	**0.676**			
Variable	**Coef.**	**Std. Error**	**t**	**P**	**VIF**
Constant	96.592	2.468	39.143	<0.001	0.000
Avg NDVI	2.187	0.0675	32.407	<0.001	112.652 <
Avg CRSI	-102.854	2.540	-40.488	<0.001	5828.612 <
Avg CWSI	0.408	0.0300	13.589	<0.001	30.901 <
ln Avg NDVI	-0.215	0.0366	-5.879	<0.001	130.226 <
ln Avg CRSI	82.434	2.069	39.833	<0.001	5466.851 <
Dev Precipitation	0.0401	0.000175	229.427	<0.001	1.701
Dev Avg Min Temp	0.197	0.00252	78.261	<0.001	1.631

Table C.20 2024 All-Field Report 3 Model 8 Coefficients.

Model # 8	**R squared**	**0.676**			
Variable	**Coef.**	**Std. Error**	**t**	**P**	**VIF**
Constant	91.405	2.650	34.486	<0.001	0.000
Avg NDVI	2.256	0.0687	32.842	<0.001	116.803 <
Avg CRSI	-97.612	2.722	-35.862	<0.001	6694.172 <
Avg CWSI	0.369	0.0309	11.927	<0.001	32.756 <
ln Avg NDVI	-0.264	0.0377	-7.012	<0.001	138.530 <
ln Avg CRSI	78.166	2.217	35.253	<0.001	6277.967 <
ln Avg CWSI	0.00423	0.000790	5.356	<0.001	3.154
Dev Precipitation	0.0397	0.000188	211.112	<0.001	1.973
Dev Avg Min Temp	0.197	0.00252	77.989	<0.001	1.634

2024 All Field Report 7 Dependent Variable ln(ECe)
Best Subsets Regression Friday, April 25, 2025 5:46:57 PM

Data source: Data 1 in 2024 All Field Optimization Data

Using R squared as best criterion.

Table C.21 2024 All-Field Report 7 Variable Definitions.

Variable	Symbol
Dev Avg NDVI	A
Dev Avg CRSI	B
Dev Avg CWSI	C
ln Dev Avg NDVI	D
ln Dev Avg CRSI	E
ln Dev Avg CWSI	F
Dev Precipitation	G
Dev Avg Min Temp	H

Table C.22 2024 All-Field Report 7 Model Summary.

Model #	Variable	Cp	Rsqr	Adj Rsqr	MSerr	A	B	C	D	E	F	G	H
1	1	21052.094	0.590	0.590	0.117							*	
2	2	8185.707	0.647	0.647	0.101							*	*
3	3	5077.014	0.661	0.661	0.097				*			*	*
4	4	3234.058	0.669	0.669	0.094			*	*			*	*
5	5	585.851	0.681	0.680	0.091	*		*	*			*	*
6	6	100.296	0.683	0.683	0.090	*		*	*		*	*	*
7	7	101.090	0.683	0.683	0.090	*	*	*	*		*	*	*
8	8	9.000	0.683	0.683	0.090	*	*	*	*	*	*	*	*

Table C.23 2024 All-Field Report 7 Model 1 Coefficients.

Model # 1	**R squared**	**0.590**			
Variable	**Coef.**	**Std. Error**	**t**	**P**	**VIF**
Constant	-0.380	0.00417	-91.296	<0.001	0.000
Dev Precipitation	0.0483	0.000151	320.442	<0.001	1.000

Table C.24 2024 All-Field Report 7 Model 2 Coefficients.

Model # 2	**R squared**	**0.647**			
Variable	**Coef.**	**Std. Error**	**t**	**P**	**VIF**
Constant	-3.622	0.0304	-119.088	<0.001	0.000

Dev Precipitation	0.0394	0.000163	242.217	<0.001	1.352
Dev Avg Min Temp	0.257	0.00239	107.453	<0.001	1.352

Table C.25 2024 All-Field Report 7 Model 3 Coefficients.

Model # 3	**R squared**	**0.661**			
Variable	**Coef.**	**Std. Error**	**t**	**P**	**VIF**
Constant	-3.216	0.0308	-104.575	<0.001	0.000
ln Dev Avg NDVI	0.169	0.00314	53.893	<0.001	1.182
Dev Precipitation	0.0370	0.000166	223.525	<0.001	1.457
Dev Avg Min Temp	0.240	0.00237	101.371	<0.001	1.377

Table C.26 2024 All-Field Report 7 Model 4 Coefficients.

Model # 4	**R squared**	**0.669**			
Variable	**Coef.**	**Std. Error**	**t**	**P**	**VIF**
Constant	-3.203	0.0304	-105.433	<0.001	0.000
Dev Avg CWSI	0.752	0.0179	42.014	<0.001	11.580 <
ln Dev Avg NDVI	0.547	0.00950	57.510	<0.001	11.113 <
Dev Precipitation	0.0382	0.000166	230.122	<0.001	1.501
Dev Avg Min Temp	0.244	0.00234	104.369	<0.001	1.379

Table C.27 2024 All-Field Report 7 Model 5 Coefficients.

Model # 5	**R squared**	**0.681**			
Variable	**Coef.**	**Std. Error**	**t**	**P**	**VIF**
Constant	-1.214	0.0489	-24.811	<0.001	0.000
Dev Avg NDVI	-2.530	0.0493	-51.273	<0.001	64.367 <
Dev Avg CWSI	1.326	0.0208	63.632	<0.001	16.283 <
ln Dev Avg NDVI	1.981	0.0295	67.167	<0.001	110.995 <
Dev Precipitation	0.0372	0.000164	226.373	<0.001	1.524
Dev Avg Min Temp	0.265	0.00233	113.493	<0.001	1.421

Table C.28 2024 All-Field Report 7 Model 6 Coefficients.

Model # 6	**R squared**	**0.683**			
Variable	**Coef.**	**Std. Error**	**t**	**P**	**VIF**
Constant	-0.727	0.0535	-13.587	<0.001	0.000
Dev Avg NDVI	-3.215	0.0581	-55.285	<0.001	89.982 <
Dev Avg CWSI	1.679	0.0262	64.036	<0.001	25.965 <
ln Dev Avg NDVI	2.400	0.0350	68.579	<0.001	157.374 <
ln Dev Avg CWSI	-0.0163	0.000739	-22.066	<0.001	2.774
Dev Precipitation	0.0382	0.000170	224.618	<0.001	1.645
Dev Avg Min Temp	0.267	0.00233	114.637	<0.001	1.423

Table C.29 2024 All-Field Report 7 Model 7 Coefficients.

Model # 7	**R squared**	**0.683**			
Variable	**Coef.**	**Std. Error**	**t**	**P**	**VIF**
Constant	-0.638	0.0974	-6.554	<0.001	0.000
Dev Avg NDVI	-3.209	0.0584	-54.923	<0.001	90.825 <
Dev Avg CRSI	-0.0956	0.0872	-1.097	0.273	7.852 <
Dev Avg CWSI	1.681	0.0263	63.965	<0.001	26.082 <
ln Dev Avg NDVI	2.406	0.0354	67.965	<0.001	161.013 <
ln Dev Avg CWSI	-0.0164	0.000740	-22.090	<0.001	2.786
Dev Precipitation	0.0382	0.000177	216.601	<0.001	1.773
Dev Avg Min Temp	0.266	0.00242	110.111	<0.001	1.535

Table C.30 2024 All-Field Report 7 Model 8 Coefficients.

Model # 8	**R squared**	**0.683**			
Variable	**Coef.**	**Std. Error**	**t**	**P**	**VIF**
Constant	15.955	1.713	9.312	<0.001	0.000
Dev Avg NDVI	-3.052	0.0606	-50.383	<0.001	97.776 <
Dev Avg CRSI	-17.104	1.756	-9.743	<0.001	3189.239 <

Dev Avg CWSI	1.761	0.0275	63.992	<0.001	28.620 <
ln Dev Avg NDVI	2.389	0.0354	67.441	<0.001	161.414 <
ln Dev Avg CRSI	13.906	1.434	9.700	<0.001	3083.996 <
ln Dev Avg CWSI	-0.0180	0.000759	-23.717	<0.001	2.934
Dev Precipitation	0.0389	0.000190	205.198	<0.001	2.049
Dev Avg Min Temp	0.266	0.00242	110.173	<0.001	1.535

2024 All Field Report 8 Dependent Variable ln(ECe)
Best Subsets Regression Friday, April 25, 2025 5:47:21 PM

Data source: Data 1 in 2024 All Field Optimization Data

Using R squared as best criterion.

Table C.31 2024 All-Field Report 8 Variable Definitions.

Variable	Symbol
Mid Avg NDVI	A
Mid Avg CRSI	B
Mid Avg CWSI	C
ln Mid Avg NDVI	D
ln Mid Avg CRSI	E
ln Mid Avg CWSI	F
Annual Precipitation	G
Annual Avg Min Temp	H

Table C.32 2024 All-Field Report 8 Model Summary.

Model #	Variable	Cp	Rsqr	Adj Rsqr	MSerr	A	B	C	D	E	F	G	H
1	1	16392.609	0.587	0.587	0.118							*	
2	2	11735.674	0.609	0.609	0.111				*			*	
3	3	5584.929	0.638	0.638	0.103	*	*					*	
4	4	3028.349	0.650	0.650	0.100	*	*			*		*	
5	5	910.274	0.660	0.660	0.097	*	*			*		*	*
6	6	416.281	0.662	0.662	0.096	*	*		*	*		*	*
7	7	8.351	0.664	0.664	0.096	*	*		*	*	*	*	*
8	8	9.000	0.664	0.664	0.096	*	*	*	*	*	*	*	*

Table C.33 2024 All-Field Report 8 Model 1 Coefficients.

Model # 1	**R squared**	**0.587**			
Variable	**Coef.**	**Std. Error**	**t**	**P**	**VIF**
Constant	-0.720	0.00522	-138.038	<0.001	0.000
Annual Precipitation	0.00495	0.0000155	318.533	<0.001	1.000

Table C.34 2024 All-Field Report 8 Model 2 Coefficients.

Model # 2	**R squared**	**0.609**			
Variable	**Coef.**	**Std. Error**	**t**	**P**	**VIF**

Constant	-0.374	0.00747	-50.044	<0.001	0.000
ln Mid Avg NDVI	0.250	0.00394	63.260	<0.001	1.515
Annual Precipitation	0.00426	0.0000186	229.080	<0.001	1.515

Table C.35 2024 All-Field Report 8 Model 3 Coefficients.

Model # 3	**R squared**	**0.638**			
Variable	**Coef.**	**Std. Error**	**t**	**P**	**VIF**
Constant	3.993	0.0629	63.464	<0.001	0.000
Mid Avg NDVI	1.662	0.0172	96.823	<0.001	8.081 <
Mid Avg CRSI	-6.443	0.0840	-76.728	<0.001	7.697 <
Annual Precipitation	0.00434	0.0000176	246.501	<0.001	1.465

Table C.36 2024 All-Field Report 8 Model 4 Coefficients.

Model # 4	**R squared**	**0.650**			
Variable	**Coef.**	**Std. Error**	**t**	**P**	**VIF**
Constant	65.848	1.250	52.679	<0.001	0.000
Mid Avg NDVI	1.594	0.0169	94.158	<0.001	8.134 <
Mid Avg CRSI	-68.819	1.262	-54.546	<0.001	1797.158 <
ln Mid Avg CRSI	53.607	1.082	49.545	<0.001	1813.070 <
Annual Precipitation	0.00427	0.0000174	245.924	<0.001	1.475

Table C.37 2024 All-Field Report 8 Model 5 Coefficients.

Model # 5	**R squared**	**0.660**			
Variable	**Coef.**	**Std. Error**	**t**	**P**	**VIF**
Constant	79.636	1.268	62.785	<0.001	0.000
Mid Avg NDVI	1.696	0.0168	100.730	<0.001	8.278 <
Mid Avg CRSI	-82.563	1.279	-64.535	<0.001	1902.013 <
ln Mid Avg CRSI	65.316	1.097	59.554	<0.001	1917.466 <
Annual Precipitation	0.00402	0.0000180	223.192	<0.001	1.630
Annual Avg Min Temp	-0.0980	0.00214	-45.756	<0.001	1.173

Table C.38 2024 All-Field Report 8 Model 6 Coefficients.

Model # 6	**R squared**	**0.662**			
Variable	**Coef.**	**Std. Error**	**t**	**P**	**VIF**
Constant	97.991	1.510	64.882	<0.001	0.000
Mid Avg NDVI	2.903	0.0569	51.038	<0.001	95.119 <
Mid Avg CRSI	-102.329	1.555	-65.810	<0.001	2828.956 <
ln Mid Avg NDVI	-0.616	0.0277	-22.207	<0.001	86.724 <
ln Mid Avg CRSI	81.926	1.324	61.859	<0.001	2815.330 <
Annual Precipitation	0.00416	0.0000191	218.411	<0.001	1.837
Annual Avg Min Temp	-0.0777	0.00232	-33.463	<0.001	1.389

Table C.39 2024 All-Field Report 8 Model 7 Coefficients.

Model # 7	**R squared**	**0.664**			
Variable	**Coef.**	**Std. Error**	**t**	**P**	**VIF**
Constant	79.992	1.749	45.741	<0.001	0.000
Mid Avg NDVI	3.183	0.0584	54.525	<0.001	100.785 <
Mid Avg CRSI	-84.215	1.790	-47.045	<0.001	3770.907 <
ln Mid Avg NDVI	-0.718	0.0281	-25.541	<0.001	89.605 <
ln Mid Avg CRSI	67.010	1.512	44.313	<0.001	3691.432 <
ln Mid Avg CWSI	0.0159	0.000783	20.247	<0.001	4.404 <
Annual Precipitation	0.00405	0.0000197	205.260	<0.001	1.984
Annual Avg Min Temp	-0.0754	0.00232	-32.558	<0.001	1.392

Table C.40 2024 All-Field Report 8 Model 8 Coefficients.

Model # 8	**R squared**	**0.664**			
Variable	**Coef.**	**Std. Error**	**t**	**P**	**VIF**
Constant	79.733	1.763	45.228	<0.001	0.000
Mid Avg NDVI	3.181	0.0584	54.480	<0.001	100.846 <

Mid Avg CRSI	-83.943	1.805	-46.500	<0.001	3834.983 <
Mid Avg CWSI	0.0574	0.0494	1.162	0.245	93.603 <
ln Mid Avg NDVI	-0.687	0.0388	-17.715	<0.001	170.490 <
ln Mid Avg CRSI	66.806	1.522	43.881	<0.001	3741.404 <
ln Mid Avg CWSI	0.0158	0.000786	20.086	<0.001	4.433 <
Annual Precipitation	0.00405	0.0000198	204.646	<0.001	1.995
Annual Avg Min Temp	-0.0758	0.00234	-32.397	<0.001	1.420

Multiyear Corn Field Report 12 Dependent Variable ECe
Best Subsets Regression Wednesday, April 23, 2025 6:28:30 PM

Data source: Data 1 in Multiyear Corn Field Optimization Data

Warning: Subsets with small Tolerances encountered and omitted

Using R squared as best criterion.

Table C.41 Multiyear Corn Field Report 12 Variable Definitions.

Variable	Symbol
Dev Max Avg NDVI	A
Dev Max Avg CRSI	B
Dev Max Avg CWSI	C
ln Dev Max Avg NDVI	D
ln Dev Max Avg CRSI	E
ln Dev Max Avg CWSI	F
Annual Precipitation	G
Annual Avg Min Temp	H

Table C.42 Multiyear Corn Field Report 12 Model Summary.

Model #	Variable	Cp	Rsqr	Adj Rsqr	MSerr	A	B	C	D	E	F	G	H
1	1	9345.813	0.669	0.669	0.467						*		
2	2	445.671	0.832	0.832	0.237						*	*	
3	3	346.929	0.834	0.834	0.234			*			*	*	
4	4	35.930	0.840	0.840	0.226	*			*		*		*
5	5	9.174	0.840	0.840	0.225	*		*	*		*		*
6	6	10.793	0.840	0.840	0.225	*		*	*	*	*		*
7	7	7.000	0.840	0.840	0.225	*	*	*	*	*	*		*

Table C.43 Multiyear Corn Field Report 12 Model 1 Coefficients.

Model # 1	**R squared**	**0.669**			
Variable	**Coef.**	**Std. Error**	**t**	**P**	**VIF**
Constant	0.501	0.0160	31.241	<0.001	0.000
ln Dev Max Avg CWSI	-1.529	0.0115	-132.932	<0.001	1.000

Table C.44 Multiyear Corn Field Report 12 Model 2 Coefficients.

Model # 2	**R squared**	**0.832**			
Variable	**Coef.**	**Std. Error**	**t**	**P**	**VIF**
Constant	-3.876	0.0489	-79.267	<0.001	0.000
ln Dev Max Avg CWSI	-1.504	0.00820	-183.420	<0.001	1.001
Annual Precipitation	0.0121	0.000131	92.046	<0.001	1.001

Table C.45 Multiyear Corn Field Report 12 Model 3 Coefficients.

Model # 3	**R squared**	**0.834**			
Variable	**Coef.**	**Std. Error**	**t**	**P**	**VIF**
Constant	-5.493	0.171	-32.067	<0.001	0.000
Dev Max Avg CWSI	4.794	0.487	9.845	<0.001	272.169 <
ln Dev Max Avg CWSI	-2.805	0.132	-21.191	<0.001	263.643 <
Annual Precipitation	0.00757	0.000476	15.896	<0.001	13.329 <

Table C.46 Multiyear Corn Field Report 12 Model 4 Coefficients.

Model # 4	**R squared**	**0.840**			
Variable	**Coef.**	**Std. Error**	**t**	**P**	**VIF**
Constant	-88.023	4.307	-20.438	<0.001	0.000
Dev Max Avg NDVI	92.943	4.592	20.242	<0.001	2517.545 <
ln Dev Max Avg NDVI	-63.856	3.146	-20.296	<0.001	2291.334 <
ln Dev Max Avg CWSI	-1.114	0.0239	-46.562	<0.001	8.926 <
Annual Avg Min Temp	0.881	0.0279	31.627	<0.001	5.141 <

Table C.47 Multiyear Corn Field Report 12 Model 5 Coefficients.

Model # 5	**R squared**	**0.840**			
Variable	**Coef.**	**Std. Error**	**t**	**P**	**VIF**
Constant	-83.879	4.369	-19.199	<0.001	0.000
Dev Max Avg NDVI	86.875	4.722	18.398	<0.001	2670.983 <

Dev Max Avg CWSI	2.638	0.492	5.362	<0.001	288.846 <
ln Dev Max Avg NDVI	-59.718	3.235	-18.461	<0.001	2429.671 <
ln Dev Max Avg CWSI	-1.858	0.141	-13.203	<0.001	309.498 <
Annual Avg Min Temp	0.665	0.0489	13.595	<0.001	15.913 <

Table C.48 Multiyear Corn Field Report 12 Model 6 Coefficients.

Model # 6	**R squared**	**0.840**			
Variable	**Coef.**	**Std. Error**	**t**	**P**	**VIF**
Constant	-83.684	4.381	-19.103	<0.001	0.000
Dev Max Avg NDVI	86.615	4.741	18.270	<0.001	2692.265 <
Dev Max Avg CWSI	2.615	0.494	5.297	<0.001	290.593 <
ln Dev Max Avg NDVI	-59.473	3.259	-18.248	<0.001	2466.184 <
ln Dev Max Avg CRSI	-0.619	1.002	-0.617	0.537	7.743 <
ln Dev Max Avg CWSI	-1.858	0.141	-13.205	<0.001	309.502 <
Annual Avg Min Temp	0.670	0.0495	13.528	<0.001	16.295 <

Table C.49 Multiyear Corn Field Report 12 Model 7 Coefficients.

Model # 7	**R squared**	**0.840**			
Variable	**Coef.**	**Std. Error**	**t**	**P**	**VIF**
Constant	-325.187	100.432	-3.238	0.001	0.000
Dev Max Avg NDVI	83.523	4.911	17.009	<0.001	2890.030 <
Dev Max Avg CRSI	246.425	102.381	2.407	0.016	63598.656 <
Dev Max Avg CWSI	2.544	0.494	5.146	<0.001	291.621 <

ln Dev Max Avg NDVI	-57.253	3.386	-16.908	<0.001	2663.838 <
ln Dev Max Avg CRSI	-217.345	90.048	-2.414	0.016	62560.892 <
ln Dev Max Avg CWSI	-1.800	0.143	-12.618	<0.001	318.448 <
Annual Avg Min Temp	0.649	0.0502	12.932	<0.001	16.772 <

Multiyear Corn Field Report 14 Dependent Variable ECe
Best Subsets Regression Wednesday, April 23, 2025 6:28:45 PM

Data source: Data 1 in Multiyear Corn Field Optimization Data

Warning: Subsets with small Tolerances encountered and omitted

Using R squared as best criterion.

Table C.50 Multiyear Corn Field Report 14 Variable Definitions.

Variable	Symbol
Dev Max Avg NDVI	A
Dev Max Avg CRSI	B
Dev Max Avg CWSI	C
ln Dev Max Avg NDVI	D
ln Dev Max Avg CRSI	E
ln Dev Max Avg CWSI	F
Dev Precipitation	G
Dev Avg Min Temp	H

Table C.51 Multiyear Corn Field Report 14 Model Summary.

Model #	Variable	Cp	Rsqr	Adj Rsqr	MSerr	A	B	C	D	E	F	G	H
1	1	9345.813	0.669	0.669	0.467						*		
2	2	445.671	0.832	0.832	0.237						*		*
3	3	346.929	0.834	0.834	0.234			*			*		*
4	4	35.930	0.840	0.840	0.226	*			*		*		*
5	5	9.174	0.840	0.840	0.225	*		*	*		*		*
6	6	10.793	0.840	0.840	0.225	*		*	*	*	*		*
7	7	7.000	0.840	0.840	0.225	*	*	*	*	*	*		*

Table C.52 Multiyear Corn Field Report 14 Model 1 Coefficients.

Model # 1	**R squared**	**0.669**			
Variable	**Coef.**	**Std. Error**	**t**	**P**	**VIF**
Constant	0.501	0.0160	31.241	<0.001	0.000
ln Dev Max Avg CWSI	-1.529	0.0115	-132.932	<0.001	1.000

Table C.53 Multiyear Corn Field Report 14 Model 2 Coefficients.

Model # 2	**R squared**	**0.832**			
Variable	**Coef.**	**Std. Error**	**t**	**P**	**VIF**
Constant	-17.833	0.200	-89.386	<0.001	0.000
ln Dev Max Avg CWSI	-1.504	0.00820	-183.420	<0.001	1.001
Dev Avg Min Temp	1.302	0.0142	92.046	<0.001	1.001

Table C.54 Multiyear Corn Field Report 14 Model 3 Coefficients.

Model # 3	**R squared**	**0.834**			
Variable	**Coef.**	**Std. Error**	**t**	**P**	**VIF**
Constant	-14.240	0.415	-34.281	<0.001	0.000
Dev Max Avg CWSI	4.794	0.487	9.845	<0.001	272.169 <
ln Dev Max Avg CWSI	-2.805	0.132	-21.191	<0.001	263.643 <
Dev Avg Min Temp	0.816	0.0514	15.896	<0.001	13.329 <

Table C.55 Multiyear Corn Field Report 14 Model 4 Coefficients.

Model # 4	**R squared**	**0.840**			
Variable	**Coef.**	**Std. Error**	**t**	**P**	**VIF**
Constant	-101.043	4.103	-24.626	<0.001	0.000
Dev Max Avg NDVI	92.943	4.592	20.242	<0.001	2517.545 <
ln Dev Max Avg NDVI	-63.856	3.146	-20.296	<0.001	2291.334 <
ln Dev Max Avg CWSI	-1.114	0.0239	-46.562	<0.001	8.926 <
Dev Avg Min Temp	0.991	0.0313	31.627	<0.001	5.141 <

Table C.56 Multiyear Corn Field Report 14 Model 5 Coefficients.

Model # 5	**R squared**	**0.840**			
Variable	**Coef.**	**Std. Error**	**t**	**P**	**VIF**
Constant	-93.709	4.319	-21.697	<0.001	0.000
Dev Max Avg NDVI	86.875	4.722	18.398	<0.001	2670.983 <

Dev Max Avg CWSI	2.638	0.492	5.362	<0.001	288.846 <
ln Dev Max Avg NDVI	-59.718	3.235	-18.461	<0.001	2429.671 <
ln Dev Max Avg CWSI	-1.858	0.141	-13.203	<0.001	309.498 <
Dev Avg Min Temp	0.748	0.0550	13.595	<0.001	15.913 <

Table C.57 Multiyear Corn Field Report 14 Model 6 Coefficients.

Model # 6	**R squared**	**0.840**			
Variable	**Coef.**	**Std. Error**	**t**	**P**	**VIF**
Constant	-93.583	4.324	-21.643	<0.001	0.000
Dev Max Avg NDVI	86.615	4.741	18.270	<0.001	2692.265 <
Dev Max Avg CWSI	2.615	0.494	5.297	<0.001	290.593 <
ln Dev Max Avg NDVI	-59.473	3.259	-18.248	<0.001	2466.184 <
ln Dev Max Avg CRSI	-0.619	1.002	-0.617	0.537	7.743 <
ln Dev Max Avg CWSI	-1.858	0.141	-13.205	<0.001	309.502 <
Dev Avg Min Temp	0.754	0.0557	13.528	<0.001	16.295 <

Table C.58 Multiyear Corn Field Report 14 Model 7 Coefficients.

Model # 7	**R squared**	**0.840**			
Variable	**Coef.**	**Std. Error**	**t**	**P**	**VIF**
Constant	-334.785	100.305	-3.338	<0.001	0.000
Dev Max Avg NDVI	83.523	4.911	17.009	<0.001	2890.030 <
Dev Max Avg CRSI	246.425	102.381	2.407	0.016	63598.656 <
Dev Max Avg CWSI	2.544	0.494	5.146	<0.001	291.621 <
ln Dev Max Avg NDVI	-57.253	3.386	-16.908	<0.001	2663.838 <

ln Dev Max Avg CRSI	-217.345	90.048	-2.414	0.016	62560.892 <
ln Dev Max Avg CWSI	-1.800	0.143	-12.618	<0.001	318.448 <
Dev Avg Min Temp	0.731	0.0565	12.932	<0.001	16.772 <

Multiyear Testing Report 10.2 Report 55
Multiple Linear Regression Friday, April 25, 2025 1:14:18 AM

Data source: Data 1 in Multiyear Corn Field Optimization Data Testing Report 10.2

Ece (dS/m) = -53.946 + (57.748 * Dev Avg NDVI) + (2.151 * Dev Max Avg CWSI) - (33.118 * ln Dev Avg NDVI) - (1.639 * ln Dev Max Avg CWSI) + (0.00954 * Seasonal Precipitation)

N = 8732

R = 0.915 Rsqr = 0.838 Adj Rsqr = 0.838

Standard Error of Estimate = 0.479

Table C.59 Multiyear Testing Report 10.2 Report 55 Model Coefficients.

	Coefficient	Std. Error	t	P	VIF
Constant	-53.946	3.536	-15.256	<0.001	
Dev Avg NDVI	57.748	4.175	13.833	<0.001	3151.681
Dev Max Avg CWSI	2.151	0.517	4.161	<0.001	313.811
ln Dev Avg NDVI	-33.118	2.366	-13.997	<0.001	2637.420
ln Dev Max Avg CWSI	-1.639	0.158	-10.398	<0.001	382.376
Seasonal Precipitation	0.00954	0.000728	13.104	<0.001	14.961

Warning: Multicollinearity is present among the independent variables. The variables with the largest values of VIF are causing the problem. Consider getting more data or eliminating one or more variables from the equation. The likely candidates for elimination are: Dev Avg NDVI , Dev Max Avg CWSI , ln Dev Avg NDVI , ln Dev Max Avg CWSI , Seasonal Precipitation

Analysis of Variance:

Table C.60 Multiyear Testing Report 10.2 Report 55 Analysis of Variance

	DF	SS	MS	F	P
Regression	5	10319.656	2063.931	9010.629	<0.001
Residual	8726	1998.735	0.229		
Total	8731	12318.392	1.411		

Table C.61 Multiyear Testing Report 10.2 Report 55 Sum of Squares.

Column	SSIncr	SSMarg
Dev Avg NDVI	8900.118	43.831
Dev Max Avg CWSI	126.465	3.965

ln Dev Avg NDVI	1126.082	44.875
ln Dev Max Avg CWSI	127.659	24.766
Seasonal Precipitation	39.333	39.333

The dependent variable Ece (dS/m) can be predicted from a linear combination of the independent variables:

Table C.62 Multiyear Testing Report 10.2 Report 55 Probability of Predicting Dependent Variable.

	P
Dev Avg NDVI	<0.001
Dev Max Avg CWSI	<0.001
ln Dev Avg NDVI	<0.001
ln Dev Max Avg CWSI	<0.001
Seasonal Precipitation	<0.001

All independent variables appear to contribute to predicting Ece (dS/m) ($P < 0.05$).

Normality Test (Kolmogorov-Smirnov) Failed ($P = <0.001$)

Constant Variance Test (Spearman Rank Correlation): Failed ($P = <0.001$)

Power of performed test with alpha = 0.050: 1.000

Multiyear Testing Report 10.2 Report 56
Multiple Linear Regression Friday, April 25, 2025 1:14:23 AM

Data source: Data 1 in Multiyear Corn Field Optimization Data Testing Report 10.2

Ece (dS/m) = -60.548 + (57.748 * Dev Avg NDVI) + (2.151 * Dev Max Avg CWSI) - (33.118 * ln Dev Avg NDVI) - (1.639 * ln Dev Max Avg CWSI) + (0.658 * Seasonal Avg Min Temp)

N = 8732

R = 0.915 Rsqr = 0.838 Adj Rsqr = 0.838

Standard Error of Estimate = 0.479

Table C.63 Multiyear Testing Report 10.2 Report 56 Model Coefficients.

Coefficient	Std. Error	t	P	VIF	
Constant	-60.548	3.449	-17.556	<0.001	
Dev Avg NDVI	57.748	4.175	13.833	<0.001	3151.681
Dev Max Avg CWSI	2.151	0.517	4.161	<0.001	313.811
ln Dev Avg NDVI	-33.118	2.366	-13.997	<0.001	2637.420
ln Dev Max Avg CWSI	-1.639	0.158	-10.398	<0.001	382.376
Seasonal Avg Min Temp	0.658	0.0502	13.104	<0.001	14.961

Warning: Multicollinearity is present among the independent variables. The variables with the largest values of VIF are causing the problem. Consider getting more data or eliminating one or more variables from the equation. The likely candidates for elimination are: Dev Avg NDVI , Dev Max Avg CWSI , ln Dev Avg NDVI , ln Dev Max Avg CWSI , Seasonal Avg Min Temp

Analysis of Variance:

Table C.64 Multiyear Testing Report 10.2 Report 56 Analysis of Variance.

	DF	SS	MS	F	P
Regression	5	10319.656	2063.931	9010.629	<0.001
Residual	8726	1998.735	0.229		
Total	8731	12318.392	1.411		

Table C.65 Multiyear Testing Report 10.2 Report 56 Sum of Squares.

Column	SSIncr	SSMarg
Dev Avg NDVI	8900.118	43.831
Dev Max Avg CWSI	126.465	3.965
ln Dev Avg NDVI	1126.082	44.875
ln Dev Max Avg CWSI	127.659	24.766
Seasonal Avg Min Temp	39.333	39.333

The dependent variable Ece (dS/m) can be predicted from a linear combination of the independent variables:

Table C.66 Multiyear Testing Report 10.2 Report 56 Probability of Predicting Dependent Variable.

	P
Dev Avg NDVI	<0.001
Dev Max Avg CWSI	<0.001
ln Dev Avg NDVI	<0.001
ln Dev Max Avg CWSI	<0.001
Seasonal Avg Min Temp	<0.001

All independent variables appear to contribute to predicting Ece (dS/m) ($P < 0.05$).

Normality Test (Kolmogorov-Smirnov) Failed (P = <0.001)

Constant Variance Test (Spearman Rank Correlation): Failed (P = <0.001)

Power of performed test with alpha = 0.050: 1.000

Multiyear Testing Report 10.2 Report 91
Multiple Linear Regression Friday, April 25, 2025 1:26:49 AM

Data source: Data 1 in Multiyear Corn Field Optimization Data Testing Report 10.2

Ece (dS/m) = -52.768 + (57.634 * Dev Avg NDVI) - (1.179 * Dev Max Avg CRSI) + (2.155 * Dev Max Avg CWSI) - (32.924 * ln Dev Avg NDVI) - (1.637 * ln Dev Max Avg CWSI) + (0.00972 * Seasonal Precipitation)

N = 8732

R = 0.915 Rsqr = 0.838 Adj Rsqr = 0.838

Standard Error of Estimate = 0.479

Table C.67 Multiyear Testing Report 10.2 Report 91 Model Coefficients.

Coefficient	**Std. Error**	**t**	**P**	**VIF**	
Constant	-52.768	3.725	-14.168	<0.001	
Dev Avg NDVI	57.634	4.176	13.801	<0.001	3154.021
Dev Max Avg CRSI	-1.179	1.171	-1.007	0.314	8.183
Dev Max Avg CWSI	2.155	0.517	4.168	<0.001	313.826
ln Dev Avg NDVI	-32.924	2.374	-13.869	<0.001	2654.909
ln Dev Max Avg CWSI	-1.637	0.158	-10.383	<0.001	382.449
Seasonal Precipitation	0.00972	0.000751	12.950	<0.001	15.922

Warning: Multicollinearity is present among the independent variables. The variables with the largest values of VIF are causing the problem. Consider getting more data or eliminating one or more variables from the equation. The likely candidates for elimination are: Dev Avg NDVI , Dev Max Avg CRSI , Dev Max Avg CWSI , ln Dev Avg NDVI , ln Dev Max Avg CWSI , Seasonal Precipitation

Analysis of Variance:

Table C.68 Multiyear Testing Report 10.2 Report 91 Analysis of Variance.

	DF	**SS**	**MS**	**F**	**P**
Regression	6	10319.889	1719.981	7509.039	<0.001

Residual	8725	1998.503	0.229
Total	8731	12318.392	1.411

Table C.69 Multiyear Testing Report 10.2 Report 91 Sum of Squares.

Column	SSIncr	SSMarg
Dev Avg NDVI	8900.118	43.625
Dev Max Avg CRSI	224.014	0.232
Dev Max Avg CWSI	4.578	3.979
ln Dev Avg NDVI	1033.121	44.058
ln Dev Max Avg CWSI	119.646	24.695
Seasonal Precipitation	38.412	38.412

The dependent variable Ece (dS/m) can be predicted from a linear combination of the independent variables:

Table C.70Multiyear Testing Report 10.2 Report 91 Probability of Predicting Dependent Variable.

	P
Dev Avg NDVI	<0.001
Dev Max Avg CRSI	0.314
Dev Max Avg CWSI	<0.001
ln Dev Avg NDVI	<0.001
ln Dev Max Avg CWSI	<0.001
Seasonal Precipitation	<0.001

Not all of the independent variables appear necessary (or the multiple linear model may be underspecified).
The following appear to account for the ability to predict Ece (dS/m) ($P < 0.05$): Dev Avg NDVI , Dev Max Avg CWSI , ln Dev Avg NDVI , ln Dev Max Avg CWSI , Seasonal Precipitation

Normality Test (Kolmogorov-Smirnov) Failed (P = <0.001)

Constant Variance Test (Spearman Rank Correlation): Failed (P = <0.001)

Power of performed test with alpha = 0.050: 1.000

Multiyear Testing Report 10.2 Report 92
Multiple Linear Regression Friday, April 25, 2025 1:26:54 AM

Data source: Data 1 in Multiyear Corn Field Optimization Data Testing Report 10.2

Ece (dS/m) = -59.498 + (57.634 * Dev Avg NDVI) - (1.179 * Dev Max Avg CRSI) + (2.155 * Dev Max Avg CWSI) - (32.924 * ln Dev Avg NDVI) - (1.637 * ln Dev Max Avg CWSI) + (0.670 * Seasonal Avg Min Temp)

N = 8732

R = 0.915 Rsqr = 0.838 Adj Rsqr = 0.838

Standard Error of Estimate = 0.479

Table C.71 Multiyear Testing Report 10.2 Report 92 Model Coefficients.

	Coefficient	Std. Error	t	P	VIF
Constant	-59.498	3.603	-16.514	<0.001	
Dev Avg NDVI	57.634	4.176	13.801	<0.001	3154.021
Dev Max Avg CRSI	-1.179	1.171	-1.007	0.314	8.183
Dev Max Avg CWSI	2.155	0.517	4.168	<0.001	313.826
ln Dev Avg NDVI	-32.924	2.374	-13.869	<0.001	2654.909
ln Dev Max Avg CWSI	-1.637	0.158	-10.383	<0.001	382.449
Seasonal Avg Min Temp	0.670	0.0518	12.950	<0.001	15.922

Warning: Multicollinearity is present among the independent variables. The variables with the largest values of VIF are causing the problem. Consider getting more data or eliminating one or more variables from the equation. The likely candidates for elimination are: Dev Avg NDVI , Dev Max Avg CRSI , Dev Max Avg CWSI , ln Dev Avg NDVI , ln Dev Max Avg CWSI , Seasonal Avg Min Temp

Analysis of Variance:

Table C.72 Multiyear Testing Report 10.2 Report 92 Analysis of Variance.

	DF	SS	MS	F	P
Regression	6	10319.889	1719.981	7509.039	<0.001
Residual	8725	1998.503	0.229		
Total	8731	12318.392	1.411		

Table C.73 Multiyear Testing Report 10.2 Report 92 Sum of Squares.

Column	SSIncr	SSMarg
Dev Avg NDVI	8900.118	43.625
Dev Max Avg CRSI	224.014	0.232
Dev Max Avg CWSI	4.578	3.979
ln Dev Avg NDVI	1033.121	44.058
ln Dev Max Avg CWSI	119.646	24.695
Seasonal Avg Min Temp	38.412	38.412

The dependent variable Ece (dS/m) can be predicted from a linear combination of the independent variables:

Table C.74 Multiyear Testing Report 10.2 Report 92 Probability of Predicting Dependent Variable.

	P
Dev Avg NDVI	<0.001
Dev Max Avg CRSI	0.314
Dev Max Avg CWSI	<0.001
ln Dev Avg NDVI	<0.001
ln Dev Max Avg CWSI	<0.001
Seasonal Avg Min Temp	<0.001

Not all of the independent variables appear necessary (or the multiple linear model may be underspecified).
The following appear to account for the ability to predict Ece (dS/m) ($P < 0.05$): Dev Avg NDVI , Dev Max Avg CWSI , ln Dev Avg NDVI , ln Dev Max Avg CWSI , Seasonal Avg Min Temp

Normality Test (Kolmogorov-Smirnov) Failed (P = <0.001)

Constant Variance Test (Spearman Rank Correlation): Failed (P = <0.001)

Power of performed test with alpha = 0.050: 1.000

Multiyear Testing Report 10.2 Report 103
Multiple Linear Regression Friday, April 25, 2025 1:31:48 AM

Data source: Data 1 in Multiyear Corn Field Optimization Data Testing Report 10.2

Ece (dS/m) = -53.924 + (57.615 * Dev Avg NDVI) + (2.155 * Dev Max Avg CWSI) - (32.909 * ln Dev Avg NDVI) - (1.074 * ln Dev Max Avg CRSI) - (1.637 * ln Dev Max Avg CWSI) + (0.00973 * Seasonal Precipitation)

N = 8732

R = 0.915 Rsqr = 0.838 Adj Rsqr = 0.838

Standard Error of Estimate = 0.479

Table C.75 Multiyear Testing Report 10.2 Report 103 Model Coefficients.

	Coefficient	Std. Error	t	P	VIF
Constant	-53.924	3.536	-15.250	<0.001	
Dev Avg NDVI	57.615	4.177	13.795	<0.001	3154.608
Dev Max Avg CWSI	2.155	0.517	4.168	<0.001	313.827
ln Dev Avg NDVI	-32.909	2.375	-13.859	<0.001	2656.407
ln Dev Max Avg CRSI	-1.074	1.029	-1.043	0.297	8.045
ln Dev Max Avg CWSI	-1.637	0.158	-10.382	<0.001	382.460
Seasonal Precipitation	0.00973	0.000750	12.961	<0.001	15.913

Warning: Multicollinearity is present among the independent variables. The variables with the largest values of VIF are causing the problem. Consider getting more data or eliminating one or more variables from the equation. The likely candidates for elimination are: Dev Avg NDVI , Dev Max Avg CWSI , ln Dev Avg NDVI , ln Dev Max Avg CRSI , ln Dev Max Avg CWSI , Seasonal Precipitation

Analysis of Variance:

Table C.76 Multiyear Testing Report 10.2 Report 103 Analysis of Variance.

	DF	SS	MS	F	P
Regression	6	10319.906	1719.984	7509.115	<0.001

Residual	8725	1998.486	0.229
Total	8731	12318.392	1.411

Table C.77 Multiyear Testing Report 10.2 Report 103 Sum of Squares.

Column	**SSIncr**	**SSMarg**
Dev Avg NDVI	8900.118	43.589
Dev Max Avg CWSI	126.465	3.979
ln Dev Avg NDVI	1126.082	43.993
ln Dev Max Avg CRSI	8.891	0.249
ln Dev Max Avg CWSI	119.870	24.687
Seasonal Precipitation	38.480	38.480

The dependent variable Ece (dS/m) can be predicted from a linear combination of the independent variables:

Table C.78 Multiyear Testing Report 10.2 Report 103 Probability of Predicting Dependent Variable.

	P
Dev Avg NDVI	<0.001
Dev Max Avg CWSI	<0.001
ln Dev Avg NDVI	<0.001
ln Dev Max Avg CRSI	0.297
ln Dev Max Avg CWSI	<0.001
Seasonal Precipitation	<0.001

Not all of the independent variables appear necessary (or the multiple linear model may be underspecified).
The following appear to account for the ability to predict Ece (dS/m) (P < 0.05): Dev Avg NDVI , Dev Max Avg CWSI , ln Dev Avg NDVI , ln Dev Max Avg CWSI , Seasonal Precipitation

Normality Test (Kolmogorov-Smirnov) Failed (P = <0.001)

Constant Variance Test (Spearman Rank Correlation): Failed (P = <0.001)

Power of performed test with alpha = 0.050: 1.000

Multiyear Testing Report 10.2 Report 104
Multiple Linear Regression Friday, April 25, 2025 1:31:54 AM

Data source: Data 1 in Multiyear Corn Field Optimization Data Testing Report 10.2

Ece (dS/m) = -60.659 + (57.615 * Dev Avg NDVI) + (2.155 * Dev Max Avg CWSI) - (32.909 * ln Dev Avg NDVI) - (1.074 * ln Dev Max Avg CRSI) - (1.637 * ln Dev Max Avg CWSI) + (0.671 * Seasonal Avg Min Temp)

N = 8732

R = 0.915 Rsqr = 0.838 Adj Rsqr = 0.838

Standard Error of Estimate = 0.479

Table C.79 Multiyear Testing Report 10.2 Report 104 Model Coefficients.

	Coefficient	Std. Error	t	P	VIF
Constant	-60.659	3.450	-17.580	<0.001	
Dev Avg NDVI	57.615	4.177	13.795	<0.001	3154.608
Dev Max Avg CWSI	2.155	0.517	4.168	<0.001	313.827
ln Dev Avg NDVI	-32.909	2.375	-13.859	<0.001	2656.407
ln Dev Max Avg CRSI	-1.074	1.029	-1.043	0.297	8.045
ln Dev Max Avg CWSI	-1.637	0.158	-10.382	<0.001	382.460
Seasonal Avg Min Temp	0.671	0.0517	12.961	<0.001	15.913

Warning: Multicollinearity is present among the independent variables. The variables with the largest values of VIF are causing the problem. Consider getting more data or eliminating one or more variables from the equation. The likely candidates for elimination are: Dev Avg NDVI , Dev Max Avg CWSI , ln Dev Avg NDVI , ln Dev Max Avg CRSI , ln Dev Max Avg CWSI , Seasonal Avg Min Temp

Analysis of Variance:

Table C.80 Multiyear Testing Report 10.2 Report 104 Analysis of Variance.

	DF	SS	MS	F	P
Regression	6	10319.906	1719.984	7509.115	<0.001
Residual	8725	1998.486	0.229		
Total	8731	12318.392	1.411		

Table C.81 Multiyear Testing Report 10.2 Report 104 Sum of Squares.

Column	SSIncr	SSMarg
Dev Avg NDVI	8900.118	43.589
Dev Max Avg CWSI	126.465	3.979
ln Dev Avg NDVI	1126.082	43.993
ln Dev Max Avg CRSI	8.891	0.249
ln Dev Max Avg CWSI	119.870	24.687
Seasonal Avg Min Temp	38.480	38.480

The dependent variable Ece (dS/m) can be predicted from a linear combination of the independent variables:

Table C.82 Multiyear Testing Report 10.2 Report 104 Probability of Predicting Dependent Variable.

	P
Dev Avg NDVI	<0.001
Dev Max Avg CWSI	<0.001
ln Dev Avg NDVI	<0.001
ln Dev Max Avg CRSI	0.297
ln Dev Max Avg CWSI	<0.001
Seasonal Avg Min Temp	<0.001

Not all of the independent variables appear necessary (or the multiple linear model may be underspecified).
The following appear to account for the ability to predict Ece (dS/m) ($P < 0.05$): Dev Avg NDVI , Dev Max Avg CWSI , ln Dev Avg NDVI , ln Dev Max Avg CWSI , Seasonal Avg Min Temp

Normality Test (Kolmogorov-Smirnov)	Failed (P = <0.001)

Constant Variance Test (Spearman Rank Correlation):	Failed (P = <0.001)

Power of performed test with alpha = 0.050: 1.000

Multiyear Testing Report 13.1 Report 78
Multiple Linear Regression Friday, April 25, 2025 10:23:02 AM

Data source: Data 1 in Multiyear Corn Field Optimization Data Testing Report 13.1

Ece (dS/m) = -89.592 + (92.943 * Dev Max Avg NDVI) - (63.856 * ln Dev Max Avg NDVI) - (1.114 * ln Dev Max Avg CWSI) + (0.0134 * Seasonal Precipitation)

N = 8732

R = 0.916 Rsqr = 0.840 Adj Rsqr = 0.840

Standard Error of Estimate = 0.476

Table C.83 Multiyear Testing Report 13.1 Report 78 Model Coefficients.

	Coefficient	Std. Error	t	P	VIF
Constant	-89.592	4.281	-20.929	<0.001	
Dev Max Avg NDVI	92.943	4.592	20.242	<0.001	2517.545
ln Dev Max Avg NDVI	-63.856	3.146	-20.296	<0.001	2291.334
ln Dev Max Avg CWSI	-1.114	0.0239	-46.562	<0.001	8.926
Seasonal Precipitation	0.0134	0.000424	31.627	<0.001	5.141

Warning: Multicollinearity is present among the independent variables. The variables with the largest values of VIF are causing the problem. Consider getting more data or eliminating one or more variables from the equation. The likely candidates for elimination are: Dev Max Avg NDVI , ln Dev Max Avg NDVI , ln Dev Max Avg CWSI , Seasonal Precipitation

Analysis of Variance:

Table C.84 Multiyear Testing Report 13.1 Report 78 Analysis of Variance.

	DF	SS	MS	F	P
Regression	4	10344.610	2586.152	11434.572	<0.001
Residual	8727	1973.782	0.226		
Total	8731	12318.392	1.411		

Table C.85 Multiyear Testing Report 13.1 Report 78 Sum of Squares.

Column	SSIncr	SSMarg
Dev Max Avg NDVI	7239.755	92.673
ln Dev Max Avg NDVI	2607.114	93.162
ln Dev Max Avg CWSI	271.514	490.343

Seasonal Precipitation	226.227	226.227

The dependent variable Ece (dS/m) can be predicted from a linear combination of the independent variables:

Table C.86 Multiyear Testing Report 13.1 Report 78 Probability of Predicting Dependent Variable.

	P
Dev Max Avg NDVI	<0.001
ln Dev Max Avg NDVI	<0.001
ln Dev Max Avg CWSI	<0.001
Seasonal Precipitation	<0.001

All independent variables appear to contribute to predicting Ece (dS/m) ($P < 0.05$).

Normality Test (Kolmogorov-Smirnov) Failed ($P = <0.001$)

Constant Variance Test (Spearman Rank Correlation): Failed ($P = <0.001$)

Power of performed test with alpha = 0.050: 1.000

Multiyear Testing Report 13.1 Report 79
Multiple Linear Regression Friday, April 25, 2025 10:23:07 AM

Data source: Data 1 in Multiyear Corn Field Optimization Data Testing Report 13.1

Ece (dS/m) = -98.874 + (92.943 * Dev Max Avg NDVI) - (63.856 * ln Dev Max Avg NDVI) - (1.114 * ln Dev Max Avg CWSI) + (0.924 * Seasonal Avg Min Temp)

N = 8732

R = 0.916 Rsqr = 0.840 Adj Rsqr = 0.840

Standard Error of Estimate = 0.476

Table C.87 Multiyear Testing Report 13.1 Report 79 Model Coefficients.

	Coefficient	Std. Error	t	P	VIF
Constant	-98.874	4.135	-23.912	<0.001	
Dev Max Avg NDVI	92.943	4.592	20.242	<0.001	2517.545
ln Dev Max Avg NDVI	-63.856	3.146	-20.296	<0.001	2291.334
ln Dev Max Avg CWSI	-1.114	0.0239	-46.562	<0.001	8.926
Seasonal Avg Min Temp	0.924	0.0292	31.627	<0.001	5.141

Warning: Multicollinearity is present among the independent variables. The variables with the largest values of VIF are causing the problem. Consider getting more data or eliminating one or more variables from the equation. The likely candidates for elimination are: Dev Max Avg NDVI , ln Dev Max Avg NDVI , ln Dev Max Avg CWSI , Seasonal Avg Min Temp

Analysis of Variance:

Table C.88 Multiyear Testing Report 13.1 Report 79 Analysis of Variance.

	DF	SS	MS	F	P
Regression	4	10344.610	2586.152	11434.572	<0.001
Residual	8727	1973.782	0.226		
Total	8731	12318.392	1.411		

Table C.89 Multiyear Testing Report 13.1 Report 79 Sum of Squares.

Column	**SSIncr**	**SSMarg**

Dev Max Avg NDVI	7239.755	92.673
ln Dev Max Avg NDVI	2607.114	93.162
ln Dev Max Avg CWSI	271.514	490.343
Seasonal Avg Min Temp	226.227	226.227

The dependent variable Ece (dS/m) can be predicted from a linear combination of the independent variables:

Table C.90 Multiyear Testing Report 13.1 Report 79 Probability of Predicting Independent Variable.

	P
Dev Max Avg NDVI	<0.001
ln Dev Max Avg NDVI	<0.001
ln Dev Max Avg CWSI	<0.001
Seasonal Avg Min Temp	<0.001

All independent variables appear to contribute to predicting Ece (dS/m) (P < 0.05).

Normality Test (Kolmogorov-Smirnov) Failed (P = <0.001)

Constant Variance Test (Spearman Rank Correlation): Failed (P = <0.001)

Power of performed test with alpha = 0.050: 1.000

Multiyear Testing Report 13.2 Report 21
Multiple Linear Regression Friday, April 25, 2025 10:56:32 AM

Data source: Data 1 in Multiyear Corn Field Optimization Data Testing Report 13.2

Ece (dS/m) = -88.111 + (92.450 * Dev Max Avg NDVI) - (1.137 * Dev Max Avg CRSI) - (63.411 * ln Dev Max Avg NDVI) - (1.126 * ln Dev Max Avg CWSI) + (0.0135 * Seasonal Precipitation)

N = 8732

R = 0.916 Rsqr = 0.840 Adj Rsqr = 0.840

Standard Error of Estimate = 0.476

Table C.91 Multiyear Testing Report 13.2 Report 21 Model Coefficients.

	Coefficient	Std. Error	t	P	VIF
Constant	-88.111	4.530	-19.450	<0.001	
Dev Max Avg NDVI	92.450	4.618	20.019	<0.001	2546.657
Dev Max Avg CRSI	-1.137	1.138	-0.999	0.318	7.824
ln Dev Max Avg NDVI	-63.411	3.178	-19.955	<0.001	2337.202
ln Dev Max Avg CWSI	-1.126	0.0265	-42.436	<0.001	10.967
Seasonal Precipitation	0.0135	0.000430	31.372	<0.001	5.279

Warning: Multicollinearity is present among the independent variables. The variables with the largest values of VIF are causing the problem. Consider getting more data or eliminating one or more variables from the equation. The likely candidates for elimination are: Dev Max Avg NDVI , Dev Max Avg CRSI , ln Dev Max Avg NDVI , ln Dev Max Avg CWSI , Seasonal Precipitation

Analysis of Variance:

Table C.92 Multiyear Testing Report 13.2 Report 21 Analysis of Variance.

	DF	SS	MS	F	P
Regression	5	10344.836	2068.967	9147.856	<0.001
Residual	8726	1973.556	0.226		
Total	8731	12318.392	1.411		

Table C.93 Multiyear Testing Report 13.2 Report 21 Sum of Squares.

Column	SSIncr	SSMarg
Dev Max Avg NDVI	7239.755	90.644
Dev Max Avg CRSI	926.323	0.226
ln Dev Max Avg NDVI	1771.425	90.065
ln Dev Max Avg CWSI	184.730	407.297
Seasonal Precipitation	222.603	222.603

The dependent variable Ece (dS/m) can be predicted from a linear combination of the independent variables:

Table C.94 Multiyear Testing Report 13.2 Report 21 Probability of Predicting Dependent Variable.

	P
Dev Max Avg NDVI	<0.001
Dev Max Avg CRSI	0.318
ln Dev Max Avg NDVI	<0.001
ln Dev Max Avg CWSI	<0.001
Seasonal Precipitation	<0.001

Not all of the independent variables appear necessary (or the multiple linear model may be underspecified).
The following appear to account for the ability to predict Ece (dS/m) (P < 0.05): Dev Max Avg NDVI , ln Dev Max Avg NDVI , ln Dev Max Avg CWSI , Seasonal Precipitation

Normality Test (Kolmogorov-Smirnov) Failed (P = <0.001)

Constant Variance Test (Spearman Rank Correlation): Failed (P = <0.001)

Power of performed test with alpha = 0.050: 1.000

Multiyear Testing Report 13.2 Report 22
Multiple Linear Regression Friday, April 25, 2025 10:56:37 AM

Data source: Data 1 in Multiyear Corn Field Optimization Data Testing Report 13.2

Ece (dS/m) = -97.441 + (92.450 * Dev Max Avg NDVI) - (1.137 * Dev Max Avg CRSI) - (63.411 * ln Dev Max Avg NDVI) - (1.126 * ln Dev Max Avg CWSI) + (0.929 * Seasonal Avg Min Temp)

N = 8732

R = 0.916 Rsqr = 0.840 Adj Rsqr = 0.840

Standard Error of Estimate = 0.476

Table C.95 Multiyear Testing Report 13.2 Report 22 Model Coefficients.

	Coefficient	Std. Error	t	P	VIF
Constant	-97.441	4.377	-22.265	<0.001	
Dev Max Avg NDVI	92.450	4.618	20.019	<0.001	2546.657
Dev Max Avg CRSI	-1.137	1.138	-0.999	0.318	7.824
ln Dev Max Avg NDVI	-63.411	3.178	-19.955	<0.001	2337.202
ln Dev Max Avg CWSI	-1.126	0.0265	-42.436	<0.001	10.967
Seasonal Avg Min Temp	0.929	0.0296	31.372	<0.001	5.279

Warning: Multicollinearity is present among the independent variables. The variables with the largest values of VIF are causing the problem. Consider getting more data or eliminating one or more variables from the equation. The likely candidates for elimination are: Dev Max Avg NDVI , Dev Max Avg CRSI , ln Dev Max Avg NDVI , ln Dev Max Avg CWSI , Seasonal Avg Min Temp

Analysis of Variance:

Table C.96 Multiyear Testing Report 13.2 Report 22 Analysis of Variance.

	DF	SS	MS	F	P
Regression	5	10344.836	2068.967	9147.856	<0.001
Residual	8726	1973.556	0.226		
Total	8731	12318.392	1.411		

Table C.97 Multiyear Testing Report 13.2 Report 22 Sum of Squares.

Column	SSIncr	SSMarg
Dev Max Avg NDVI	7239.755	90.644
Dev Max Avg CRSI	926.323	0.226
ln Dev Max Avg NDVI	1771.425	90.065
ln Dev Max Avg CWSI	184.730	407.297
Seasonal Avg Min Temp	222.603	222.603

The dependent variable Ece (dS/m) can be predicted from a linear combination of the independent variables:

Table C.98 Multiyear Testing Report 13.2 Report 22 Probability of Predicting Dependent Variable.

	P
Dev Max Avg NDVI	<0.001
Dev Max Avg CRSI	0.318
ln Dev Max Avg NDVI	<0.001
ln Dev Max Avg CWSI	<0.001
Seasonal Avg Min Temp	<0.001

Not all of the independent variables appear necessary (or the multiple linear model may be underspecified).
The following appear to account for the ability to predict Ece (dS/m) ($P < 0.05$): Dev Max Avg NDVI , ln Dev Max Avg NDVI , ln Dev Max Avg CWSI , Seasonal Avg Min Temp

Normality Test (Kolmogorov-Smirnov) Failed ($P = <0.001$)

Constant Variance Test (Spearman Rank Correlation): Failed ($P = <0.001$)

Power of performed test with alpha = 0.050: 1.000

Multiyear Testing Report 13.2 Report 38
Multiple Linear Regression Friday, April 25, 2025 10:56:37 AM

Data source: Data 1 in Multiyear Corn Field Optimization Data Testing Report 13.2

Ece (dS/m) = -97.441 + (92.450 * Dev Max Avg NDVI) - (1.137 * Dev Max Avg CRSI) - (63.411 * ln Dev Max Avg NDVI) - (1.126 * ln Dev Max Avg CWSI) + (0.929 * Seasonal Avg Min Temp)

N = 8732

R = 0.916 Rsqr = 0.840 Adj Rsqr = 0.840

Standard Error of Estimate = 0.476

Table C.99 Multiyear Testing Report 13.2 Report 38 Model Coefficients.

	Coefficient	Std. Error	t	P	VIF
Constant	-97.441	4.377	-22.265	<0.001	
Dev Max Avg NDVI	92.450	4.618	20.019	<0.001	2546.657
Dev Max Avg CRSI	-1.137	1.138	-0.999	0.318	7.824
ln Dev Max Avg NDVI	-63.411	3.178	-19.955	<0.001	2337.202
ln Dev Max Avg CWSI	-1.126	0.0265	-42.436	<0.001	10.967
Seasonal Avg Min Temp	0.929	0.0296	31.372	<0.001	5.279

Warning: Multicollinearity is present among the independent variables. The variables with the largest values of VIF are causing the problem. Consider getting more data or eliminating one or more variables from the equation. The likely candidates for elimination are: Dev Max Avg NDVI , Dev Max Avg CRSI , ln Dev Max Avg NDVI , ln Dev Max Avg CWSI , Seasonal Avg Min Temp

Analysis of Variance:

Table C.100 Multiyear Testing Report 13.2 Report 38 Analysis of Variance.

	DF	SS	MS	F	P
Regression	5	10344.836	2068.967	9147.856	<0.001
Residual	8726	1973.556	0.226		
Total	8731	12318.392	1.411		

Table C.101 Multiyear Testing Report 13.2 Report 38 Sum of Squares.

Column	SSIncr	SSMarg
Dev Max Avg NDVI	7239.755	90.644
Dev Max Avg CRSI	926.323	0.226
ln Dev Max Avg NDVI	1771.425	90.065
ln Dev Max Avg CWSI	184.730	407.297
Seasonal Avg Min Temp	222.603	222.603

The dependent variable Ece (dS/m) can be predicted from a linear combination of the independent variables:

Table C.102 Multiyear Testing Report 13.2 Report 38 Probability of Predicting Dependent Variable.

	P
Dev Max Avg NDVI	<0.001
Dev Max Avg CRSI	0.318
ln Dev Max Avg NDVI	<0.001
ln Dev Max Avg CWSI	<0.001
Seasonal Avg Min Temp	<0.001

Not all of the independent variables appear necessary (or the multiple linear model may be underspecified).
The following appear to account for the ability to predict Ece (dS/m) ($P < 0.05$): Dev Max Avg NDVI , ln Dev Max Avg NDVI , ln Dev Max Avg CWSI , Seasonal Avg Min Temp

Normality Test (Kolmogorov-Smirnov) Failed ($P = <0.001$)

Constant Variance Test (Spearman Rank Correlation): Failed ($P = <0.001$)

Power of performed test with alpha = 0.050: 1.000

Multiyear Testing Report 13.2 Report 39
Multiple Linear Regression Friday, April 25, 2025 11:02:31 AM

Data source: Data 1 in Multiyear Corn Field Optimization Data Testing Report 13.2

Ece (dS/m) = -98.544 + (92.419 * Dev Max Avg NDVI) - (63.387 * ln Dev Max Avg NDVI) - (1.030 * ln Dev Max Avg CRSI) - (1.126 * ln Dev Max Avg CWSI) + (0.929 * Seasonal Avg Min Temp)

N = 8732

R = 0.916 Rsqr = 0.840 Adj Rsqr = 0.840

Standard Error of Estimate = 0.476

Table C.103 Multiyear Testing Report 13.2 Report 39 Model Coefficients.

	Coefficient	Std. Error	t	P	VIF
Constant	-98.544	4.147	-23.761	<0.001	
Dev Max Avg NDVI	92.419	4.620	20.006	<0.001	2548.456
ln Dev Max Avg NDVI	-63.387	3.179	-19.938	<0.001	2339.447
ln Dev Max Avg CRSI	-1.030	1.001	-1.030	0.303	7.696
ln Dev Max Avg CWSI	-1.126	0.0265	-42.562	<0.001	10.906
Seasonal Avg Min Temp	0.929	0.0296	31.394	<0.001	5.272

Warning: Multicollinearity is present among the independent variables. The variables with the largest values of VIF are causing the problem. Consider getting more data or eliminating one or more variables from the equation. The likely candidates for elimination are: Dev Max Avg NDVI , ln Dev Max Avg NDVI , ln Dev Max Avg CRSI , ln Dev Max Avg CWSI , Seasonal Avg Min Temp

Analysis of Variance:

Table C.104Multiyear Testing Report 13.2 Report 39 Analysis of Variance.

	DF	SS	MS	F	P
Regression	5	10344.850	2068.970	9147.932	<0.001
Residual	8726	1973.542	0.226		
Total	8731	12318.392	1.411		

Table C.105Multiyear Testing Report 13.2 Report 39 Sum of Squares.

Column	SSIncr	SSMarg
Dev Max Avg NDVI	7239.755	90.520
ln Dev Max Avg NDVI	2607.114	89.909
ln Dev Max Avg CRSI	88.210	0.240
ln Dev Max Avg CWSI	186.856	409.715
Seasonal Avg Min Temp	222.914	222.914

The dependent variable Ece (dS/m) can be predicted from a linear combination of the independent variables:

Table C.106 Multiyear Testing Report 13.2 Report 39 Probability of Predicting Dependent Variable.

	P
Dev Max Avg NDVI	<0.001
ln Dev Max Avg NDVI	<0.001
ln Dev Max Avg CRSI	0.303
ln Dev Max Avg CWSI	<0.001
Seasonal Avg Min Temp	<0.001

Not all of the independent variables appear necessary (or the multiple linear model may be underspecified).

The following appear to account for the ability to predict Ece (dS/m) (P < 0.05): Dev Max Avg NDVI , ln Dev Max Avg NDVI , ln Dev Max Avg CWSI , Seasonal Avg Min Temp

Normality Test (Kolmogorov-Smirnov) Failed (P = <0.001)

Constant Variance Test (Spearman Rank Correlation): Failed (P = <0.001)

Power of performed test with alpha = 0.050: 1.000

2024 Non-Corn Field Report 3 Dependent Variable ln(ECe)
Best Subsets Regression Friday, April 25, 2025 6:24:23 PM

Data source: Data 1 in 2024 Non Corn Optimization Data

Using R squared as best criterion.

Table C.107 2024 Non-Corn Field Report 3 Variable Definitions.

Variable	Symbol
Avg NDVI	A
Avg CRSI	B
Avg CWSI	C
ln Avg NDVI	D
ln Avg CRSI	E
ln Avg CWSI	F
Dev Precipitation	G
Dev Avg Min Temp	H

Table C.108 2024 Non-Corn Field Report 3 Model Summary.

Model #	Variable	Cp	Rsqr	Adj Rsqr	MSerr	A	B	C	D	E	F	G	H
1	1	12442.060	0.632	0.632	0.121							*	
2	2	7368.929	0.659	0.659	0.112							*	*
3	3	5072.206	0.671	0.671	0.108	*	*					*	
4	4	2760.426	0.684	0.684	0.104	*	*			*		*	
5	5	1296.974	0.692	0.692	0.101	*	*		*	*		*	
6	6	115.489	0.698	0.698	0.099	*	*		*	*		*	*
7	7	7.141	0.699	0.699	0.099	*	*		*	*	*	*	*
8	8	9.000	0.699	0.699	0.099	*	*	*	*	*	*	*	*

Table C.109 2024 Non-Corn Field Report 3 Model 1 Coefficients.

Model # 1	**R squared**	**0.632**			
Variable	**Coef.**	**Std. Error**	**t**	**P**	**VIF**
Constant	-0.691	0.00542	-127.514	<0.001	0.000
Dev Precipitation	0.0582	0.000188	309.260	<0.001	1.000

Table C.110 2024 Non-Corn Field Report 3 Model 3 Coefficients.

Model # 2	**R squared**	**0.659**			
Variable	**Coef.**	**Std. Error**	**t**	**P**	**VIF**
Constant	-3.202	0.0379	-84.560	<0.001	0.000
Dev Precipitation	0.0477	0.000239	199.565	<0.001	1.745

Dev Avg Min Temp	0.208	0.00310	66.957	<0.001	1.745

Table C.111 2024 Non-Corn Field Report 3 Model 3 Coefficients.

Model # 3	**R squared**	**0.671**			
Variable	**Coef.**	**Std. Error**	**t**	**P**	**VIF**
Constant	2.808	0.0802	35.031	<0.001	0.000
Avg NDVI	1.493	0.0205	72.687	<0.001	6.682 <
Avg CRSI	-4.919	0.107	-45.944	<0.001	6.782 <
Dev Precipitation	0.0514	0.000220	233.784	<0.001	1.532

Table C.112 2024 Non-Corn Field Report 3 Model 4 Coefficients.

Model # 4	**R squared**	**0.684**			
Variable	**Coef.**	**Std. Error**	**t**	**P**	**VIF**
Constant	127.437	2.655	47.993	<0.001	0.000
Avg NDVI	2.100	0.0239	87.731	<0.001	9.437 <
Avg CRSI	-132.044	2.709	-48.736	<0.001	4514.785 <
ln Avg CRSI	103.841	2.211	46.956	<0.001	4281.669 <
Dev Precipitation	0.0541	0.000223	242.446	<0.001	1.639

Table C.113 2024 Non-Corn Field Report 3 Model 5 Coefficients.

Model # 5	**R squared**	**0.692**			
Variable	**Coef.**	**Std. Error**	**t**	**P**	**VIF**
Constant	163.273	2.788	58.570	<0.001	0.000
Avg NDVI	4.683	0.0722	64.838	<0.001	88.126 <
Avg CRSI	-170.875	2.865	-59.637	<0.001	5178.867 <
ln Avg NDVI	-1.257	0.0332	-37.846	<0.001	75.664 <
ln Avg CRSI	135.673	2.340	57.980	<0.001	4916.966 <
Dev Precipitation	0.0583	0.000247	235.745	<0.001	2.070

Table C.114 2024 Non-Corn Field Report 3 Model 6 Coefficients.

Model # 6	**R squared**	**0.698**			
Variable	**Coef.**	**Std. Error**	**t**	**P**	**VIF**
Constant	165.930	2.760	60.126	<0.001	0.000
Avg NDVI	4.368	0.0721	60.616	<0.001	89.575 <
Avg CRSI	-174.766	2.838	-61.588	<0.001	5187.125 <

ln Avg NDVI	-1.251	0.0329	-38.054	<0.001	75.667 <
ln Avg CRSI	139.570	2.318	60.201	<0.001	4928.751 <
Dev Precipitation	0.0545	0.000270	202.094	<0.001	2.508
Dev Avg Min Temp	0.118	0.00342	34.368	<0.001	2.397

Table C.115 2024 Non-Corn Field Report 3 Model 7 Coefficients.

Model # 7	**R squared**	**0.699**			
Variable	**Coef.**	**Std. Error**	**t**	**P**	**VIF**
Constant	152.900	3.023	50.576	<0.001	0.000
Avg NDVI	4.525	0.0735	61.543	<0.001	93.456 <
Avg CRSI	-161.546	3.102	-52.083	<0.001	6209.347 <
ln Avg NDVI	-1.317	0.0334	-39.392	<0.001	78.490 <
ln Avg CRSI	128.836	2.532	50.893	<0.001	5888.036 <
ln Avg CWSI	0.00959	0.000913	10.505	<0.001	2.559
Dev Precipitation	0.0540	0.000273	197.619	<0.001	2.581
Dev Avg Min Temp	0.113	0.00344	32.867	<0.001	2.433

Table C.116 2024 Non-Corn Field Report 3 Model 8 Coefficients.

Model # 8	**R squared**	**0.699**			
Variable	**Coef.**	**Std. Error**	**t**	**P**	**VIF**
Constant	152.549	3.164	48.211	<0.001	0.000
Avg NDVI	4.513	0.0800	56.427	<0.001	110.585 <
Avg CRSI	-161.182	3.249	-49.607	<0.001	6813.874 <
Avg CWSI	0.0145	0.0387	0.376	0.707	35.497 <
ln Avg NDVI	-1.307	0.0432	-30.248	<0.001	131.046 <
ln Avg CRSI	128.555	2.639	48.712	<0.001	6398.989 <
ln Avg CWSI	0.00947	0.000962	9.847	<0.001	2.843
Dev Precipitation	0.0540	0.000274	196.748	<0.001	2.605
Dev Avg Min Temp	0.114	0.00360	31.557	<0.001	2.658

2024 Non-Corn Field Report 5 Dependent Variable ln(ECe)
Best Subsets Regression Friday, April 25, 2025 6:24:57 PM

Data source: Data 1 in 2024 Non Corn Optimization Data

Using R squared as best criterion.

Table C.117 2024 Non-Corn Field Report 5 Variable Definitions.

Variable	Symbol
Dev Avg NDVI	A
Dev Avg CRSI	B
Dev Avg CWSI	C
ln Dev Avg NDVI	D
ln Dev Avg CRSI	E
ln Dev Avg CWSI	F
Annual Precipitation	G
Annual Avg Min Temp	H

Table C.118 2024 Non-Corn Field Report 5 Model Summary.

Model #	Variable	Cp	Rsqr	Adj Rsqr	MSerr	A	B	C	D	E	F	G	H
1	1	5760.246	0.609	0.609	0.128							*	
2	2	4795.192	0.615	0.615	0.126				*			*	
3	3	2627.434	0.629	0.629	0.122			*	*			*	
4	4	876.438	0.640	0.640	0.118	*		*	*			*	
5	5	331.909	0.644	0.644	0.117	*		*	*		*	*	
6	6	314.212	0.644	0.644	0.117	*		*	*		*	*	*
7	7	25.483	0.646	0.646	0.116	*	*	*	*	*	*	*	
8	8	9.000	0.646	0.646	0.116	*	*	*	*	*	*	*	*

Table C.119 2024 Non-Corn Field Report 5 Model 1 Coefficients.

Model # 1	**R squared**	**0.609**			
Variable	**Coef.**	**Std. Error**	**t**	**P**	**VIF**
Constant	-0.879	0.00629	-139.694	<0.001	0.000
Annual Precipitation	0.00541	0.0000183	294.904	<0.001	1.000

Table C.120 2024 Non-Corn Field Report 5 Model 2 Coefficients.

Model # 2	**R squared**	**0.615**			
Variable	**Coef.**	**Std. Error**	**t**	**P**	**VIF**
Constant	-0.675	0.00925	-72.885	<0.001	0.000

ln Dev Avg NDVI	0.142	0.00477	29.842	<0.001	1.424
Annual Precipitation	0.00506	0.0000217	232.841	<0.001	1.424

Table C.121 2024 Non-Corn Field Report 5 Model 3 Coefficients.

Model # 3	**R squared**	**0.629**			
Variable	**Coef.**	**Std. Error**	**t**	**P**	**VIF**
Constant	-0.743	0.00921	-80.690	<0.001	0.000
Dev Avg CWSI	1.133	0.0249	45.523	<0.001	10.910 <
ln Dev Avg NDVI	0.631	0.0117	53.877	<0.001	8.904 <
Annual Precipitation	0.00560	0.0000244	229.246	<0.001	1.867

Table C.122 2024 Non-Corn Field Report 5 Model 4 Coefficients.

Model # 4	**R squared**	**0.640**			
Variable	**Coef.**	**Std. Error**	**t**	**P**	**VIF**
Constant	1.453	0.0536	27.088	<0.001	0.000
Dev Avg NDVI	-2.461	0.0592	-41.546	<0.001	50.151 <
Dev Avg CWSI	1.719	0.0283	60.780	<0.001	14.520 <
ln Dev Avg NDVI	2.041	0.0359	56.932	<0.001	86.081 <
Annual Precipitation	0.00557	0.0000241	231.225	<0.001	1.869

Table C.123 2024 Non-Corn Field Report 5 Model 5 Coefficients.

Model # 5	**R squared**	**0.644**			
Variable	**Coef.**	**Std. Error**	**t**	**P**	**VIF**
Constant	2.186	0.0619	35.283	<0.001	0.000
Dev Avg NDVI	-3.457	0.0728	-47.480	<0.001	76.532 <
Dev Avg CWSI	2.197	0.0348	63.093	<0.001	22.220 <
ln Dev Avg NDVI	2.621	0.0435	60.254	<0.001	128.000 <
ln Dev Avg CWSI	-0.0243	0.00104	-23.310	<0.001	2.716
Annual Precipitation	0.00571	0.0000247	231.038	<0.001	1.987

Table C.124 2024 Non-Corn Field Report 5 Model 6 Coefficients.

Model # 6	**R squared**	**0.644**			
Variable	**Coef.**	**Std. Error**	**t**	**P**	**VIF**
Constant	2.256	0.0640	35.276	<0.001	0.000
Dev Avg NDVI	-3.570	0.0772	-46.273	<0.001	85.967 <
Dev Avg CWSI	2.239	0.0361	61.979	<0.001	23.942 <
ln Dev Avg NDVI	2.688	0.0461	58.376	<0.001	143.464 <
ln Dev Avg CWSI	-0.0250	0.00105	-23.706	<0.001	2.772
Annual Precipitation	0.00572	0.0000251	228.473	<0.001	2.046
Annual Avg Min Temp	0.0123	0.00278	4.426	<0.001	1.155

Table C.125 2024 Non-Corn Field Report 5 Model 7 Coefficients.

Model # 7	**R squared**	**0.646**			
Variable	**Coef.**	**Std. Error**	**t**	**P**	**VIF**
Constant	40.170	2.159	18.610	<0.001	0.000
Dev Avg NDVI	-3.235	0.0737	-43.885	<0.001	78.853 <
Dev Avg CRSI	-38.872	2.208	-17.607	<0.001	2633.601 <
Dev Avg CWSI	2.480	0.0383	64.729	<0.001	27.054 <
ln Dev Avg NDVI	2.685	0.0443	60.554	<0.001	133.682 <
ln Dev Avg CRSI	31.617	1.800	17.564	<0.001	2543.924 <
ln Dev Avg CWSI	-0.0290	0.00107	-27.023	<0.001	2.896
Annual Precipitation	0.00593	0.0000277	214.073	<0.001	2.513

Table C.126 2024 Non-Corn Field Report 5 Model 8 Coefficients.

Model # 8	**R squared**	**0.646**			
Variable	**Coef.**	**Std. Error**	**t**	**P**	**VIF**
Constant	40.183	2.158	18.619	<0.001	0.000
Dev Avg NDVI	-3.348	0.0783	-42.766	<0.001	88.997 <

Dev Avg CRSI	-38.805	2.207	-17.579	<0.001	2633.734 <
Dev Avg CWSI	2.519	0.0394	63.943	<0.001	28.628 <
ln Dev Avg NDVI	2.743	0.0463	59.190	<0.001	146.069 <
ln Dev Avg CRSI	31.642	1.800	17.580	<0.001	2543.951 <
ln Dev Avg CWSI	-0.0296	0.00108	-27.359	<0.001	2.949
Annual Precipitation	0.00595	0.0000280	212.386	<0.001	2.569
Annual Avg Min Temp	0.0122	0.00285	4.299	<0.001	1.216

2024 Non-Corn Field Report 7 Dependent Variable ln(ECe)
Best Subsets Regression Friday, April 25, 2025 6:25:17 PM

Data source: Data 1 in 2024 Non Corn Optimization Data

Using R squared as best criterion.

Table C.127 2024 Non-Corn Field Report 7 Variable Definitions.

Variable	Symbol
Dev Avg NDVI	A
Dev Avg CRSI	B
Dev Avg CWSI	C
ln Dev Avg NDVI	D
ln Dev Avg CRSI	E
ln Dev Avg CWSI	F
Dev Precipitation	G
Dev Avg Min Temp	H

Table C.128 2024 Non-Corn Field Report 7 Model Summary.

Model #	Variable	Cp	Rsqr	Adj Rsqr	MSerr	A	B	C	D	E	F	G	H
1	1	12744.254	0.632	0.632	0.121							*	
2	2	7648.645	0.659	0.659	0.112							*	*
3	3	5351.596	0.671	0.671	0.108				*			*	*
4	4	3205.416	0.683	0.683	0.104			*	*			*	*
5	5	1447.750	0.692	0.692	0.101	*		*	*			*	*
6	6	1140.858	0.694	0.694	0.100		*	*	*	*		*	*
7	7	494.350	0.697	0.697	0.099	*	*	*	*	*		*	*
8	8	9.000	0.700	0.700	0.098	*	*	*	*	*	*	*	*

Table C.129 2024 Non-Corn Field Report 7 Model 1 Coefficients.

Model # 1	**R squared =**	**0.632**			
Variable	**Coef.**	**Std. Error**	**t**	**P**	**VIF**
Constant	-0.691	0.00542	-127.514	<0.001	0.000
Dev Precipitation	0.0582	0.000188	309.260	<0.001	1.000

Table C.130 2024 Non-Corn Field Report 7 Model 2 Coefficients.

Model # 2	**R squared**	**0.659**			
Variable	**Coef.**	**Std. Error**	**t**	**P**	**VIF**
Constant	-3.202	0.0379	-84.560	<0.001	0.000

Dev Precipitation	0.0477	0.000239	199.565	<0.001	1.745
Dev Avg Min Temp	0.208	0.00310	66.957	<0.001	1.745

Table C.131 2024 Non-Corn Field Report 7 Model 3 Coefficients.

Model # 3	**R squared**	**0.671**			
Variable	**Coef.**	**Std. Error**	**t**	**P**	**VIF**
Constant	-2.513	0.0401	-62.682	<0.001	0.000
ln Dev Avg NDVI	0.196	0.00428	45.803	<0.001	1.343
Dev Precipitation	0.0453	0.000240	188.755	<0.001	1.829
Dev Avg Min Temp	0.170	0.00315	54.021	<0.001	1.871

Table C.132 2024 Non-Corn Field Report 7 Model 4 Coefficients.

Model # 4	**R squared**	**0.683**			
Variable	**Coef.**	**Std. Error**	**t**	**P**	**VIF**
Constant	-2.735	0.0397	-68.893	<0.001	0.000
Dev Avg CWSI	1.012	0.0224	45.074	<0.001	10.378 <
ln Dev Avg NDVI	0.644	0.0108	59.671	<0.001	8.863 <
Dev Precipitation	0.0489	0.000248	196.600	<0.001	2.029
Dev Avg Min Temp	0.187	0.00312	60.067	<0.001	1.899

Table C.133 2024 Non-Corn Field Report 7 Model 5 Coefficients.

Model # 5	**R squared**	**0.692**			
Variable	**Coef.**	**Std. Error**	**t**	**P**	**VIF**
Constant	-1.103	0.0555	-19.867	<0.001	0.000
Dev Avg NDVI	-2.419	0.0584	-41.417	<0.001	57.014 <
Dev Avg CWSI	1.588	0.0261	60.789	<0.001	14.487 <
ln Dev Avg NDVI	2.021	0.0349	57.908	<0.001	95.436 <
Dev Precipitation	0.0459	0.000255	180.145	<0.001	2.200
Dev Avg Min Temp	0.231	0.00325	71.152	<0.001	2.124

Table C.134 2024 Non-Corn Field Report 7 Model 6 Coefficients.

Model # 6	**R squared**	**0.694**			
Variable	**Coef.**	**Std. Error**	**t**	**P**	**VIF**
Constant	77.447	1.841	42.066	<0.001	0.000
Dev Avg CRSI	-81.724	1.876	-43.553	<0.001	2202.988 <
Dev Avg CWSI	1.637	0.0261	62.772	<0.001	14.517 <
ln Dev Avg NDVI	1.130	0.0164	68.895	<0.001	21.191 <
ln Dev Avg CRSI	65.699	1.531	42.911	<0.001	2130.996 <
Dev Precipitation	0.0527	0.000261	202.034	<0.001	2.320
Dev Avg Min Temp	0.196	0.00319	61.362	<0.001	2.052

Table C.135 2024 Non-Corn Field Report 7 Model 7 Coefficients.

Model # 7	**R squared**	**0.697**			
Variable	**Coef.**	**Std. Error**	**t**	**P**	**VIF**
Constant	58.611	1.976	29.668	<0.001	0.000
Dev Avg NDVI	-1.613	0.0636	-25.356	<0.001	68.804 <
Dev Avg CRSI	-61.418	2.030	-30.249	<0.001	2608.909 <
Dev Avg CWSI	1.863	0.0274	67.948	<0.001	16.239 <
ln Dev Avg NDVI	1.919	0.0351	54.621	<0.001	98.360 <
ln Dev Avg CRSI	49.448	1.652	29.937	<0.001	2508.717 <
Dev Precipitation	0.0498	0.000285	174.651	<0.001	2.796
Dev Avg Min Temp	0.224	0.00336	66.621	<0.001	2.301

Table C.136 2024 Non-Corn Field Report 7 Model 8 Coefficients.

Model # 8	**R squared**	**0.700**			
Variable	**Coef.**	**Std. Error**	**t**	**P**	**VIF**
Constant	68.887	2.021	34.080	<0.001	0.000
Dev Avg NDVI	-2.425	0.0733	-33.109	<0.001	92.023 <
Dev Avg CRSI	-71.394	2.071	-34.465	<0.001	2739.273 <

Dev Avg CWSI	2.324	0.0344	67.633	<0.001	25.714 <
ln Dev Avg NDVI	2.436	0.0421	57.873	<0.001	142.349 <
ln Dev Avg CRSI	57.567	1.685	34.160	<0.001	2634.177 <
ln Dev Avg CWSI	-0.0215	0.000974	-22.076	<0.001	2.818
Dev Precipitation	0.0506	0.000286	176.791	<0.001	2.845
Dev Avg Min Temp	0.235	0.00338	69.479	<0.001	2.355

2024 Non-Corn Field Report 8 Dependent Variable ln(ECe)
Best Subsets Regression Friday, April 25, 2025 6:25:42 PM

Data source: Data 1 in 2024 Non Corn Optimization Data

Using R squared as best criterion.

Table C.137 2024 Non-Corn Field Report 8 Variable Definitions.

Variable	Symbol
Mid Avg NDVI	A
Mid Avg CRSI	B
Mid Avg CWSI	C
ln Mid Avg NDVI	D
ln Mid Avg CRSI	E
ln Mid Avg CWSI	F
Annual Precipitation	G
Annual Avg Min Temp	H

Table C.138 2024 Non-Corn Field Report 8 Model Summary.

Model #	Variable	Cp	Rsqr	Adj Rsqr	MSerr	A	B	C	D	E	F	G	H
1	1	12382.080	0.609	0.609	0.128							*	
2	2	10980.502	0.617	0.617	0.125				*			*	
3	3	5418.101	0.649	0.649	0.115	*	*					*	
4	4	3597.704	0.660	0.660	0.112	*	*					*	*
5	5	1710.919	0.670	0.670	0.108	*	*			*		*	*
6	6	712.931	0.676	0.676	0.106	*	*		*	*		*	*
7	7	462.330	0.678	0.678	0.106	*	*		*	*	*	*	*
8	8	9.000	0.680	0.680	0.105	*	*	*	*	*	*	*	*

Table C.139 2024 Non-Corn Field Report 8 Model 1 Coefficients.

Model # 1	**R squared =**	**0.609**			
Variable	**Coef.**	**Std. Error**	**t**	**P**	**VIF**
Constant	-0.879	0.00629	-139.694	<0.001	0.000
Annual Precipitation	0.00541	0.0000183	294.904	<0.001	1.000

Table C.140 2024 Non-Corn Field Report 8 Model 2 Coefficients.

Model # 2	**R squared**	**0.617**			
Variable	**Coef.**	**Std. Error**	**t**	**P**	**VIF**

Constant	-0.570	0.0110	-51.992	<0.001	0.000
ln Mid Avg NDVI	0.181	0.00528	34.246	<0.001	2.137
Annual Precipitation	0.00475	0.0000265	178.880	<0.001	2.137

Table C.141 2024 Non-Corn Field Report 8 Model 3 Coefficients.

Model # 3	**R squared**	**0.649**			
Variable	**Coef.**	**Std. Error**	**t**	**P**	**VIF**
Constant	4.088	0.0703	58.163	<0.001	0.000
Mid Avg NDVI	1.659	0.0208	79.619	<0.001	8.868 <
Mid Avg CRSI	-6.695	0.0940	-71.231	<0.001	7.591 <
Annual Precipitation	0.00470	0.0000253	186.138	<0.001	2.110

Table C.142 2024 Non-Corn Field Report 8 Model 4 Coefficients.

Model # 4	**R squared**	**0.660**			
Variable	**Coef.**	**Std. Error**	**t**	**P**	**VIF**
Constant	4.644	0.0705	65.848	<0.001	0.000
Mid Avg NDVI	1.957	0.0218	89.979	<0.001	9.964 <
Mid Avg CRSI	-7.171	0.0933	-76.869	<0.001	7.708 <
Annual Precipitation	0.00427	0.0000270	157.985	<0.001	2.486
Annual Avg Min Temp	-0.118	0.00285	-41.378	<0.001	1.271

Table C.143 2024 Non-Corn Field Report 8 Model 5 Coefficients.

Model # 5	**R squared**	**0.670**			
Variable	**Coef.**	**Std. Error**	**t**	**P**	**VIF**
Constant	68.462	1.492	45.876	<0.001	0.000
Mid Avg NDVI	1.795	0.0217	82.554	<0.001	10.278 <
Mid Avg CRSI	-71.458	1.504	-47.498	<0.001	2070.259 <
ln Mid Avg CRSI	55.360	1.293	42.811	<0.001	2111.006 <
Annual Precipitation	0.00428	0.0000266	161.192	<0.001	2.487
Annual Avg Min Temp	-0.125	0.00281	-44.447	<0.001	1.275

Table C.144 2024 Non-Corn Field Report 8 Model 6 Coefficients.

Model # 6	**R squared**	**0.676**			
Variable	**Coef.**	**Std. Error**	**t**	**P**	**VIF**
Constant	90.902	1.643	55.339	<0.001	0.000
Mid Avg NDVI	3.888	0.0700	55.536	<0.001	108.452 <
Mid Avg CRSI	-96.237	1.687	-57.048	<0.001	2649.055 <
ln Mid Avg NDVI	-1.023	0.0326	-31.424	<0.001	95.794 <
ln Mid Avg CRSI	75.863	1.438	52.743	<0.001	2657.871 <
Annual Precipitation	0.00450	0.0000273	165.224	<0.001	2.663
Annual Avg Min Temp	-0.0973	0.00292	-33.284	<0.001	1.402

Table C.145 2024 Non-Corn Field Report 8 Model 7 Coefficients.

Model # 7	**R squared**	**0.678**			
Variable	**Coef.**	**Std. Error**	**t**	**P**	**VIF**
Constant	74.049	1.954	37.888	<0.001	0.000
Mid Avg NDVI	4.284	0.0742	57.737	<0.001	122.377 <
Mid Avg CRSI	-79.391	1.991	-39.867	<0.001	3708.053 <
ln Mid Avg NDVI	-1.159	0.0336	-34.501	<0.001	102.543 <
ln Mid Avg CRSI	61.835	1.687	36.661	<0.001	3671.282 <
ln Mid Avg CWSI	0.0144	0.000907	15.829	<0.001	4.057 <
Annual Precipitation	0.00437	0.0000285	153.079	<0.001	2.930
Annual Avg Min Temp	-0.101	0.00293	-34.561	<0.001	1.412

Table C.146 2024 Non-Corn Field Report 8 Model 8 Coefficients.

Model # 8	**R squared**	**0.680**			
Variable	**Coef.**	**Std. Error**	**t**	**P**	**VIF**
Constant	77.768	1.954	39.794	<0.001	0.000
Mid Avg NDVI	4.661	0.0760	61.343	<0.001	129.358 <

Mid Avg CRSI	-83.661	1.993	-41.969	<0.001	3745.809 <
Mid Avg CWSI	-1.663	0.0779	-21.338	<0.001	182.727 <
ln Mid Avg NDVI	-2.121	0.0561	-37.786	<0.001	288.417 <
ln Mid Avg CRSI	64.292	1.684	38.183	<0.001	3688.531 <
ln Mid Avg CWSI	0.0203	0.000946	21.500	<0.001	4.447 <
Annual Precipitation	0.00424	0.0000291	145.643	<0.001	3.069
Annual Avg Min Temp	-0.0946	0.00293	-32.300	<0.001	1.427